ABSTRACT

Late Quaternary History of the Waco Mammoth Site: Environmental Reconstruction and Interpreting the Cause of Death

John D. Bongino, M.S.

Mentor: Lee C. Nordt, Ph.D.

The Waco Mammoth site is thought to be the largest single-herd, non-human related mammoth death site in the World. Previous research has failed to determine an undisputed age and cause of death of 22 Columbian mammoths (Mammuthus *columbi*) uncovered at the site. The purpose of this study is to produce the most accurate age and interpretation of the environmental events occurring before, during, and after the death of the Waco Mammoths. Soils, sediments, and allostratigraphic units were described using several vertical measured sections. Data collected from measured sections included stratal thickness, allostratigraphic boundaries, grain size, sedimentary and pedogenic features, and the spatial and temporal ordering of stratigraphic units. Particle size distribution and micromorphologic analyses were performed to create a microstratigraphic and pedologic history of the site. This study concludes that the Waco mammoths represent at least two separate death events occurring in a tributary of the ancestral Bosque River between 53 to 73 ka B.P.

Late Quaternary History of the Waco Mammoth Site: Environmental Reconstruction and Determining the Cause of Death

by

John D. Bongino, B.A.

A Thesis

Approved by the Department of Geology

_____
Steven G. Driese, Ph.D., Chairperson

Submitted to the Graduate Faculty of
Baylor University in Partial Fulfillment of the
Requirements for the Degree
of
Master of Science

Approved by the Department of Geology

_____
Lee C. Nordt, Ph.D., Chairperson

_____
Steven G. Driese, Ph.D.

_____
Ellie B. Caston, Ph.D.

Accepted by the Graduate School
August 2007

_____
J. Larry Lyon, Ph.D., Dean

Page bearing signatures is kept on file in the Graduate School.

TABLE OF CONTENTS

LIST OF FIGURES

LIST OF TABLES

ACKNOWLEDGMENTS

This manuscript is the product of many years of determination, continued support, and love. If not for the loving support of my family and friends, this manuscript would have never met completion. I would like to express my great appreciation to Dr. Lee Nordt for giving me the opportunity to work on such an amazing site and all his patience, expertise, and time. I would like to thank Dr. Steve Driese for his generous assistance and for reviewing this manuscript. I also wish to thank Dr. Ellie Caston for her open mindedness and support in this project.

My appreciation goes to Dr. John Dubar and Sikiru Amidu for their genial assistance with resistivity surveys and processing the raw data. I want to thank Dr. Steve Forman for his help with interpreting the age of the Waco Mammoth Site using OSL age dating. I would like to thank Dr. Peter Allen for his enthusiastic interest in this study and his continued help with several aspects of this project. I express my gratitude to the entire Geology faculty for their support and kindness during the completion of this manuscript. I extend a special thank you to Paulette Penney for her unbelievable kindness and endless help throughout my time at Baylor. She is an irreplaceable asset to the Department of Geology.

My sincere appreciation goes to President Emeritus Herbert H. Reynolds for his generous financial support toward this study. The majority of this project would have not been possible without Dr. Reynold's support. I would also like to thank the Geological Society of America for a sizable grant, allowing me to expand my analytical opportunities.

I especially want to thank Anita Benedict for her assistance in my study. Anita provided a wealth of information and documentation that proved invaluable. I extend my gratitude towards Dr. Greg McDonald for his expertise in Pleistocene paleotology. My appreciation also extends to Bill Walker for his gracious help in digging out profiles.

Lastly I would like to express my sincere gratitude to my fiancée Stephanie for her support through my Masters and my parents for their never-ending support and love.

CHAPTER ONE

Introduction

The Waco Mammoth Site was discovered in 1978 in a gully dissecting an alluvial terrace within the confluence of the Brazos and Bosque Rivers in McLennan County, Texas (Figure 1). During the initial Phase I excavation (1978-1987), 16 articulated to semi-articulated female and juvenile Columbian mammoths (*Mammuthus columbi*) were unearthed (Fox et al., 1992) (Figure 1). During Phase II and III excavations (1991-1997), the remains of an additional five female and one bull mammoths, and a fully articulated camel (*Camelops hesternus*) (Greg Mcdonald 2005, pers. comm.), and an unidentified large-tooth feline were uncovered (Anita Benedict 2005, Personal Communication) (Figure 1). Subsurface coring by Hilliard (1997), approximately 23 m northeast of the Phase II & III excavation area, encountered bone from another mammoth buried approximately four meters beneath the coring surface, bringing the total number of known mammoths at the site to 23.

After excavation was completed in 1990, several hypotheses were formulated concerning the cause of death of the mammoths. Early investigation (Naryshkin, 1982; Hiernrich, 1985) of the sediments surrounding the mammoth bones suggested that the mammoths did not die *in situ* from rapid burial, but rather were transported and buried over time by finely laminated sediments. Conversely, Fox et al. (1992) concluded that taphonomic data and the *in situ* nature of the bone bed suggested a quick burial by flash-flood-derived sediments, causing the mammoths to form a defensive posture around the younger females and juveniles.

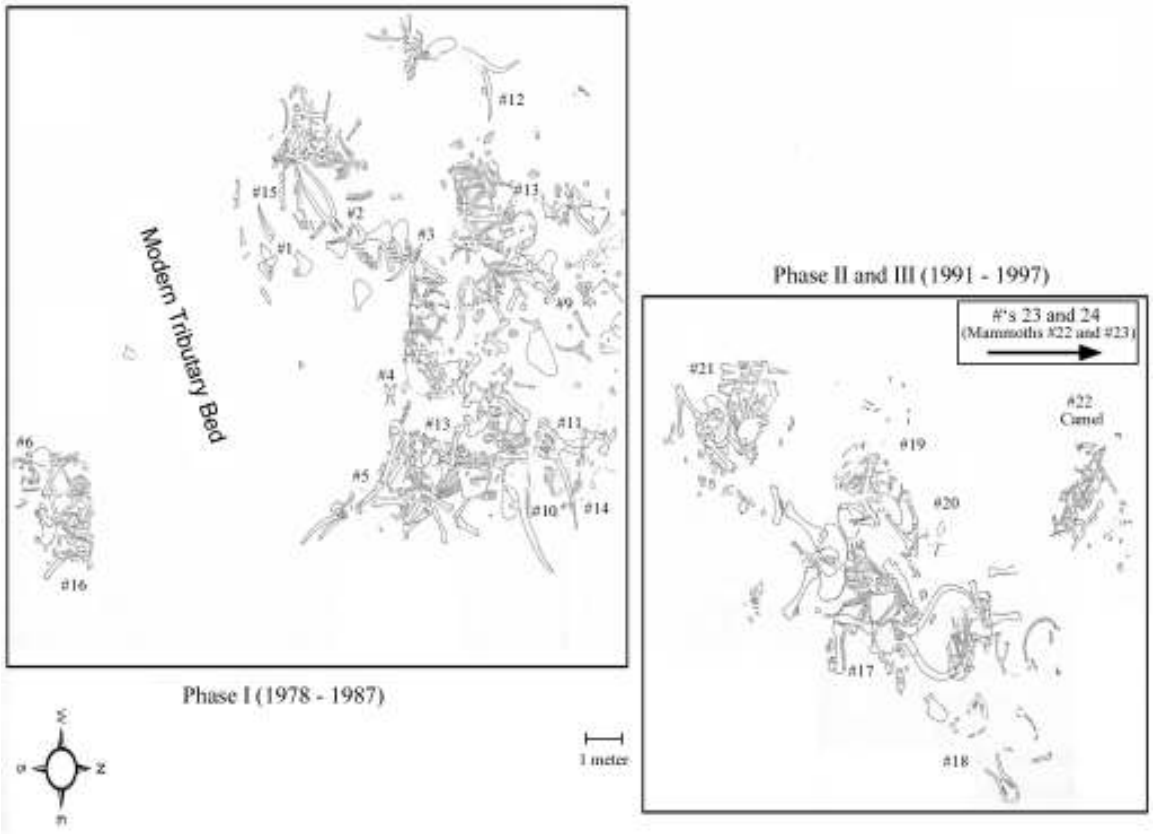

Figure 1. Waco Mammoth Site bone bed, showing locations of excavated mammoths and camel. Adapted from original plan map of Phase I, II, and III excavations by Ralph Vincent. Out of view to the north are Mammoths #22 and #23.

According to Naryshkin (1982), Heinrich (1985), and Fox et al. (1992), the Waco Mammoth site is buried in Brazos River alluvium.

Three dating techniques have been employed at the Waco Mammoth site since its discovery in 1978. Initial standard radiocarbon dating of bone apatite performed approximately twenty years ago positioned the death of one mammoth from the Phase I excavation at the site to 28,670 ± 720 ^{14}C yr B.P. (SMU-155C). Two uranium series ages retained from mammoth tooth enamel in 1990 (SMU-198E2b, 198E1) and four Optically Stimulated Lumenescense ages from associated sediment (UIC1345-1348) obtained in

2004 (Lee Nordt 2005, pers. comm.) both indicate that the demise of the herd occurred sometime between 58,000 and 73,000 yr B.P.

The Waco Mammoth Site is a unique Columbian mammoth site, because it is proposed as the largest single herd, non-human-related death site discovered in the world. However, since its discovery in 1978, scientific studies (Naryshkin, 1981; Heinrich, 1985; Strickland, 1988; Fox et al., 1992; Hilliard, 1997; Hoppe, 2004) have produced differing interpretations, leading to controversy over the absolute age of the site and cause of death. The purpose of this paper is to (1) construct an allostratigraphic and chronostratigraphic framework to interpret the depositional history and age of the site, (2) investigate the cause of death of the Waco mammoths through environmental reconstruction, and (3) to determine whether all the mammoths died during a single event or if several individual death assemblages exist.

More specifically, the following are objectives of the Waco Mammoth Site study are:

1. Refine the most current age estimates of the mammoths using additional optically stimulated luminescence dating,

2. Reconstruct the paleoenvironment in which the mammoths lived and died (using geomorphological, sedimentological, stratigraphic and pedological approaches),

3. Determine the environmental mechanisms resulting in the mammoths deaths (using depositional characteristics, and stable carbon and oxygen isotope analysis for climate conditions and approaches listed above), and

4. Determine whether the 22 mammoths existed collectively as a single herd or as a number of smaller, individual assemblages separated spatially and temporally.

Study Area

Location

The Waco Mammoth Site (WMS) is situated in a narrow valley (~100 meters wide) inset to a large paired alluvial terrace of the Brazos and Bosques rivers in northwest Waco of central Mclennan County, Texas (Figure 2). The WMS is located at 31°36'N, 97°11'W, and mapped on the northeast quadrant of the Waco West USGS 7.5" quadrangle (USGS photo revised, 1975). The WMS is approximately 2 km north of the present confluence of the Brazos and Bosque Rivers. The site lies within a large meander loop known as Steinbeck Bend, approximately 0.6 km and 3 km from the Bosque and Brazos rivers, respectively (Fox et al., 1992) (Figure 2).

Physiography

The WMS is positioned on the interior margin of the Gulf Coastal Plain, at the border where the Blackland Prairie, Grand Prairie and northeast corner of the Edwards Plateau physiographic regions meet (Figure 3). The Blackland Prairie is an approximately 80-kilometer wide, north-south trending belt spanning Central Texas from just north of San Antonio to the Red River in North Texas (Flawn and Burket, 1965) (Figure 3). The WMS is within the Brazos River basin containing the Brazos and Bosque River systems, which is bordered to the east and northeast by the Trinity River Basin (Figure 4). The Brazos River basin upstream from the Waco Mammoth Site encompasses other physiographic regions that influence its hydrology and sediment sourcing. Provinces included within the upper Brazos River basin are the North Central Plains and the High Plains (Figure 3).

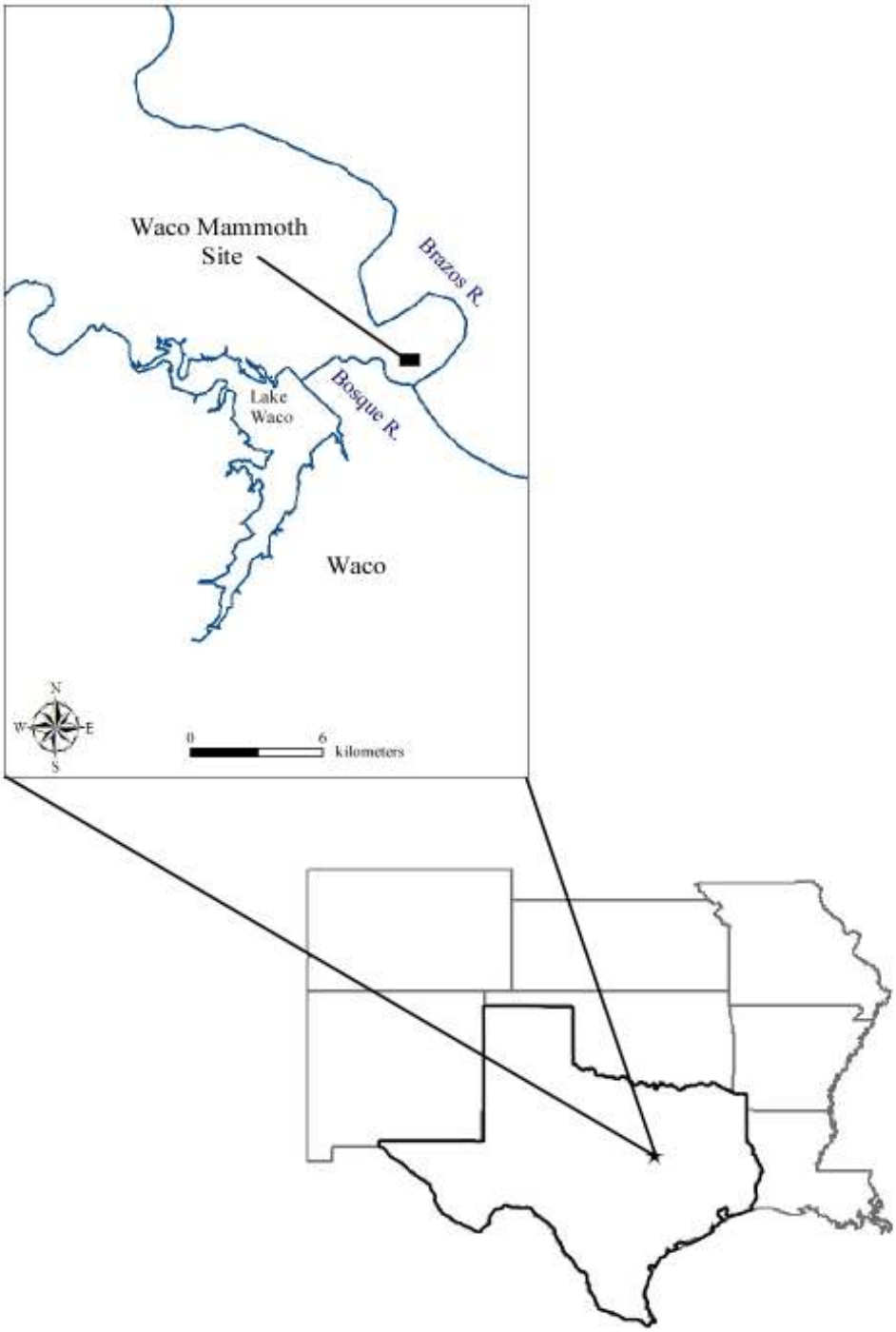

Figure 2. Location of the Waco Mammoth Site approximately 2 km north of the confluence of the Brazos and Bosque rivers, within the northern city limits of Waco in McLennan County, Texas.

The topography consists of gentle rolling hills with deep clayey soils (Blackland Prairie) in the east grading into a more rolling prairie (Washita Prairie – part of the Grand Praire) with shallow calcareous soils to the west (Flawn and Burket, 1965).

Geology

The Blackland Prairie region is underlain by Cretaceous shales and limestones of the Eagle Ford Group, Austin Chalk and Taylor Marl (Flawn and Burket, 1965). The neighboring Washita Prairie to the west lies above the Washita Group, which consists of Cretaceous limestones of the Buda, Del Rio, and Georgetown formations (Flawn and Burket, 1965). The two prairie systems are separated by the Bosque Escarpment, a fault line scarp extending across the northwest portion of Waco (Flawn and Burket, 1965) (Figures 3 and 5). This stair-stepped, fault-controlled feature is part of the much larger and longer White Rock escarpment, a northeastern trending two-stepped topographic escarpment spanning across Central Texas. The White Rock escarpment and its smaller counterpart, the Bosque escarpment are capped on their high step primarily by the Cretaceous Austin Chalk with the lower step being supported by limestones of the Eagle Ford Group (Flawn and Burket, 1965).

Brazos River alluvium is mapped at the site as Fluviatile terrace deposits (Qta) on the Geologic Atlas of Texas Waco sheet (Figure 5). Flawn and Burket (1965) mapped these deposits as Brazos Terrace (Qbrl). North of the excavation area, the Brazos alluvium is directly underlain by the Eagle Ford Group and Early Gulfian (Cretaceous) shales with limestone fragments (Figure 5). The central and southern portions of the site are underlain by Cretaceous-age Austin Chalk (Kau), which is exposed at the surface to the south, west and north of the site (Figure 5).

The Brazos and Bosque rivers are both meandering streams, creating a series of three alluvial fill terraces that represent older, abandoned floodplains. The Waco Mammoth Site is inset to the third and highest terrace of a well defined three-level system of terraces between the Brazos and Bosque rivers (Figure 6). These terraces are labeled T1 through T3 and are 11 m, 16 m, and 24 m above mean river elevation correspondingly (Flawn and Burkett, 1965; Hilliard, 1997). The mammoth and other faunal remains were excavated within and adjacent to a modern low-order tributary that has cut down through the T3 terrace.

Hydrology

The Brazos drainage basin begins with its headwaters in central-eastern New Mexico and continues southeastward through Texas, where it terminates into the Gulf of Mexico (Figure 4). Beginning from its headwaters to where the Brazos and Bosque Rivers converge, the Brazos basin drains approximately 110,703 km^2, with 8,611 km^2 considered noncontributing (Greiner, 1978). Flowing southeast through Erath, Somervell, Bosque, Hamilton, Coryell, and McLennan counties, the Bosque River is bounded by the Leon River to the west, the Brazos River to the east, and the White Rock escarpment to the southeast (Bishop, 1977). The Bosque River drainage basin, within the larger Brazos River basin, drains approximately 4,286 km^2.

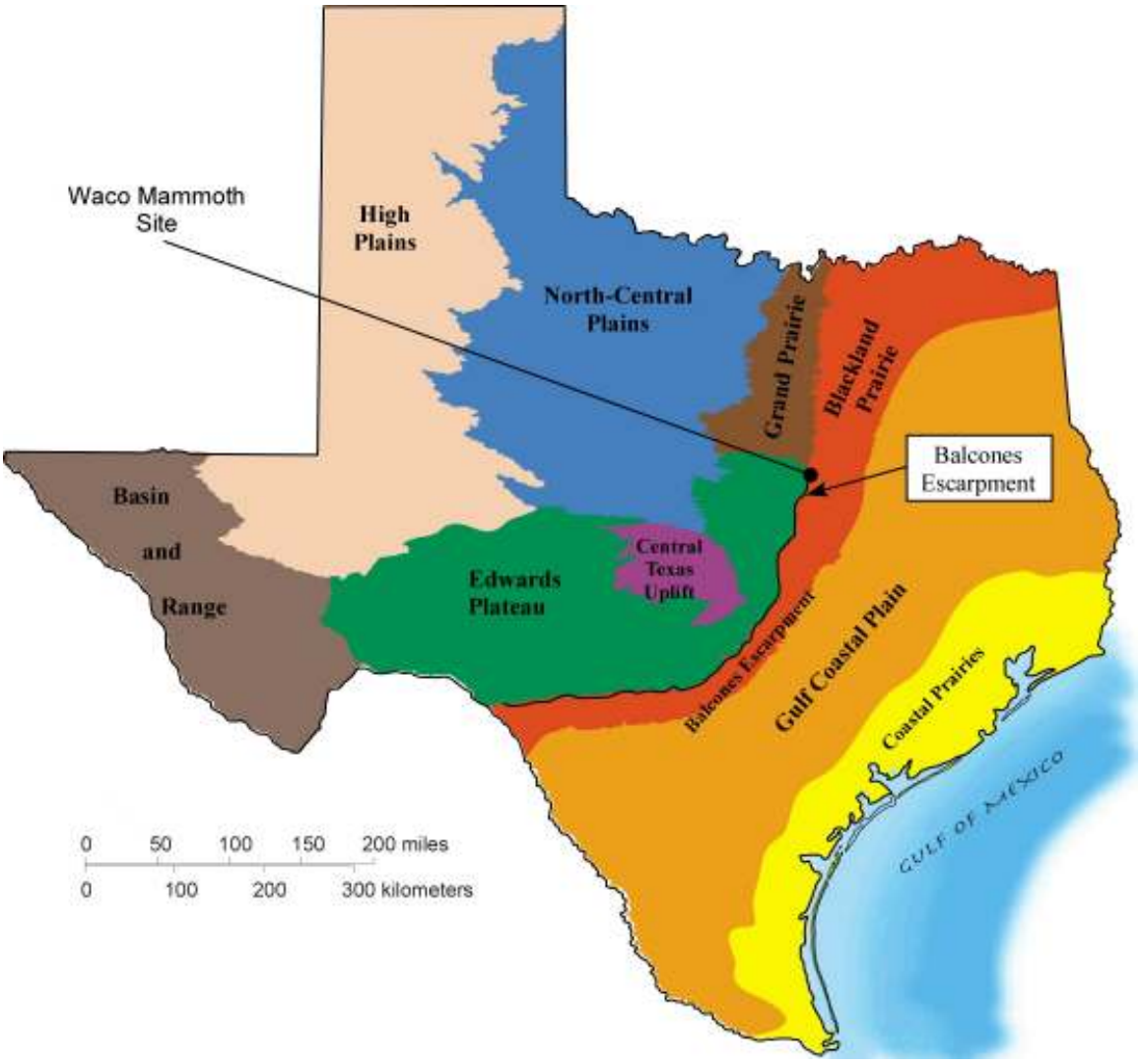

Figure 3. The location of the Waco Mammoth Site, shown on the physiographic map of Texas. Adapted from Bureau of Economic Geology, Austin, Texas (1996).

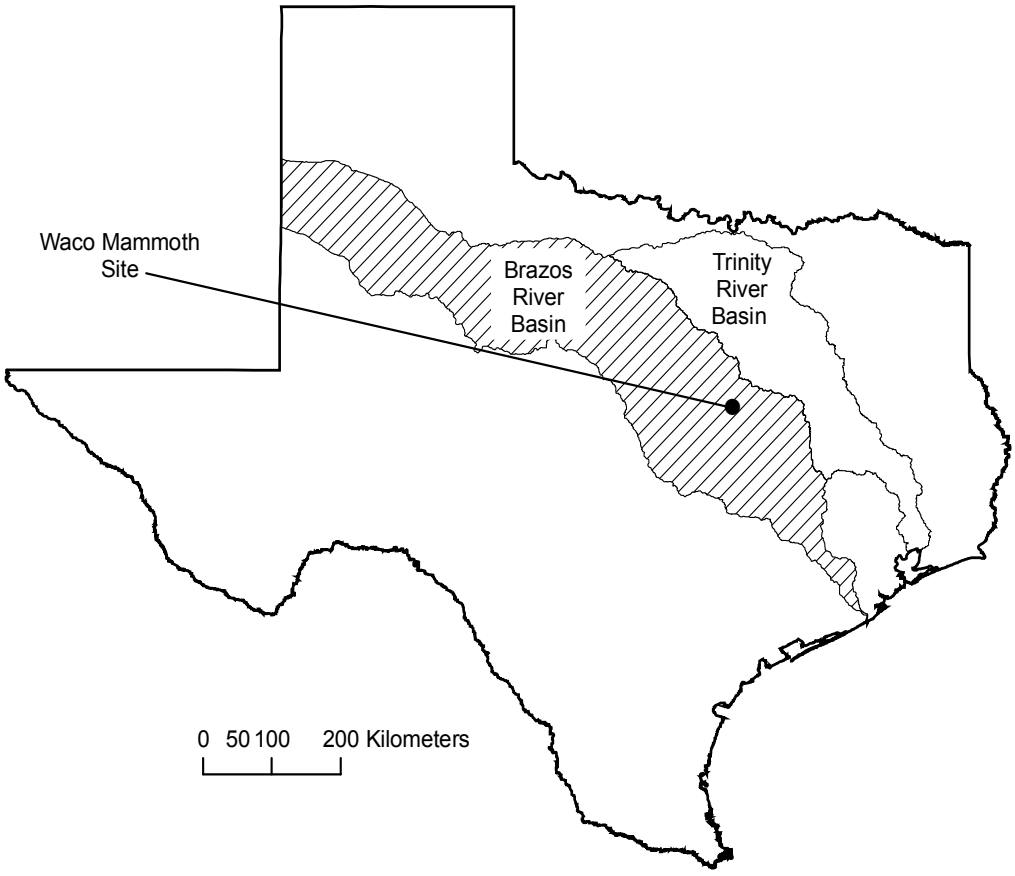

Figure 4. Map showing location of Waco Mammoth Site within the Brazos River Basin. The Brazos River basin is bordered to the north and northeast by the Trinity River basin.

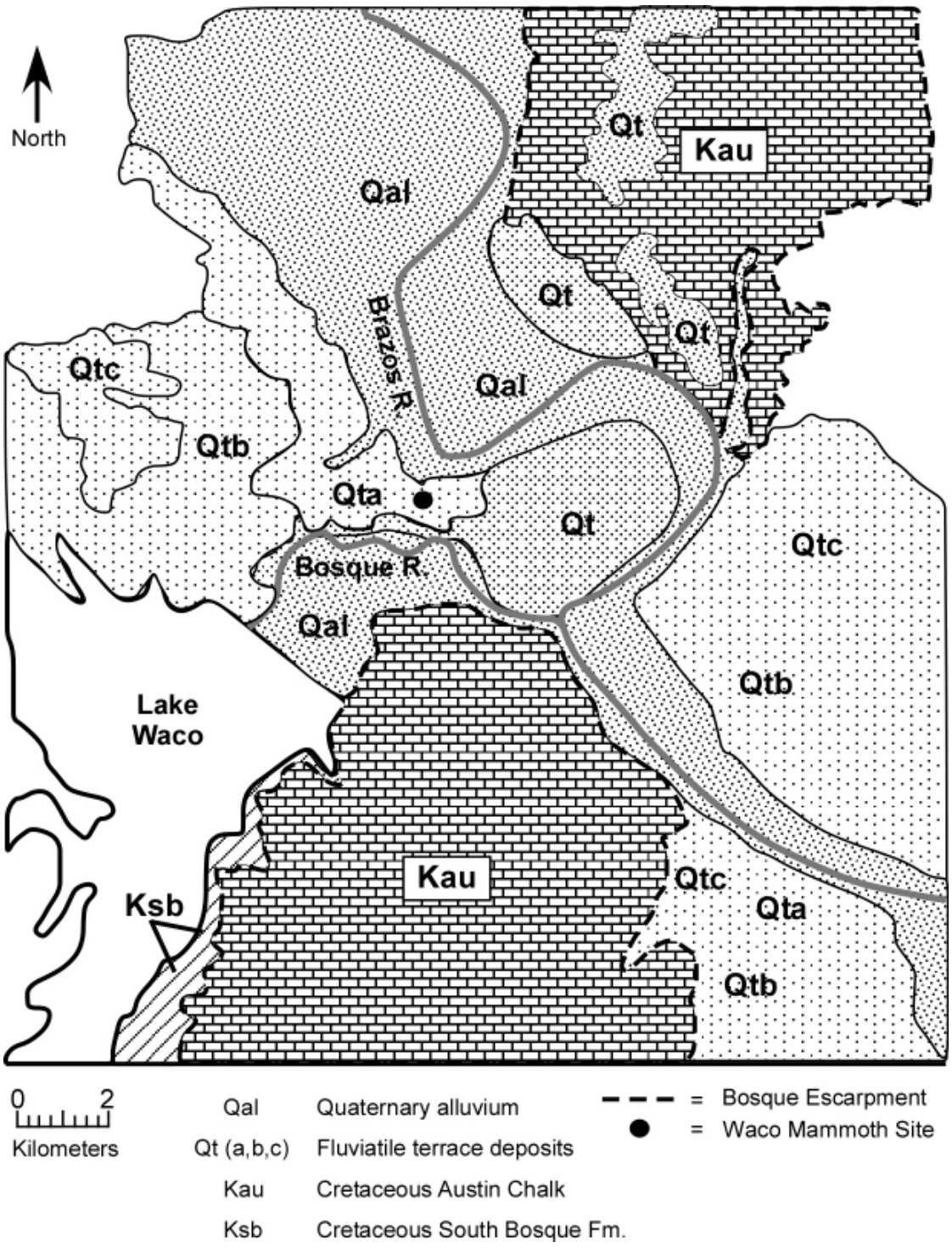

Figure 5. Geologic map of the Waco Mammoth Site and surrounding area, including the associated reaches of the Brazos and Bosque Rivers. One centimeter equals 2.5 km (adapted from the Bureau of Economic Geology, Waco sheet, 1979).

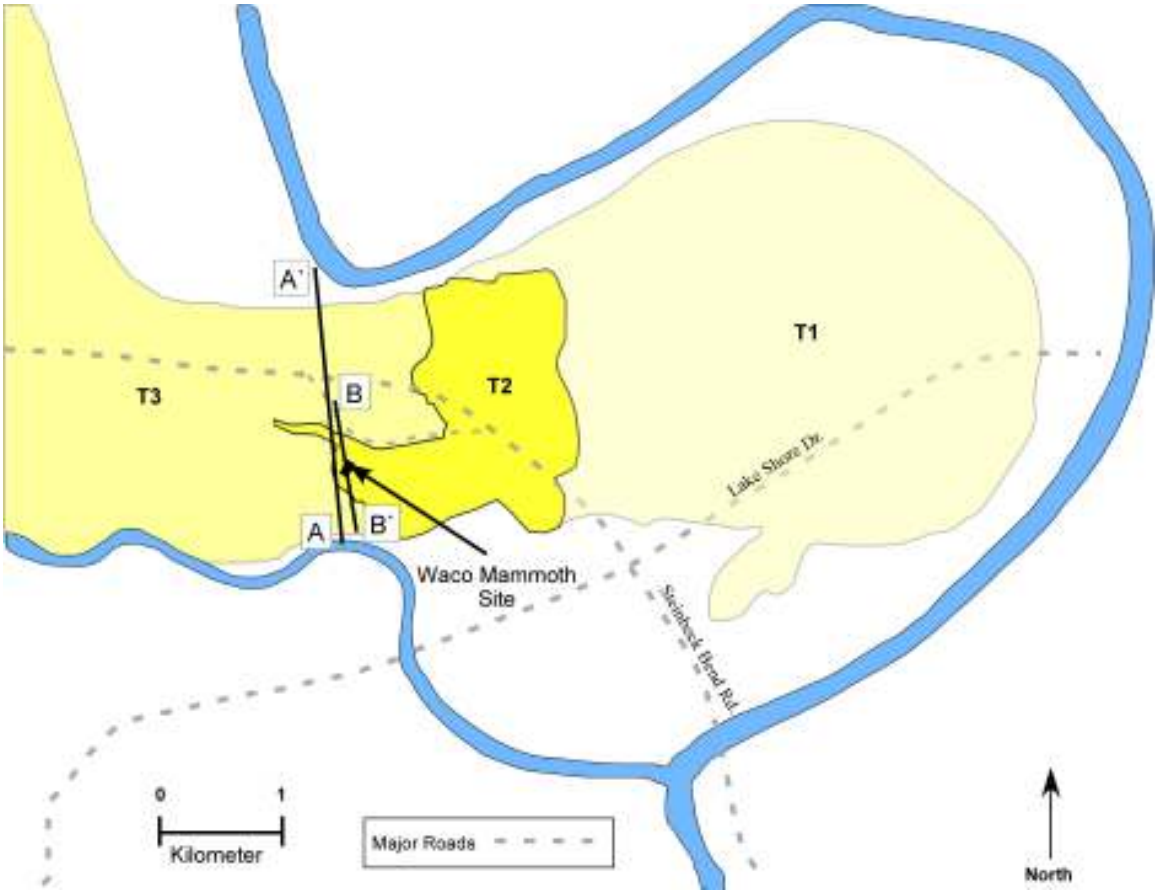

Figure 6. Map of study area showing Brazos/Bosque River alluvial terraces. Terrace boundaries based on USGS Waco West 7.5" topographic quadrangle (1975), with cross section transect (A to A`) and cross section transect (B to B`) (adapted from Hilliard, 1979). Transects A to A` and B to B` are shown in Figures 6 and 13, respectively.

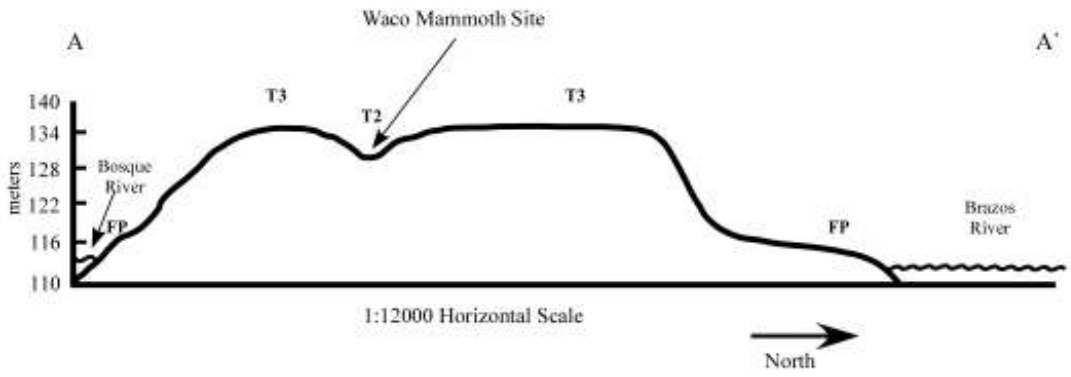

Figure 7. Cross section of T2 and T3 alluvial terraces derived from the USGS Waco West 7.5" quadrangle (photo revised 1975) along transect A to A` (see Figure 6) (Adapted from Hilliard, 1997).

Soils

Soils principally associated with the Bosque River terrace alluvium to the south of the site are calcareous and clayey Mollisols formed under grassland prairies (Figure 8). These soils contain organic-rich mineral surface horizons, typically underlain by clayey and carbonitic subsurface horizons that include the Burleson, Sunev, Queeny, Lewisville, and Frio series (USDA, 2001) (Figure 8). The southern (Bosque River side) portion of the Waco Mammoth Site is dominated by the Sunev series in the uplands (fine-loamy, carbonatic, thermic Udic Calciustolls) and the Frio series in the floodplain (fine, montmorillonitic, thermic Cumulic Haplustolls) (USDA, 2001) (Figure 8).

The Brazos River soils on the north side of the Waco Mammoth site are Alfisols formed under oak-grassland savanna with deep, loamy-siliceous properties containing a greater abundance of quartz derived from the Paluxy Formation of the Fredricksburg Group (Hilliard, 1997) (Figure 8). Brazos alluvium-parented soils in the study area are members of the Bastil, Wilson, McLennan, Gholson, Payne, Branyon, Burleson,

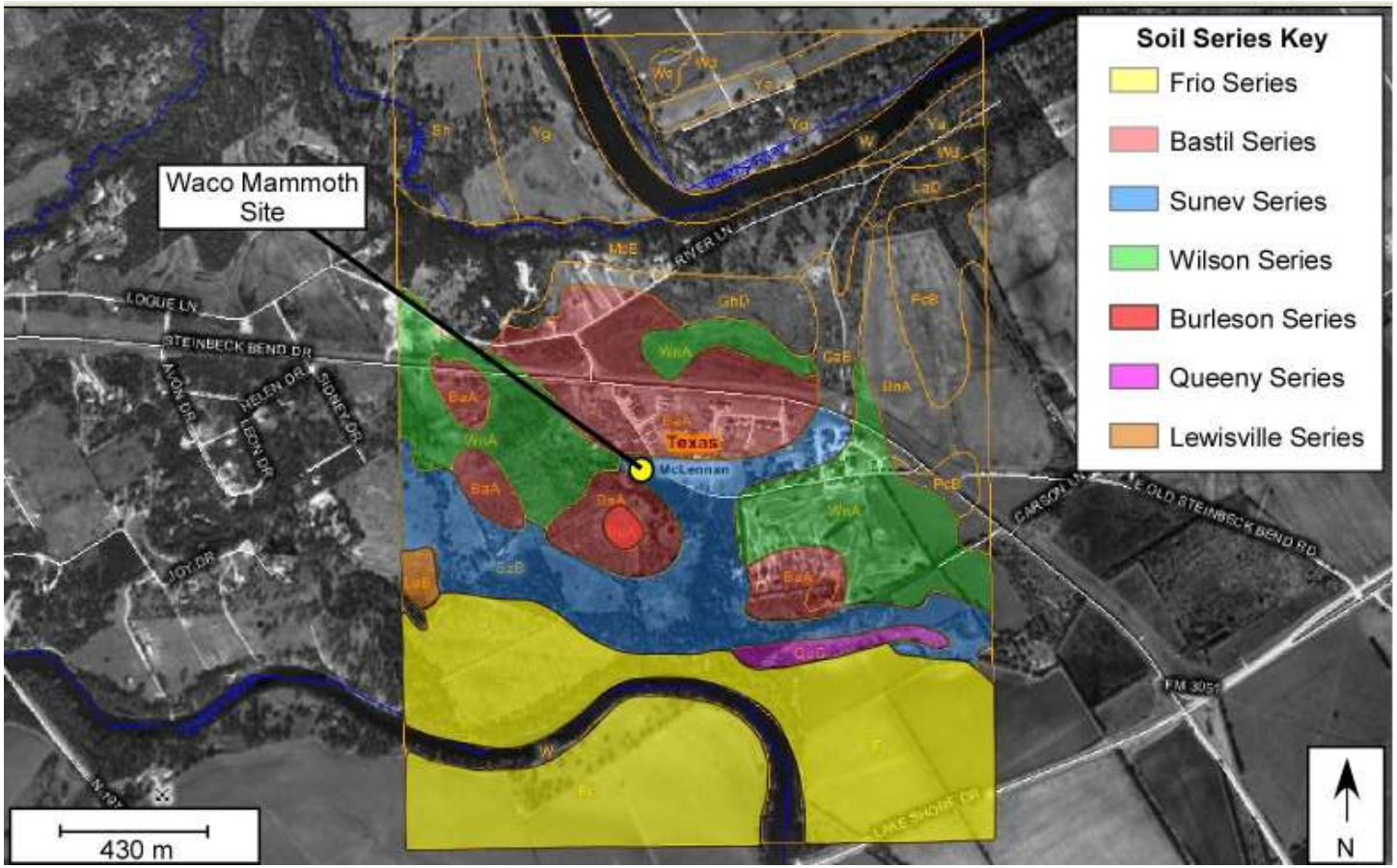

Figure 8. McLennan County Soil Survey map showing soil series distributions within and surrounding the Waco Mammoth Site. Adapted from the NRCS Web Soil Survey (2007).

Weswood, and Yahola soils series (USDA, 2001) (Figure 8). The primary soil series are the Bastil series (fine-loamy, siliceous, thermic Udic Paleustalfs) and the Wilson series (fine, montmorillonitic, thermic Oxyaquic Vertic Haplustalfs) (USDA, 2001) (Figure 8).

CHAPTER TWO

Related and Previous Work

Columbian Mammoths

Taxonomy and Evolution

Classified by Falconer (1857) as *Mammuthus columbi*, Columbian mammoths existed in North American for close to 1.9 million years (Saunders, 1990). Identified primarily based on the frequency and number of lamellar plates and enamel thickness (range of 5 – 8 plates/100 mm and a range of 8 – 20+ plates; Osborn, 1922; Hay 1924; Lundelius, 1972; Maglio, 1973; Kurten and Anderson, 1980; Graham, 1986; Dalquest and Schultz, 1992; Fox et al., 1992; Webb, 1992; Finsley, 1996), the Columbian mammoth (*Mammuthus columbi*) was one of the largest species of mammoth (*Mammuthus*) measuring from 300 to 400 cm tall at the shoulder (Agenbroad, 1984; Haynes, 1991; Lister and Bahn, 1994; Dutrow, 1980) with adults weighing up to 7,700 kg (Shipman, 1992). Columbian mammoth (*M. columbi*) evolved from its Early Pleistocene ancestor *Mammuthus meridionalis* (approximately 1.9 mya) (Agenbroad, 1984; Haynes, 1991; Lister and Bahn, 1994). Unlike its colder-adapted Eurasian cousin the Wooly mammoth (*M. primigenius*), the Columbian mammoth moved southward from Asia (via the land bridge Beringia), across North America, adapting to more temperate open grazing environments (Fox et al., 1992; Haynes, 1991; Lister and Bahn, 1994; Webb, 1992) stretching from the southwest states, then northeastward to the Great Lakes region (Agenbroad, 1984) (Figure 9).

Columbian mammoths (*Mammuthus columbi*) migrated into Texas approximately 1.2-1.3 my B.P. (Izett, 1977; Madden, 1983; Morgan et al., 1998).

Figure 9. Columbian Mammoth (*Mammuthus columbi*) distribution in North American from known excavations (Agenbroad, 1984). Contour interval = 20 individuals. Adapted from Agenbroad, (1984).

Other North American Mammoth Sites

Several sites containing *Mammuthus columbi* remains have been discovered throughout Texas and surrounding Western states, including Arizona, New Mexico, and Colorado (Agenbroad, 1984a). Notable Columbian Mammoth sites in Texas include the Duewall-Newberry Site in Brazos County (Carlson et al., 1984; Steele and Carlson,

1989a, 1989b; Haynes, 1991; Fox and Smith, 1992; Fox et al., 1992; Carlson and Steele, 1992), the Friesenhahn Cave Site in Bexar County (Milstead, 1956; Glen and Grayson, 1961), and the Maimi Site in Roberts County (Steele and Carlson, 1989a, 1989b; Graham, 1976; Sellards, 1952; Holliday et al., 1994). During excavation of the Duewall-Newberry Site, the remains of a single mammoth were found on the muddy sand sediments of a buried natural levee of the Brazos River, which was estimated to date 12,000 to 10,000 years ago, however, collagen present in the bone was not sufficient to obtain an accurate radiocarbon age estimate (Carlson and Steele, 1992). The Friesenhahn Cave Site, a one-room cave carved into the Edwards Limestone in south-central Texas, has yielded 300 whole and 200 broken Columbian Mammoth teeth, along with the remains of several other large fauna (Graham, 1976). Radiocarbon ages produced at the Friesenhahn Cave Site suggest that large assemblage habitation occurred from 10,000 yr B.P. to 20,000 yr B.P. (Graham, 1976). The Friesenhahn Site contains an abundance of sabertoothed cat (*Homotherium serum*) remains, suggesting that this site was a saber-toothed cat den (Graham, 1976; Marean and Ehrhardt 1995). The Miami Site, located near the eastern boundary of the Southern High Plains contains the partial remains of five Columbian mammoths dating from 10,000 yr B.P. to 11,400 yr B.P., all found resting on the surface of silty clay sediments deposited in a shallow ephemeral pond (Sellards, 1952; Holliday et al., 1994).

Several similar studies have been performed on Columbian mammoth sites in Texas, Iowa, and Oklahoma. A mammoth site dating to 22,000 yr B.P. located in Pattawattamie County, Iowa was investigated by Davis et al. (1972), who was concerned with placing the mammoth stratigraphically within its Pleistocene sediments to determine

potential associations with prehistoric man or other mammals. Similar to the Waco Mammoth Site, the stratigraphic investigation revealed no apparent evidence to support a fluvial redeposition of the mammoth after their death. The bones were, however, fragmented and disarticulated suggesting weathering and possible scavenger activity.

The La Paloma Mammoth Site, containing 145 partially articulated bones relatively undisturbed by moving water or scavenging activity, was discovered buried in fluvial sediments in Kenedy County, Texas, (Weir, 1978). Sedimentological and stratigraphic evidence retained from the site suggests the possibility of rapid burial, which has also been suggested at the Waco Mammoth Site.

The Hajny Mammoth Site, Dewey County, Oklahoma has been extensively studied by Wyckoff et al. (1992), who focused on geological and paleontological aspects. Located in a Quaternary alluvial terrace, the Hajny Site contains the remains of two adult Imperial or Columbian mammoths, of which a definite classification has not been made (Wyckoff et al., 1992). The study of this site included the application of site stratigraphy, radiocarbon dating, and local geomorphology to determine the age, local stratigraphic and spatial contexts of the site. The Hajny Site mammoths died in sediments associated with a natural spring, with two sizably different dates; one radiocarbon age of approximately 9,000 yr B.P. and one uranium/thorium age range of 140,000 to 165,000 yr B.P. (Wyckoff et al., 1992), resulting in a conflict concerning the absolute age of the site. Regardless of the unresolved age of the Hajny Site, the geological implications and methodology was used to interpret the paleoenvironmental conditions during the Hajny Site mammoth occupation (Wyckoff et al., 1992).

Several human-related mammoth kill sites dating to the Late Pleistocene and Early Holocene transition (10,000 to 15,000 yr B.P.), contain useful depositional information for comparison with the Waco Mammoth Site. These sites include: the Taylor Ranch Mammoth Site in Kleberg County, Texas (Suhm, 1979); the Naco Mammoth Site, southeastern Arizona (Haury, 1953); and the Rawlins Mammoth Site in Wyoming (McGrew, 1961). All of these sites are located in fluvial environments and contain depositional evidence similar to that found at the Waco Mammoth Site.

Previous Work

Since its discovery in 1978, several phases of research have been employed at the Waco Mammoth Site including excavation, classification and casting of most of the 22 mammoths, two tortoises, a large-tooth feline and one camel (*Camelops hesternus*), absolute dating of faunal material and sediment, initial stratigraphic and soil analysis and stable isotope analysis (Naryshkin, 1981; Hienrich, 1985; Strickland, 1988, Fox et al., 1992; Haynes, 1992; Hoppe, 2004). Three dating techniques have been employed at the Waco Mammoth Site. Initial standard radiocarbon dating of bone apatite performed approximately twenty years ago positioned the death of one mammoth at the site at approximately 29,000 ^{14}C yr B.P. (SMU-155C). Two uranium series ages retained from mammoth tooth enamel in 1990 (SMU-198E2b, 198E1) and four Optically Stimulated Luminescence ages from associated sediment (UIC1345-1348) obtained in 2004 both indicate that the herd died sometime between 58,000 and 73,000 yr B.P.

Preliminary investigations were initiated by Fox et al. (1992) and Haynes (1992) concerning the herd dynamics of the Waco Mammoth Site using data collected from 1978 to 1987. Their study produced evidence suggesting that the mammoths were part of

a single matriarchal herd all dying during the same event (Fox et al., 1992). The position of the mammoths, sexual dimorphism, and ages suggest that the 16 adult females and juveniles were all members of a single family assemblage (Haynes, 1991, 1992; Fox et al., 1992). Fox et al. (1992) used stratigraphic, faunal, and spatial evidence to compose a number of potential hypotheses explaining the cause of the mammoths' deaths. Evidence assembled by Fox et al. (1992) was also used to challenge previous hypotheses (Naryshkin, 1981; Hienrich, 1985; Strickland, 1988) indicating that the mammoths died not *in situ* from drowning and slow burial. Fox et al. (1992) concluded that the Waco mammoth bones were naturally preserved *in situ* likely due to a sudden catastrophic event resulting in immediate burial. However, Fox et al. (1992) suggested that the exact cause of death of the mammoths remains problematic.

A taphonomic study on 10 of the mammoths from the Waco Mammoth Site was conducted by Haynes (1992). Haynes (1992) determined the life-ages of the 10 individuals and found that at least two of the mammoths were juveniles and approximately 20-30% were subadults. According to Haynes (1991), modern elephant populations consist of approximately 30-50% subadults within the population. Based on the lack of sexually productive mammoths and skeletal size and bone lengths, Haynes (1992) concluded that the Waco mammoths may have suffered from environmental stresses or significant predation.

Two faculty-supported undergraduate research studies through Baylor University, (Naryshkin, 1981; Hilliard, 1997), were completed on the Waco site, both concentrating on the geologic investigation and age of the site. Naryshkin (1981) attempted to determine the site's significance to the Pleistocene history of Central Texas. He

combined fossil and sedimentary data in an effort to form an environmental interpretation of the site by determining any relationships between the Pleistocene history of the site and the alluvial terrace history of the Brazos River Valley. Naryshkin (1981) concluded that lithologic evidence suggested that the herd met their demise upstream and were transported downstream, where they were deposited on a point bar.

Additionally, two brief studies (Hienrich, 1985; Strickland, 1988) focusing on the stratigraphy and site formation processes were carried out on the Waco Mammoth Site. Hienrich (1985) suggested that the stratigraphy of the site was not consistent with a single episodic event, but rather a more systematic series of depositional events that over time completely buried the 16 mammoths from the first phase of excavation. He proposed that the mammoths were situated on an abandoned channel, once part of an active floodplain of the Bosque River. The mammoths were partially buried by approximately 25 cm of finely laminated flood deposits, leaving bone exposed to be weathered. Hienrich (1985) suggested that the depositional sequence of events may have resulted from the infilling of an abandoned meander loop of the Bosque River. Furthermore, Hienrich (1985) concluded that the flood history of the Bosque River should be considered in the interpretation of the cause of death.

Strickland (1988) studied site formation processes at the Waco Mammoth Site, considering the mammoths as a thanatocose (i.e. animals present died in *in situ*). This study compared the previous works of Naryshkin (1981), Heinrich (1985), and Haynes (1987). Strickland (1988) concluded that the mammoths were likely part of a single family group and recommended the application of microenvironmental analysis to the interpretation of the Waco mammoth death event.

A study by Hoppe (2004) presented isotopic analyses of several known Pleistocene mammoth sites, including the Waco Mammoth Site. Hoppe (2004) focused on mammoth herd structure, migration patterns, and Clovis hunting strategies using carbon, oxygen, and strontium isotope ratios in mammoth tooth enamel. Isotopic ratios from the Waco Mammoth Site were compared to the Friesenhahn Cave site (a natural accumulation of non-related Columbian mammoths) in South Texas. For the Waco Mammoth Site, 17 samples were obtained from molars representing 12 mammoths (Hoppe, 2004). Carbon and oxygen isotopic ratios were measured from all samples except one and strontium ratios were measured from 11 of the 17 samples (Hoppe, 2004). The Waco mammoths showed little variability of either carbon or oxygen isotope values (Hoppe, 2004). Strontium isotopic ratios were determined not to be sufficient for identifying related individuals among the Waco mammoths; however, these ratios suggest an influence from sediments associated with the Bosque River (Hoppe, 2004). Oxygen isotopes suggested that the mammoths drank from a variety of source areas and were not traceable to any one source (Hoppe, 2004). Hoppe (2004) concluded that the close range of carbon isotope ratios from the Waco mammoth teeth suggested a similar diet of primarily C_4 (warm season grasses) vegetation among the mammoths. Conversely, the unrelated individuals at the Friesenhahn Cave site showed a wider range of $\delta^{13}C$ values, suggesting those individuals were from different areas, or lived at different times (Hoppe, 2004).

CHAPTER THREE

Methodology

Field Description and Sampling

Locations for field description, sampling, and geology map were chosen using topographic sheets, aerial photographs, the Soil Survey of McLennan County, Texas (2001), the Environmental Atlas of McLennan County (Yelderman and Cervenka, 1992), the Geologic Atlas of Texas, Waco sheet (1970), and field observations. Seven vertical sediment profiles, eight backhoe trenches, and nine subsurface cores (Figures 10, 11 and 12; Appendices A, B, and C) were used for description and identification of unconformably bound stratigraphic units, associated depositional facies, and surface and buried soils. Depositional facies and soils were described in the field using texture grain-size and color, sedimentary structures, and reaction to HCl. Backhoe trenches were dug to depths of 2 to 4 meters depending on machine capabilities.

Detailed soil descriptions were completed on seven existing vertical soil profiles within the excavation area (Figure 10; Appendix B). In addition, detailed soil descriptions were completed on all backhoe trenches excavated (Figures 11 and 12; Appendices A and B). Soil characteristics from the vertical profiles and soil trenches were identified and described in correspondence with the standards and procedures of the Soil Survey Division Staff (1993), including: texture, structure, consistence, color, reaction to HCl, carbonate content, coarse fragments, and other diagnostic features such as reduction/oxidation, rooting, and slickensides.

Bulk samples were collected from each soil horizon and associated parent material for particle-size distribution, thin-section analysis, and $\delta^{13}C$ and $\delta^{18}O$ isotopic analysis. Thin section samples with natural integrity were also collected from each soil horizon for micromorphological analysis. Samples for optically stimulated luminescence (OSL) dating were taken from sandy sediment layers associated with the six mammoths, camel, large-tooth feline, and turtle excavated during the Phase II and III excavations. OSL samples were excavated using a 30 cm long hollow galvanized metal pipe that was capped on one end to assure the capture of unexposed sandy sediment.

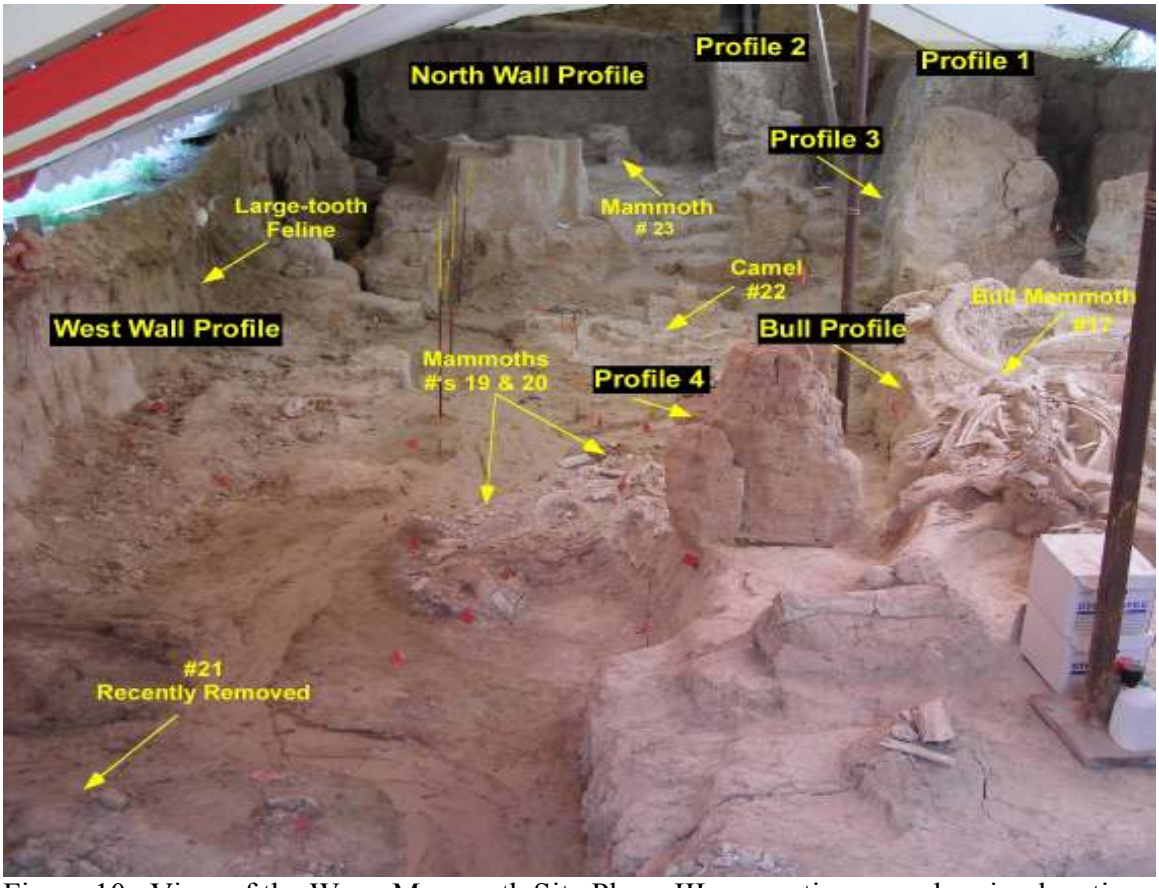

Figure 10. View of the Waco Mammoth Site Phase III excavation area showing locations of exposed vertical wall profiles, with view to the north.

Figure 11. Aerial photograph of Waco Mammoth Site area, showing locations of soil test trenches and T3 and T2 alluvial terraces (Aerial photo adapted from Google Earth, 2006).

Sediment was collected using a 12 in (~30 cm) by 1.25 in (~3 cm) cylindrical metal tube, which was hammered perpendicular into the center of each sediment layer to a depth of at least 30 cm. Sediment was also collected within a 20 cm radius around each sample core for dose rate determinations and to check samples for proper particle size (4-11 μm) and mineralogy (quartz and/or feldspar), prior to analysis.

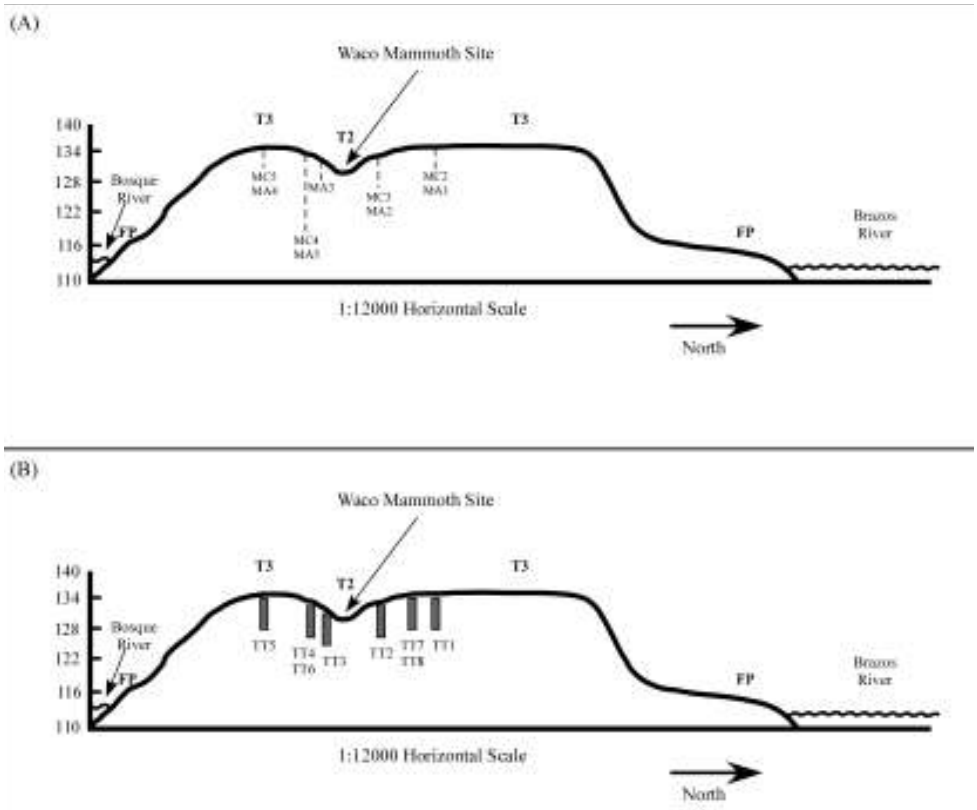

Figure 12. Cross section of T2 and T3 alluvial terraces associated with Waco Mammoth Site, showing terrace elevations and (A) Core (Hilliard, 1997) and Auger flight localities (2005 to 2006), and (B) Soil Trench locations, relative to the positions of the Brazos and Bosque Rivers (Adapted from Hilliard, 1997).

Laboratory Analyses

Particle-Size Distribution

Particle-size distribution was completed using the hydrometer method following the standards and procedures of Gee and Bauder (1986). For this study, the 40-second hydrometer reading for sand fraction calculations was not performed. Alternatively, samples were washed over a 52 µm sieve after the 6-hour reading for clay content, dried and weighed. Dried samples were then placed in a sieve shaker device and sieved for 15 minutes each for sand size separates. Sample fractions used for this study include sand (2-0.062 mm), silt (0.062-0.0039 mm), and clay (> 0.0039). Particle size distributions

were computed for each profile and test trench sampled. Soil texture was also determined using particle size.

Micromorphology

Micromorphologic description and identification were made on 42 (2 X 3 inch formatted) thin section samples taken from several identified soil horizons (from both vertical soil profiles and soil trenches) within study area. For this study, micromorphologic analysis was focused on the identification of diagnostic features associated with morphological and sedimentological similarities to correlate sedimentary beds and/or units and interpret the environments of deposition across the study area. Furthermore, morphological analysis was used to determine the influences of the soil forming factors and environmental controls on pedogenesis for the surface and buried soils. Terminology used for the micromorphological description of thin sections is derived from Brewer's (1976) and Bullock et al. (1985).

Dating

^{14}C and Uranium/Thorium age dating. In 1985, one standard radiocarbon age of 28,670 ± 720 yr B.P. was estimated on a bone sample from the Waco Mammoth Site by the Southern Methodist University Radiocarbon Laboratory, Dallas, Texas. Due to an insufficient amount of organic material (bone collagen), three mineral fractions (hydroxyapatite) were extracted and dated using standard Accelerated Mass Spectrometry (AMS) ^{14}C dating. The first fraction was assumed to be contaminated by secondary carbonate, the second fraction was dated as a check and the third fraction yielded the ~29,000 yr B.P. age (Herbert Haas 1998, pers.comm.). Four additional samples were

obtained for further AMS dating, which included bone from Mammoth #17 (1997.1), the camel (1997.2), and Mammoth #23 (1997.3) and a bulk sediment sample from below Mammoth #21. All of these additional samples were determined to have insufficient datable carbon (collagen) for dating by either AMS or standard methods because of extreme chemical degradation (Thomas W. Stafford, Jr., Ph.D. 2000, pers. comm.). A study by Grun et al. (1997) suggested that AMS dating of hydroxyapatite from human teeth uncovered from archaeological sites when compared to ages estimated from collagen or inorganic carbon, resulted in serious age underestimations.

Two Uranium-series ($^{230}Th/^{234}U$) ages were estimated from enamel extracted from an unidentified molar of an unidentified mammoth from the Phase I excavation (SMU McKinney, 1990). The two estimated ages were calculated from enamel from an interior and exterior portion of the molar and are 70,924 ± 5261 yr B.P. (198E1) and 73,442 ± 2735 yr B.P. (198E2b), respectively. The Uranium series dating method (Ivanovich and Harmon, 1982) was extensively tested by McKinney (1991), who focused on the reliability of Uranium-series dating of enamel, bone, and dentine. McKinney (1977) argued that enamel was a better material for Uranum-series dating than bone, because of enamel has a much more dense crystal structure. Uranium content in enamel seems to be limited to the outer edges of the enamel, and, in cases when enamel is weathered, the Uranium content tends to be highest in the weathered zone, commonly resulting in overestimated ages (McKinney, 1991). McKinney (1991) concluded that when used with multiple samples and repeated analysis, U-series dating of enamel can be reliable.

Optically stimulated luminescence. Optically stimulated luminescence dating is dependent on the time-dependent dosimetric properties of silicate minerals, especially quartz and feldspar (Aitken, 1985, 1998). The reliability of dating fluvial sediments using OSL has been addressed in several studies over the past eight years (Olley et al., 1999; Wallinga et al., 2001; Wallinga, 2002; Zhang et al., 2003; Feathers et al., 2006). A common problem that arises with OSL dating of fluvial sediments is that sand in fluvial systems may receive inadequate light exposure during transport, resulting in incomplete resetting of the OSL signal by incomplete bleaching prior to burial (Olley et al., 1999; Wallinga et al., 2001; Wallinga, 2002; Zhang et al., 2003; Feathers et al., 2006). This can result in overestimations of the actual burial ages. To avoid overestimation of OSL ages due to possible variability in radiation exposure (degree of resetting), it is recommended to use small subsamples or aliquots of a single to few grains to determine if the radiation dose rate from cosmic rays (grays/1000 yr) or equivalent dose (D_e) is sufficient to produce consistent burial ages (Olley et al., 1999; Wallinga et al., 2001; Wallinga, 2002; Zhang et al., 2003; Feathers et al., 2006). However the multiple aliquot additive dose method (MAAD) is most commonly used for fine-grained polymineral or quartz fraction and is a more suitable method for fluvial sediments (Singhvi et al., 1982; Forman and Pierson, 2002). This method consists of applying additional doses (beta or gamma) to separate aliquots of a larger sample to build a dose response curve and ultimately simulating an equivalent dose (D_e) to the solar reset level (Singhvi et al., 1982; Forman and Pierson, 2002). For this study, the multiple aliquot additive dose method of Singhvi et al. (1982) and Forman and Pierson (2002) was used on the polymineral fraction of the bulk sediment samples.

Bulk sediment samples obtained for OSL dating were analyzed by the Luminescence Dating Research Laboratory, University of Illinois at Chicago, Chicago, Illinois. Four samples were analyzed in 2004 and nine samples were analyzed in 2006. The 4-11 μm polymineral fractions from both the 2004 and 2006 samples were analyzed using the multiple aliquot additive dose method from Singhvi et al. (1982) and Forman and Pierson (2002). The Uranium (U) and Thorium (Th) content from all samples were determined by thick-source alpha counting in order to determine dosing rates (Sjostrand and Prescott, 2002). Uranium, Thorium, and Potassium oxide of the 2006 samples were assayed using an Inductively Coupled Plasma Mass Spectrometer (ICP-MS) at Activation Laboratories, Ontario, Canada. The 2006 samples were designated either GR for excitation by green light (514 ± 20 nm) or IR for excitation by infrared wavelengths (880 ± 80 nm), with the equivalent dose determined by the multiple aliquot regenerative dose technique (Jain et al., 2003). All calculated ages (2004 and 2006 samples) include a cosmic ray dose rate of 16 mGray/ka determined from calculations of Prescott and Hutton (1994). Each age also included an assumed burial moisture content of 20 ± 5% and a measured alpha efficiency factor, which is defined by Aitken and Bowman (1975). The moisture content affects the dose rate by absorbing ionizing radiation. The wetter the sample, the more moisture in pore spaces and thus the greater absorption of generated alpha, beta and gamma particles to varying degrees (dependent on particle energy). The wetter the sample, the lower the dose rate, and ultimately the greater the age estimate. The reliability of OSL dating is dependent on the suitability of the sandy sediments and the preferred sediments for OSL dating are those that (1) less than one hour of sunlight exposure, (2) accumulated as a relatively homogeneous unit, and (3) have not undergone

significant water-content variations or diagenetic alteration during burial (Steve Forman 2005, pers. comm.). After OSL sampling at the Waco Mammoth Site in 2004, the sediments were determined to be suitable for dating (Steve Forman 2005, pers. comm.).

Carbon and oxygen isotopes. A total of 21 whole pedogenic carbonate nodules were collected from soil trenches and exposed wall profiles, representing soil horizons and sediment layers throughout the site. Isotopic ratios of ^{18}O and ^{16}O and ^{13}C and ^{12}C of each sample was measured using a VG SIRA Model 12 dual-inlet continuous gas-source mass spectrometer operated by Coastal Science Laboratories in Austin, Texas. Isotopic ratios of oxygen and carbon were analyzed by liberating CO_2 gas from the bulk carbonate samples using a weak acid. The ratios of ^{18}O to ^{16}O and ^{13}C to ^{12}C measured from CO_2 is expressed as the per mil (‰) difference relative to the Pee Dee Belemnite (PDB) standard, as represented by the $\delta^{18}O$ and $\delta^{13}C$ notations, respectively. For this study, carbon and oxygen measurements are accurate to ± 0.2‰ PDB (CSL Ref.#FP44).

Electrical Resistivity

Electrical-resistivity surveys measure the electrical resistive properties of earthen materials, where by variations in resistivity are correlated to subsurface geologic, hydrologic and chemical properties. In archaeological studies, the method is widely used for detecting, mapping, and studying the characteristics of various types of objects and structures in the subsurface as well as in mapping subsurface stratigraphy (Darwin et al., 1990; Scollar et al., 1990; Osella et al., 2005; Papadopoulos et al., 2006)

Conventionally, artificially generated electric current is injected into the ground through a pair of current electrodes and the resulting potential difference is measured

through a pair of potential electrodes. The relationship between the injected current, measured potential difference and the electrical resistivity is given as:

$$\rho_a = \frac{\Delta V}{I} K$$

where, ρ_a is known as apparent resistivity, V is voltage, I is current, and $K = 2\pi / f(r)$ is known as the geometric or form factor whose values depend on the type of electrode configuration used. Figure 13 shows the electrode arrangements and the corresponding geometric factors for the dipole-dipole and Schlumberger arrays used in this study. In the dipole-dipole array, current and potential electrodes are located on either side of the array, whereas for the Schlumberger array, the current electrodes are placed between the two potential electrodes. By increasing the distance between the electrodes, the depth of investigation increases and deeper zones within the subsurface can be studied. The dipole-dipole array has low EM (electromagnetic) coupling between the potential and current circuits and is sensitive to horizontal changes in resistivity, whereas the Schlumberger array is sensitive to vertical changes in resistivity (Loke, 2000; Furman et al., 2003; Dhalin and Zhou, 2004). By combining the two arrays for the resistivity survey in this study, it is presumed that the horizontal and vertical changes in resistivity are optimally resolved.

The field survey was carried out with an AGI SuperSting R8 resistivity system (Advanced Geosciences Inc. AGI, Austin, Texas). The system consists of a portable earth resistivity meter with 28 smart electrodes in a cable segment. The system was pre-programmed before the field survey for automatic resistivity measurements using the dipole-dipole and Schlumberger arrays at a minimum dipole and electrode spacings of 5 m. Two-cycle stacking was used for the measurements. For each reading, the resistivity

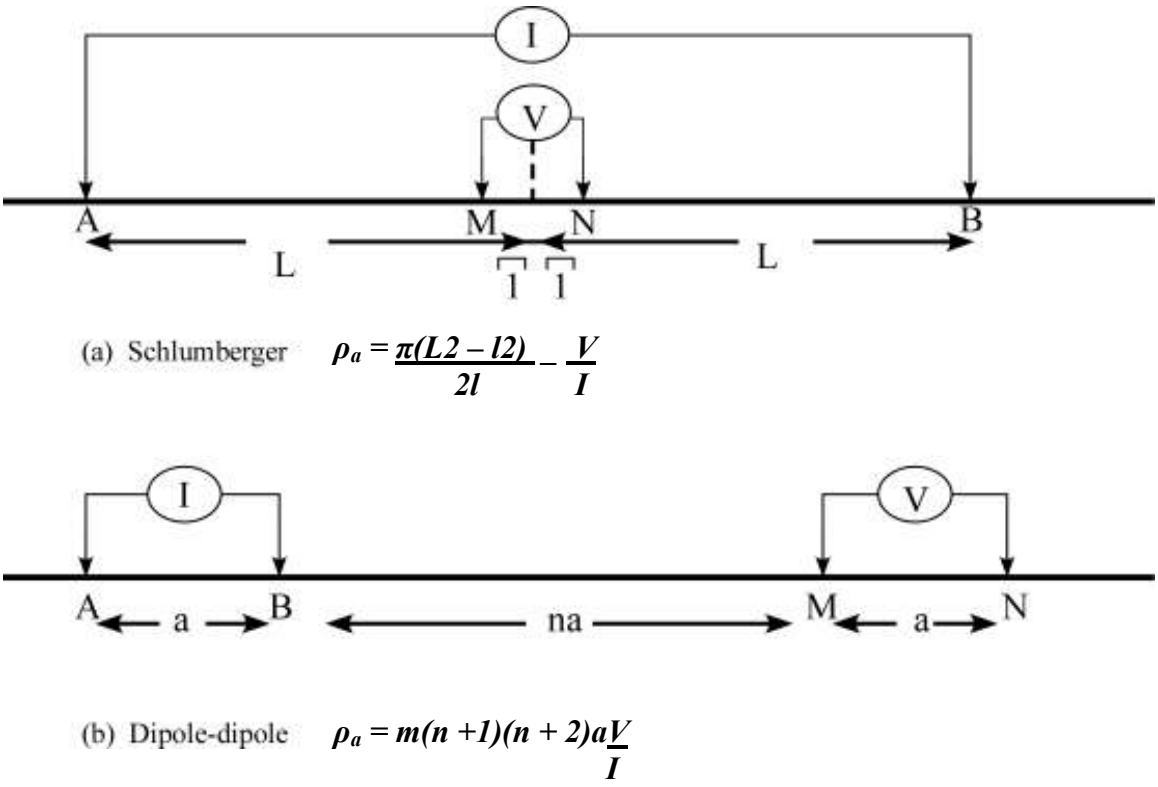

Figure 13. Electrode arrays and corresponding geometric factors for (a) Schlumberger and (b) Dipole-dipole electrode configuration, used in this study. A and B are the current electrodes and M and N are the potential electrodes.

meter recorded the apparent resistivity value and the corresponding standard error from The error values were less than 5% throughout the survey.

The measured apparent resistivity data required numerical modeling and inversion, to obtain the true two-dimensional (2D) distribution of resistivity within the subsurface. This was carried out using the program *EarthImager 2D* (AGI, 2006). This is a computer program that automatically determines a 2D resistivity model of the subsurface for the input-apparent resistivity data. The program uses an array of rectangular blocks (finite elements) to model the subsurface, and by forward modeling, calculates resistivity values that agree with the actual measurements (Loke and Barker, 1996). An optimization method, which may be a least-squares or robust scheme, is then

used to adjust the resistivity of the model blocks and iteratively reduce the difference between the calculated and measured apparent resistivity values. The robust method, which attempts to minimize the sum of the absolute values of the spatial changes in the model resistivity, was used for the data inversion (Claerbout and Muir, 1973; Olayinka and Yaramanci, 2000; Loke et al., 2003). This generated a model in which the features in the resistivity section were delineated by relatively constant resistivity values, and were separated from each other by sharp boundaries (Loke et al., 2003). The observed resistivity distribution in the inverted resistivity section was then tied to available geological and paleontological information at the site.

CHAPTER FOUR

Results

Stratigraphy

The Waco Mammoth Site is associated with two Late Pleistocene paired alluvial landforms: T3 terrace and T2 terrace (Figure 14). Represented in seven vertical profiles (Figure 15), eight soil test-trench exposures (Figure 14) and nine subsurface cores (Figure 14), the Late Quaternary sediments in the terrace system are divided into five major allostratigraphic units, labeled I to V, from oldest to youngest (Figure 14). The five unconformably-bound alluvial stratigraphic units include: Pleistocene channel gravels (Ia) and floodplain alluvium (Ib and Ic) beneath T3, Late Pleistocene channel gravels (IIa and IIb) and floodplain alluvium (IIc) beneath T2, Late Pleistocene floodplain alluvium (III) beneath T2, Late Pleistocene floodplain alluvium (IV) facies, and Late Pleistocene floodplain alluvium (V) overlying Unit IV. The Pleistocene and Late Pleistocene gravels were labeled as subunits of the larger allostratigraphic units (i.e., Ia, IIa, and IIb). The two channel facies (IIa and IIb) of Unit II fill two separate channels that are deeply incised into Cretaceous bedrock (Figure 14). All of the faunal remains uncovered at the Waco Mammoth Site are associated with Unit III (Figure 15). Particle size and soil textural analysis data for several vertical exposures and test trenches are presented in Appendix D.

In addition to vertical profiles, test trench and core exposures, electrical resistivity increases the resolution of the subsurface geometry, providing a continuous view of subsurface features at greater depths than either trenching or coring. (Figure 16). An

inversion of the electrical resistivity data shows a large continuous, highly resistant body of material (approximately 125-466 ohm m) that spans from the southern boundary of the excavation area southward, terminating against bedrock and alluvium of T3 terrace (Figure 16). The continuous body appears to have two channels incised deeper into surrounding, less resistant material (Figure 16). The channel located under the excavation area shows a distinctive body of highly resistant material in the shape of a narrowly incised channel (Figure 16). This subsurface body is consistent with the previously interpreted channel that lies beneath the Phase I mammoth bone bed based on gravels encountered during hand augering and unit excavation.

Unit I

The oldest unit in the study area is Unit I (T3) and is identified in cores MC2 and MC5 (Hilliard, 1997), augers MA1 and MA4 and test trenches 1, 5, 7, and 8 (Figures 12, 14, and 17). Unit I is approximately 6.4 m and 5.0 m thick to the north and south, respectively. Unit I is unconformably underlain by the Cretaceous Austin Chalk Formation (Figure 14). Unit I consists of three dominant facies, including a channel facies (Unit Ia to the north) and two sandy clay to silty clay floodplain facies (Ib, Ic). The channel facies (Ia) consists of well sorted, subrounded to subangular, grain-supported siliceous and carbonatic gravels (~3 mm – 10 mm in diameter), with intermittent sand beds that thicken towards the surface (0.5 m – 1.5 m). The channel facies of Unit I appears to be laterally confined by the limestone bedrock (Figure 14). The sand and gravel deposits (Ia) are conformably overlain by a layer of vertical accretion deposits (Ib) that grade upward into well developed soils. These soils are

Figure 14. Geologic cross section of the Waco Mammoth Site along transect B-B`, showing four major allostratigraphic units and associated facies and the T2/T3 terrace boundary. The geologic cross-section was drafted using vertical exposures, soil test trenches, subsurface cores, and electrical resistivity.

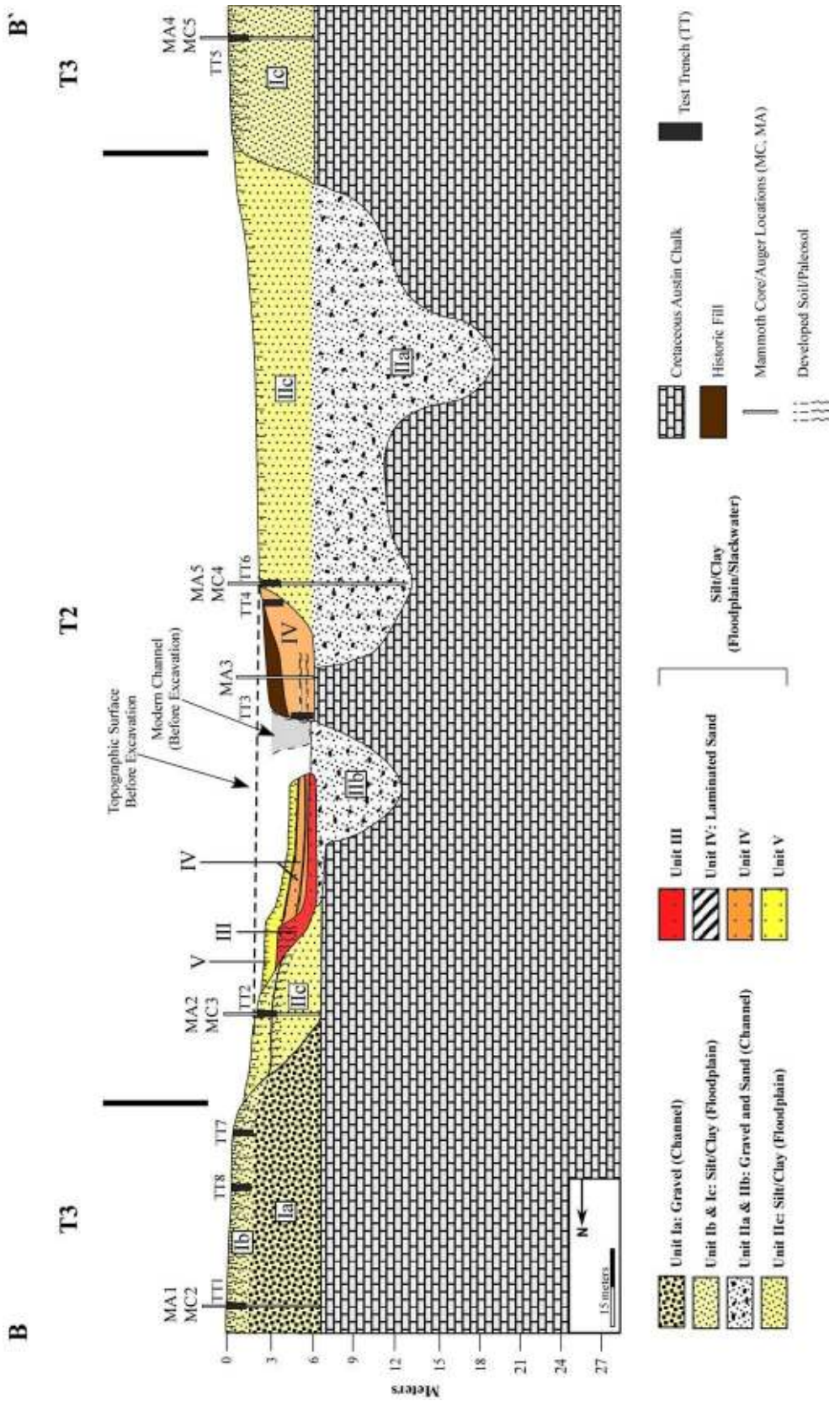
B
B'
T3
T2
T3
MA1
MC2
TT1
TT8
TT7
MA2
MC3
TT2
MA3
TT3
MA5
MC4
TT4
TT6
MA4
MC5
TT5
Topographic Surface
Before Excavation
Modern Channel
(Before Excavation)
Ia
Ib
Ic
IIa
IIb
IIc
III
IV
V
N
15 meters
Meters
0
3
6
9
12
15
18
21
24
27
Unit Ia: Gravel (Channel)
Unit Ib & Ic: Silt/Clay (Floodplain)
Unit IIa & IIb: Gravel and Sand (Channel)
Unit IIc: Silt/Clay (Floodplain)
Unit III
Unit IV: Laminated Sand
Unit IV
Unit V
Silt/Clay
(Floodplain/Slackwater)
Cretaceous Austin Chalk
Historic Fill
Developed Soil/Paleosol
Test Trench (TT)
Mammoth Core/Auger Locations (MC, MA)

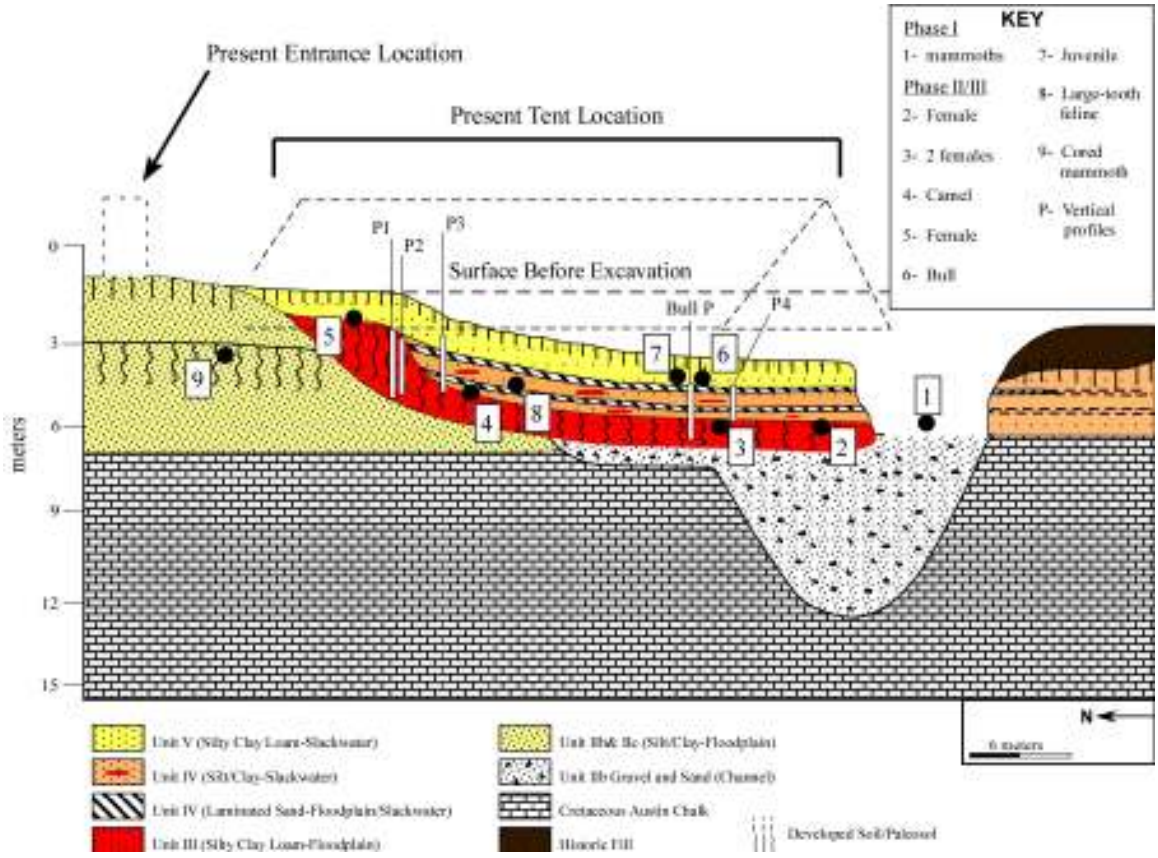

Figure 15. Geologic cross-section of the excavation area showing the spatial distribution of faunal remains in relation to allostratigraphic units and locations of vertical profiles within the Phase II/III excavation area.

Figure 16. Electrical resistivity inversion of (A) Dipole-Dipole/Schlumberger combined array of a transect trending north to south from the south end of the excavation tent to north edge of T3 terrace and (B) Dipole-Dipole array of a transect trending north to south covering the entire excavation area. Resistivity is measured in Ohm meters.

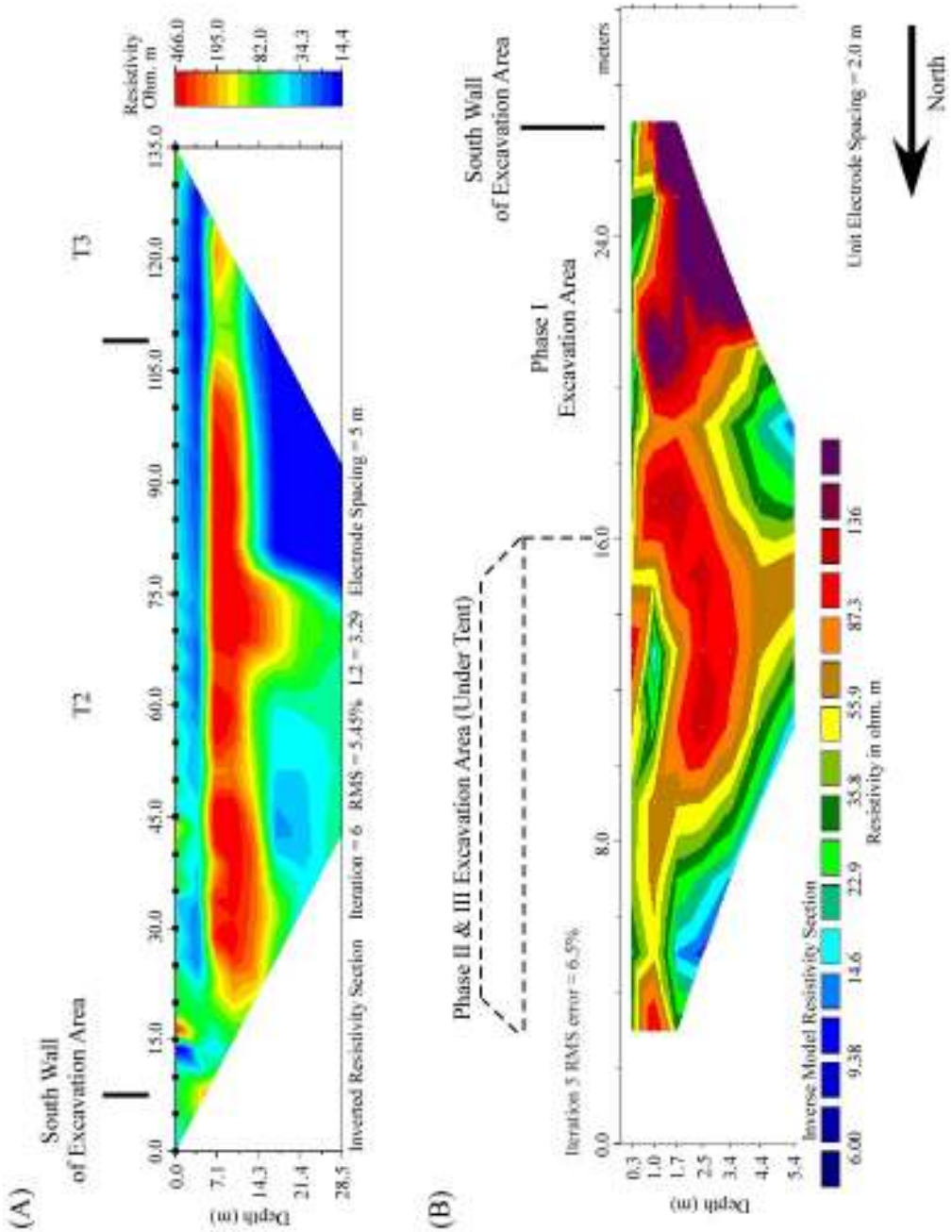
(A)
South Wall
of Excavation Area
T2
T3
Resistivity
Ohm. m
466.0
195.0
82.0
34.3
14.4
0.0
15.0
30.0
45.0
60.0
75.0
90.0
105.0
120.0
135.0
Depth (m)
0.0
7.1
14.3
21.4
28.5
Inverted Resistivity Section Iteration = 6 RMS = 5.45% L2 = 3.29 Electrode Spacing = 5 m
(B)
South Wall
of Excavation Area
Phase I
Excavation Area
Phase II & III Excavation Area (Under Tent)
meters
0.0
8.0
16.0
24.0
Depth (m)
0.3
1.0
1.7
2.5
3.4
4.4
5.4
Iteration 5 RMS error = 6.5%
Inverse Model Resistivity Section
6.00
9.38
14.6
22.9
35.8
55.9
87.3
136
Resistivity in ohm. m
Unit Electrode Spacing = 2.0 m
North

relatively thick (>1.5 m) and siliceous-dominated Alfisols (Bastil series) to the north (Ib) and thick (>2 m) carbonitic Mollisols (Sunev series) to the south (Ic) (Figures 8 and 14).

The Alfisol (Test Trench 1) in Unit Ib contains a thin surface (A) horizon and subsurface Bt1, Bt2, Btss, and Btg horizons (Appendices A and B). The entire soil profile down to the Ck horizon was completely decalcified, showing no reaction to Hydrochloric (HCl) acid. The Bt1 and Bt2 horizons are characterized by the presence of significant accumulation of translocated clay in the form of clay films and clay coats. The Btss horizon is characterized by the presence of clay films and occasional slickensides. The Btg horizon is characterized by the presence of clay argillans and significant gleying from periodic saturation.

Unit Ic, identified in core MC5, auger MC4, and Test Trench 5, consists of relatively thick (~6 m) silty clay floodplain facies unconformably overlying Cretaceous-age Austin Chalk to the south (Figures 14 and 17). Unit Ic grades upward into a well developed Mollisol (Test Trench 5) containing a horizon succession of A, Bw, Bss, Bssk, and Bk grading down into silty clay parent material. The Bss and Bk horizons are characterized by the presence of slickensides and nodules of secondary calcium carbonate, respectively.

Micromorphological analysis of the modern Alfisol (Ib) shows fine-grain matrices expressing various pedogenic features. The Bt horizons show significant amounts of illuviated clay (i.e. grain and pore argillans), abundant Fe oxide accumulation and common Fe/Mn redoximorphic features (Figures 18A and 18B; Appendix E) The Btss horizon shows sepic-plasmic fabric and abundant illuviated clay (Figure 18B; Appendix E). The Mollisol horizons of Unit Ic contain clay and carbonate-rich matrices showing

weak to moderate sepic-plasmic fabric throughout and illuviated clays, especially in the Bssk horizon (Figure 18C; Appendix E). Abundant carbonate nodules are present in the lower horizons (especially the Bssk and Bk horizons), some with septarian shrinkage cracks from drying (Figure 18D; Appendix E). Redoximorphic features (i.e. Fe/Mn nodules and concretions) are common throughout, some present with distinct banding.

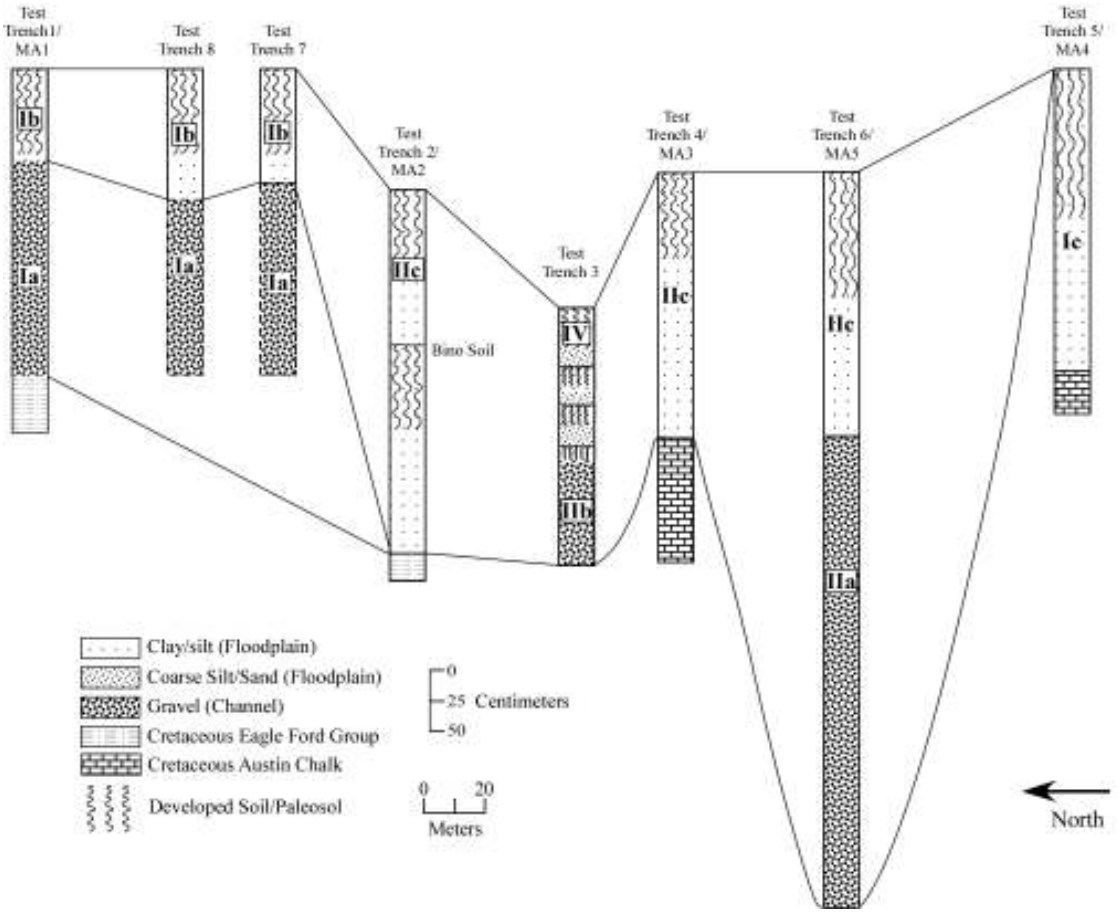

Figure 17. Correlation of soil trench and auger data across the Waco Mammoth Site, but excluding the site itself showing associated allostratigraphic units and facies. Buried soils in Test Trench 3 are discontinuous.

Unit II

Unit II is composed of both channel (IIa and IIb) and floodplain (IIc) facies that unconformably cross cuts Unit I (Figure 14). Unit II is identified in cores MC3 and

MC4, augers MA2, MA3, and MA5, and test trenches 2, 3, 4, and 6 (Figures 12, 14, and 17). The Channel facies of Unit IIa (gravels with interbedded sands in the upper portion) fills a large channel entrenched into Cretaceous Austin Chalk bedrock according to subsurface trenching and electrical resistivity (Figures 14, 16, and 17). This channel appears to be confined within steeply dipping bedrock slopes, likely an active meander of the ancestral Bosque River (Figure 14). The gravels of IIa are fine (3-10 mm, limitations of the auger flight) grain-supported, well sorted, subrounded to subangular carbonatic gravels with intermittent lenses of coarser gravels (10-20 mm). A second channel facies (IIb) was identified in Test Trench 3, with through hand excavation into the subsurface beneath the Phase II excavation area, and, with electrical resistivity (Figures 14, 15, 16, and 17). This channel facies (IIb) fills a relatively deeply entrenched channel that lies beneath the Phase I bone bed surface and thins to the north, where it underlies the Phase II bone bed surface (Figures 14 and 15). This channel is also contained within Cretaceous bedrock. The filled channel appears to have been a low order tributary of, and a relatively short distance from, the confluence of the larger trunk channel of the ancestral Bosque River.

The floodplain facies (IIc) to the north consists of thick (5.5 m thick in the south and 5.8 m thick in the north), horizontally bedded overbank silts and clays (Figures 14). Here, the vertical accretion deposits of Unit IIc are unconformably inset to Units Ia and Ib. Exposed in Test Trench 2 (north of the excavation site), a buried soil (Bino soil) is present (Figures 14 and 17), overlain by the carbonate-rich surface Mollisol. The Bino paleosol consists of two clay loam, pale reddish brown Bk horizons with common nodules and filaments of secondary calcium carbonate.

Figure 18. Photomicrographs of thin section samples, including: (A) Asepic fabric and Fe/Mn concentration from TT1 Bt2 horizon (Unit Ib); (B) Sepic plasmic and abundant illuviated clay in the form of linings and grain argillans from TT1 Btss horizon (Unit Ib); (C) Clay argillans around grains from TT5 Bssk horizon (Unit Ic); (D) Large pedogenic carbonate nodule with distinct septarian shrinkage cracks from TT5 Bk horizon (Unit Ic); (E) Large multi-generational pedogenic nodule with distinct shrinkage cracks from TT2 Bk1 horizon (Unit IIc); (F) Concentrically banded Fe/Mn concretion from TT2 Bk2 horizon (Unit IIc); (G) Pedogenic carbonate disseminated throughout matrix and infilling biopores (brown streaks) from horizon TT2 Bk1b (Bino soil) (Unit IIc); (H) biopore infilled with detrital matrix material from TT2 Bk2b (Bino soil) horizon (Unit IIc);

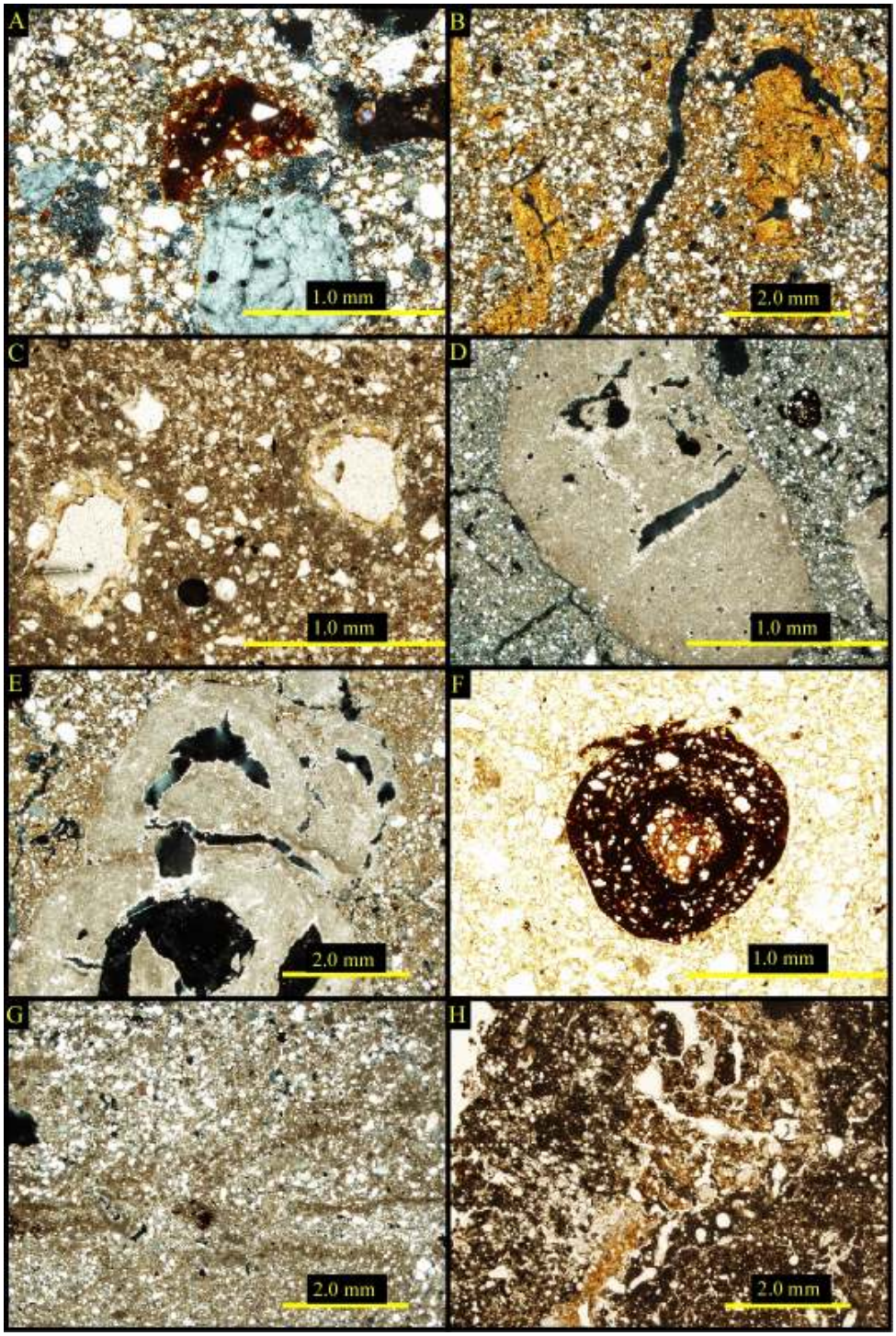
A
1.0 mm
B
2.0 mm
C
1.0 mm
D
1.0 mm
E
2.0 mm
F
1.0 mm
G
2.0 mm
H
2.0 mm

In thin section, the upper Bk horizon (Bkb1) of the Bino paleosol consists of a clay loam, carbonate-rich matrix, with abundant masses of pedogenic calcium carbonate present throughout. The lower Bk horizon (Bkb2) consists of a carbonate-rich, clay matrix with abundant embedded silt-size quartz grains. Pedogenic carbonate disseminated throughout the soil matrix and biopores infilled with coarser grain detrital material are also present in the Bk2b horizon (Figures 18 E, 18G, and 18H; Appendix E).

The Bino paleosol appears to be conformably underlying the modern surface Mollisol in Test Trench 2 (Figures 14 and 15). In the north, the suface of Unit IIc is weathered to a moderately developed carbonate-rich Mollisol (Test Trench 2). This surface soil consists of a silty-clay to clay loam, pale yellowish brown to yellowish brown, A-Bk horizon sequence. The Bk horizons (Test Trench 2) are characterized by abundant nodules and filaments of secondary calcium carbonate. The Mollisol to the south (Test Trench 4) of the site consists of a loamy clay, brown to light brown, A-Bk-BC horizon sequence. The Bk horizons (Test Trench 4) are characterized by the presence of nodules and filaments of secondary calcium carbonate.

Petrographically, the surface Mollisol of Unit IIc (Test Trench 2) consists of a clay matrix with abundant very fine to fine silt-size embedded quartz grains (Figure 18E, Appendix E). The A, Bk1 and Bk2 horizons exhibit distinct mosepic to bimasepic plasmic fabric. The Bk horizons show abundant pedogenic carbonate nodules, many with substantial septarian shrinkage cracks and development of secondary sparry calcite (Figure 18E; Appendix E). The Bk horizons also contain clay argillans, lining root pores and coating larger mineral particles as grain argillans. Biopores (i.e., root and soil pores)

and redoximorphic features (i.e., iron masses, banded Fe/Mn concretions, iron pore linings) commonly occur in all horizons of the surface soil (Figures 18E and 18F; Appendix E).

Unit III

Unit III consists of loamy, reddish-yellow floodplain deposits that truncate Unit IIc, are truncated by Unit IV, and are unconformably bound at their top by Unit V (Figures 14 and 15). Unit III is completely exposed in Profile 1 and Profile 2 (Figure 15), just north of the bull mammoth within the current excavation area (Figures 10 and 14). A well developed paleosol, the Boncap soil, has formed through Unit III. The surface A horizon and possibly upper B horizon (upper portion of Unit III) of the Boncap soil appear to have been erosionally truncated (Figures 14 and 15). The Boncap paleosol consists of a clayey, reddish yellow to gleyed Bkgb1-Bkgb2-Bkssgb horizon sequence. The Bkg horizons are characterized by common nodules and filaments of secondary calcium carbonate, abundant carbonate rhizoliths and iron depletions. The Bkssg horizon is characterized by common nodules and filaments of secondary calcium carbonate, substantial gleying and occasional pedogenic slickensides.

Thin section analysis of the Boncap paleosol reveals a fine-grained, calcareous clay matrix with abundant and embedded very fine to fine silt-size quartz grains. The Bkg1b and Bkg2b horizons contain larger (coarse silt to sand) embedded quartz grains, some well rounded. Few pedogenic carbonate nodules are present with common septarian shrinkage cracks in both the Bkg1b and Bkssgb horizons. Illuviated clay features (i.e., grain and pore argillans), potential sepic plasmic fabric, and Fe/Mn nodules and pore linings commonly occur in the Bkg1b and Bkg2b horizons (Figures 19A, 19B, and 19C;

Appendix E). The Bkssgb horizon contains a possible mosepic plasmic fabric, but is generally masked by significant calcium carbonate staining within the matrix (Figure

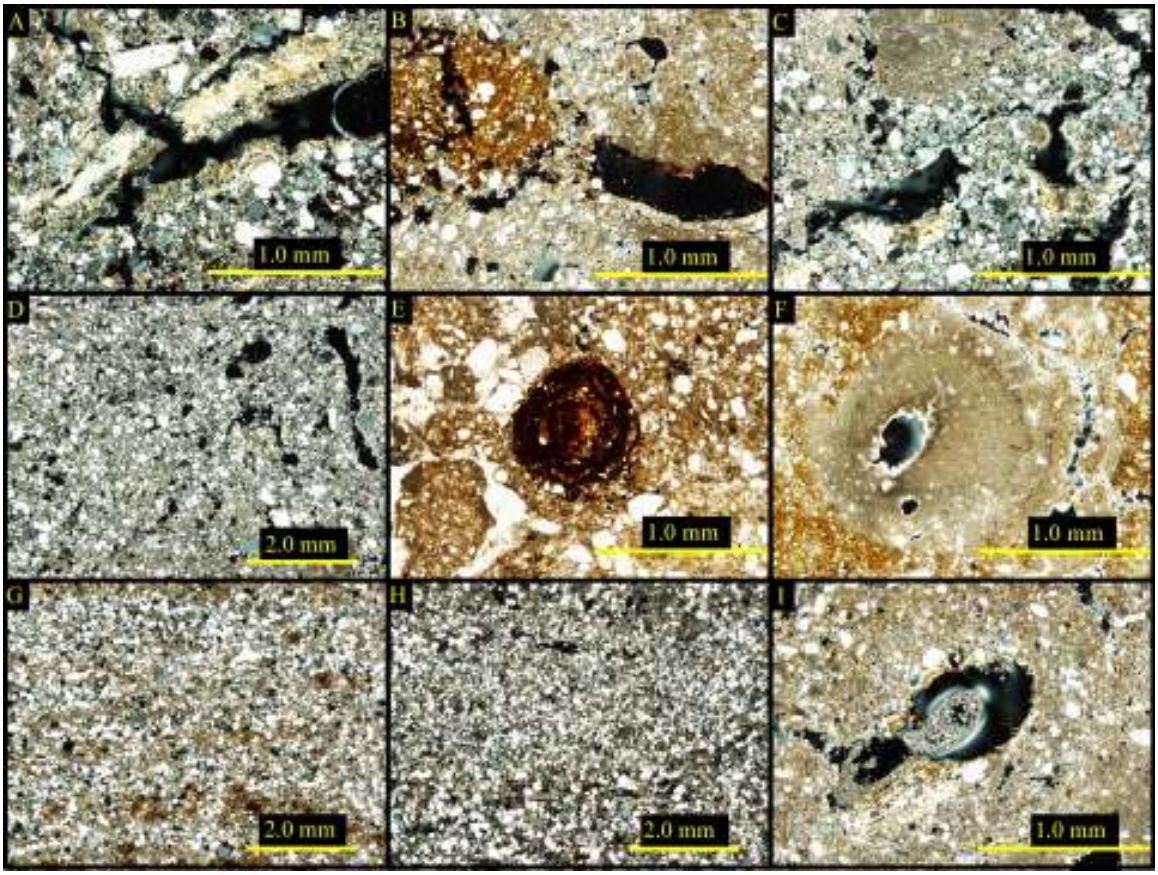

Figure 19. Photomicrographs from soil horizons showing pedogenic features: (A) Root pore lined by lluviated clay with possible sepic plasmic fabric from Bkg1b horizon of the Boncap soil of Profile 1 (Unit III); (B) Fe/Mn pore lining and concentration from Bkg1b horizon of the Boncap soil of Profile 1 (Unit III); (C) Pedogenic carbonate formation and translocated clays from Bkg2b horizon of the Boncap soil of Profile 1 (Unit III); (D) Fine-grained clay soil matrix with embedded quartz grains Bkssgb of the Boncap soil of Profile 1(Unit III); (E) Concentrically banded Fe/Mn concretion from lower silty clay sediments of the Bull Profile (Unit IV); (F) Pedogenic carbonate nodule in lower silty clay sediments of Unit IV; (G) Fine distinct laminations in upper laminated bed of the Bull Profile (Unit IV); (H) Coarse silt to very fine sand matrix of TT3 Cb2 horizon correlated to upper laminated bed of the Bull Profile (Unit IV); (I) Thin illuviated clay argillans lining a root pore in Bk1 horizon of Profile 1 (Unit V).

19D; Appendix E). The Bkg1b, Bkg2b and Bkssgb horizons also contain abundant biopores, some containing Fe coatings (Figures 19A, 19B, 19C, and 19D; Appendix E).

Unit IV

Unit IV unconformably overlies and truncates Unit III and unconformably underlies Unit V (Figures 14 and 15). Unit IV is a relatively thick (~3 m) unit exposed in Profile 3, Profile 4, and the Bull Profile within the excavation area (Figures 10 and 15). This unit consists of four layers composed of carbonate-rich silty clay and fine sand slackwater deposits likely derived from the ancestral Bosque River, based on the carbonatic (Bosque-like) lithology of the sediments and the tributary's proximity to the trunk stream (Figure 14).

Unit IV consists of horizontally bedded, carbonate-rich, yellowish-red clay and fine silt (1st and 3rd layer from bottom to top), and finely laminated coarse silt to very fine sand (2nd and 4th layer from bottom to top) (Figure 14). Erosion of sediments is evidenced by the presence of lensoidal deposits of material from Unit III stratum dispersed throughout the lowermost layer (1st layer) of Unit IV (Figures 14 and 15). The lower laminated sand bed (2nd layer) consists of very finely laminated coarse silt- to very fine-grain quartz sand (Figures 14 and 15), dipping 7 degrees to the south. The lower sand appears to be the associated ground surface for the unidentified large-tooth feline (Figures 14, 15). The silty clay sediments of the third layer of Unit IV (between the lower and upper sand) contain pedogenic features eroded and transported from Unit III as colluvium during erosional events. Remnants of the detrital pedogenic features include pedogenic calcium carbonate nodules and filaments and common Fe depletions, which are confined to the Boncap paleosol of Unit III. The upper sand bed (4th layer) consists of

very finely laminated very fine quartz sand, dipping 10 degrees to the south, and contains the skeletal remains of the elder Bull mammoth and a young adolescent female mammoth (Figures 14 and 15).

The slackwater facies (IV) was exposed in the south wall of the excavation area in Test Trench 3 (TT3) (Figure 14). The vertical profile of TT3 consists of a series of weakly developed Bw-C horizon sequences unconformably overlying Cretaceous bedrock (Figure 14). Two stacked, finely laminated sandy horizons (Cb1/Cb2) are present in TT3, which show macroscopic features (i.e., fine laminations and grain size) that correlate to the laminations and grain size of the upper sand bed of Unit IV within the excavation area (Figure 14).

Micromorphologically, the silty clay horizons below the lower sand bed and between the lower and upper sand beds of Unit IV, exposed in the Bull Profile (Figures 10 and 15), contains a fine, carbonate-rich clay matrices with abundant embedded, fine silt-size quartz grains. Abundant pedogenic carbonate nodules and soft masses are present in the two layers (Figure 19G; Appendix E). Concentrically banded iron/manganese concretions (redoximorphic features) are present in the horizon beneath the lower sand bed (Figure 19F; Appendix E). Abundant biopores (i.e., root pores and wasp burrows), some partially infilled with detrital material, also occur in the two silty clay layers below and above the lower sand bed.

Six optically stimulated luminescence (OSL) ages, four obtained in 2004 and two in 2006, were from sandy sediments within the floodplain deposits of Unit IV just below and burying the bull mammoth (Figure 20; Table 1). These ages range from 52.1 ± 4.2 ka yr B.P. (WOSL02a) to 73.4 ± 6.8 ka B.P. (WMS03-04) (Figure 20; Table 1). The

lower sand bed yielded OSL ages from 2004 and 2006 of 62.1 ± 6.0 ka yr B.P. (WMS01-04) and five ages ranging from 52.1 ± 6.8 to 64.1 ± 5.6 ka B.P (WMSL-03a), respectively (Figure 20; Table 1). The upper sand bed yielded OSL ages of 64.6 ± 6.2 ka yr B.P. (WMS02-04) and two ages of 52.6 ± 4.2 ka B.P. and 53.3 ± 4.6 ka B.P. (WOSL02a), respectively (Figure 19; Table 1). Two OSL ages of 58.1 ± 6.0 ka yr B.P. and 73.4 ± 6.8 ka B.P. in 2004 were obtained from sandy sediments (upper and lower sand beds) within unit IV, below the bull mammoth (Figure 20; Table 1). Additionally, two optically stimulated luminescence (OSL) ages were obtained in 2006 from a sandy sediment horizon (C1b3 horizon) located ~210 cm below the surface in Test Trench 3 (Figure 20; Table 1). The two ages from this horizon yielded ages of 67.9 ± 5.9 ka B.P. and 70.6 ± 5.9 ka B.P. (WOSL01a), respectively.

Unit V

Unit V is exposed in Profiles 1, 2, and 3 and consists of a silty clay floodplain/slackwater facies (Figures 10, 14, and 15). Unit V unconformably overlies Unit III and Unit IV, and is inset to Unit II (Figures 14 and 15). The exact lateral extent of Unit V is not known because a portion of Unit V was removed during earlier excavations, but it is assumed that it is inset to and confined by Unit II to the north and south (Figures 14 and 15). Unit V grades upward into the modern surface soil (Figures 14 and 15). Only the subsurface horizons are present in the profile exposures due to soil removal during prior excavations. The soil consists of a Bk1-Bk2 horizon sequence that is characterized by the presence of a buff-colored (very pale brown) clayey matrix with abundant nodules and filaments of secondary calcium carbonate. Micromorphologically, both Bk horizons contain a fine-grained, carbonate-rich matrix with weakly developed

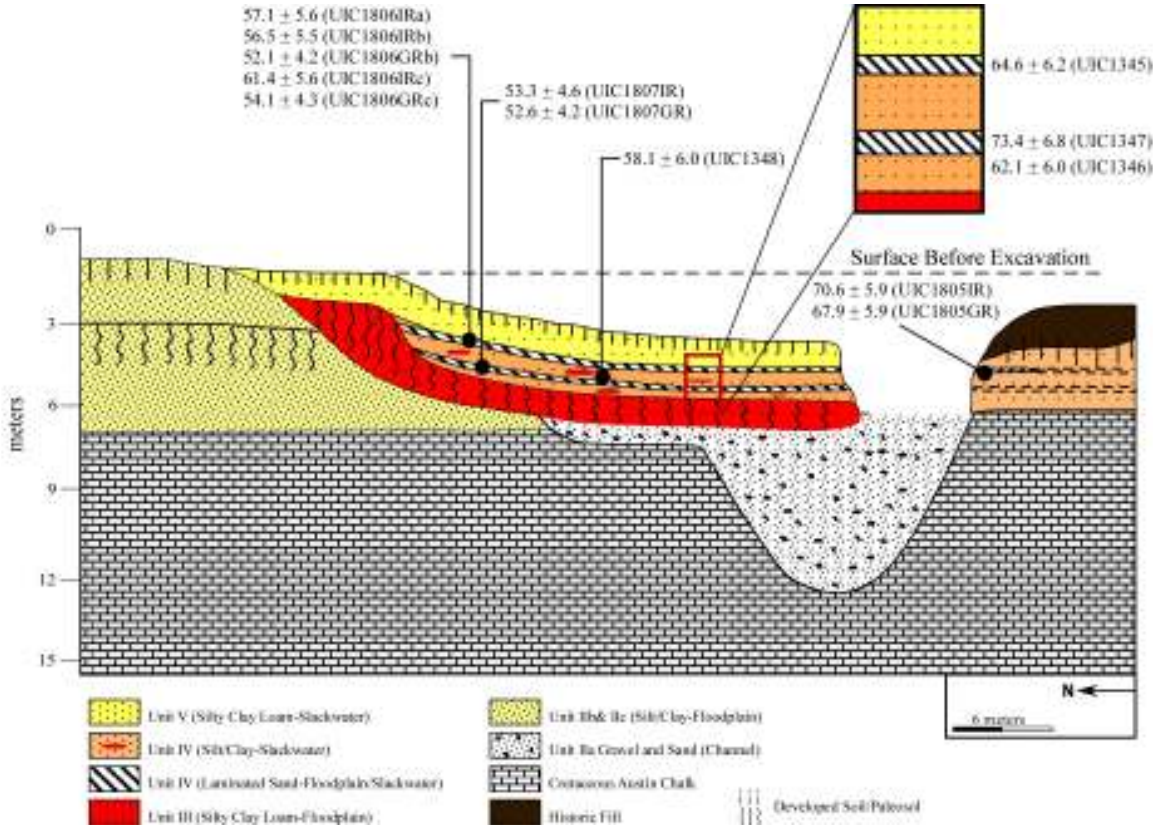

Figure 20. Geologic cross section of the Waco Mammoth Site within the excavation area, showing locations of optically stimulated luminescence ages within the excavation area.

Table 1. Optically stimulated luminescence (OSL) ages on fine-grained polymineral extracts from fluvial sediments from the Waco Mammoth Site.

Field#	Laboratory #	Equivalent dose	U (ppm)[c]	Th (ppm)[c]	K_2O (%)[d]	Dose rate (Gy/ka)	OSL age (ka)[e]
2004							
WM01-04	UIC1346[a]	153.73 ± 0.56a	3.2 ± 0.4b	5.6 ± 1.0c	0.76 ± 0.02	2.48 ± 0.10	62.1 ± 6.0
WM02-04	UIC1345[a]	151.21 ± 0.37a	3.0 ± 0.4b	5.9 ± 1.0c	0.79 ± 0.02	2.34 ± 0.09	64.6 ± 6.2
WM03-04	UIC1347[a]	161.48 ± 0.40a	2.6 ± 0.3b	5.1 ± 0.8c	0.82 ± 0.02	2.20 ± 0.09	73.4 ± 6.8
WM04-04	UIC1348[a]	144.78 ± 0.29a	2.5 ± 0.4b	8.9 ± 1.3c	0.73 ± 0.02	2.49 ± 0.10	58.1 ± 6.0
2006							
WOSL-01a	UIC1805IR[b]	153.73 ± 0.56	1.8 ± 0.1c	4.9 ± 0.1d	0.83 ± 0.02	1.85 ± 0.08	70.6 ± 5.9
WOSL-01a	UIC1805GR[b]	117.75 ± 0.56	1.8 ± 0.1c	4.9 ± 0.1d	0.83 ± 0.02	1.73 ± 0.07	67.9 ± 5.9
WOSL-02a	UIC1807IR	140.43 ± 6.30	2.0 ± 0.1c	12.4 ± 0.1d	0.76 ± 0.02	2.63 ± 0.11	53.3 ± 4.6
WOSL-02a	UIC1807GR	123.90 ± 2.50	2.0 ± 0.1c	12.4 ± 0.1d	0.76 ± 0.02	2.51 ± 0.10	52.6 ± 4.2
WOSL-03a	UIC1806IR[a]	144.43 ± 0.52	1.7 ± 0.1c	9.3 ± 0.1d	0.085 ± 0.02	2.25 ± 0.09	57.1 ± 5.6
WOSL-03a	UIC1806IR[b]	142.84 ± 0.40	1.7 ± 0.1c	9.3 ± 0.1d	0.085 ± 0.02	2.23 ± 0.09	56.5 ± 5.5
WOSL-03a	UIC1806GR[b]	108.93 ± 1.00	1.7 ± 0.1c	9.3 ± 0.1d	0.085 ± 0.02	2.09 ± 0.09	52.1 ± 4.2
WOSL-03a	UIC1806IR[c]	154.72 ± 0.40	1.7 ± 0.1c	9.3 ± 0.1d	0.085 ± 0.02	2.52 ± 0.10	64.1 ± 5.6
WOSL-03a	UIC1806GR[c]	112.66 ± 0.51	1.7 ± 0.1c	9.3 ± 0.1d	0.085 ± 0.02	2.08 ± 0.09	54.1 ± 4.3

a Multiple aliquot additive dose method from Singhvi et al.(1982) and Forman and Pierson (2002) on 4-11 µm polymineral fraction.
b The GR designation indicates excitation by green light (514 ± 20 nm) and the IR designation indicates excitation by infrared wavelengths (880 ± 80 nm with the equivalent dose determined by the multiple aliquot regenerative dose technique (Jain et al. 2003).
c U, and Th content determined by thick-source alpha counting.
d U, Th and K20 assayed by ICP-MS at Activation Laboratories, Ontario, Canada.
e Ages included a cosmic ray dose rate of 16 mGray/ka from calculations of Prescott and Hutton, 1994, an assumed burial moisture content of 20 ± 5 %, and a measured alpha efficiency factor (a value) as defined by Aitken and Bowman (1975).
All errors are at one sigma. Analyses by the Luminescence Dating Research Laboratory, University of Illinois at Chicago.

sepic plasmic fabric. Abundant pedogenic carbonate masses and hard nodules are present in both horizons, with significant septarian shrinkage cracks and the formation of secondary sparry calcite. Common clay argillans are present in both horizons, lining root pores and possible small animal burrows (Figure 19I; Appendix E).

Optically Stimulated Luminescence Ages

Variability among the 13 OSL ages (4 from 2004 and 9 from 2006) from the Waco Mammoth Site sediments was analyzed by constructing a probability density distribution, completed by the Luminescence Dating Research Laboratory, University of Illinois at Chicago. The distribution of all the samples was plotted, indicating that the ages represent one age population, according to central tendency statistics and most probable age spread (Figure 21). The unweighted mean average for the age population is 60.0 ± 2.5 ka yr B.P. (at 1-sigma, 68% confidence) as shown on the distribution plot (Figure 21). Thus, at 2-sigma error (95% confidence), the sediments of Unit IV would have been deposited sometime between ca. 55 and 65 ka yr B.P. The two ages from the Unit IV sediments in the south wall (TT3) of the excavation site (UIC1805IR and UIC1805GR) are 70.6 ± 5.9 and 67.9 ± 5.9 ka yr B.P. at 1-sigma error and at 2 sigma yield an age range of 58.8-82.4 and 56.1-79.7 ka yr B.P, respectively, which does overlap with the Unit IV strata ages. Statistically, the Unit IV sediment ages could be penecontemporaneous to as much as 20 ka yr younger than the south wall (TT3 of Unit IIc) sediments based on the estimated OSL ages. Moreover, at 1-sigma error the ages from within Phase II and III excavation areas and from the sandy sediments of Test Trench 3 (south wall of Phase I excavation area) are statistically distinct, but at 2-sigma error they overlap, indicating that these sediments are penecontemporaneous to ca. 12 ka yr difference (twice the error of the 70.6 and 67.9 ka yr B.P. ages).

Stable Isotope Analysis

Carbon and oxygen isotopic compositions were measured ($\delta^{13}C_{PDB}$ and $\delta^{18}O_{PDB,}$ respectively) from pedogenic carbonate nodules of 21 soil horizons exposed in vertical

profiles and test trenches (Table 2). For this study, the three vertical profiles (Profile 1, Profile 2, and Profile 3) and one test trench (Test Trench 2) with the most complete data sets are presented in Figure 22. All 21 isotope samples were used for environmental reconstruction. Isotopic ratios recorded for carbon and oxygen range from -0.7‰ to 9.2‰ $\delta^{13}C_{PDB}$ and -3.2‰ to -4.6‰ $\delta^{18}O_{PDB}$, respectively, and average -4.48‰ and 3.80‰, respectively (Table 2). Given the wide range of $\delta^{13}C$ values, neither a temporal nor stratigraphic relationship was found within the stratigraphic section.

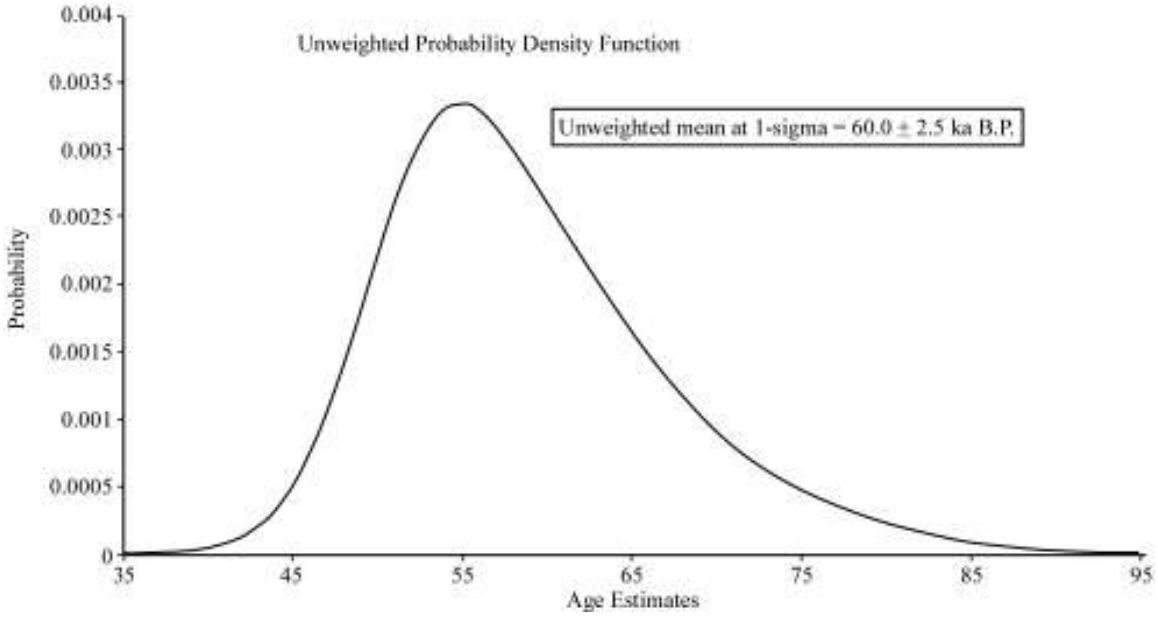

Figure 21. Probability density distribution analysis plot of all (2004 and 2006) ages obtained from Unit IV sandy sediments performed by the Luminescence Dating Research Laboratory, University of Illinois at Chicago. The plot indicates that all the ages represent one population and shows the populations central Tendency and associated most probably age spread.

$\delta^{13}C$ values of soil organic matter (SOM) were estimated from the $\delta^{13}C$ values of pedogenic carbonate nodules, using a temperature constant of 20°C (Nordt et al. 1998). The SOM $\delta^{13}C$ values are presented in Table 2. Following a linear mixing model (Nordt

Table 2. Carbon and oxygen isotope values from pedogenic carbonate samples obtained from vertical profiles and test trenches and converted to $\delta^{13}C$ values of soil organic matter (SOM) using a temperature constant of 20°C (Nordt et al., 1998), showing estimated mean annual July temperature in °C (Nordt et al., 2007), and showing C4 and C3 biomass percentages (Nordt et al., 2002).

Profile/ Horizon	Unit	$\delta^{13}C$ PDB	$\delta^{18}O$ PDB	Depth cm	$\delta^{13}C$ SOM at 20ºC	$\delta^{13}C$ ºC July Est.	Soil Biomass % C_4	Soil Biomass % C_3
P1Bk1	V	-1.7	-3.8	-10	-15.57		74	26
P1Bk2	V	-1.7	-3.8	-45	-15.57		74	26
P1Bkg1b	III	-2.0	-4.1	-83	-15.87	26.7	72	28
P1Bkg2b	III	-9.2	-3.9	-122	-23.00		21	79
P1Bkssgb	III	-7.4	-4.0	-182	-21.22		34	66
P2Bk1	V	-3.1	-3.7	-14	-16.96		65	35
P2Bk2	V	-2.8	-3.7	-56	-16.66		67	33
P2Bkssg	III	-3.9	-3.5	-201	-17.75		59	41
P3Bkg1b	IV	-5.5	-3.7	-70	-19.34		48	52
P3Bkg2b	IV	-7.5	-3.4	-145	-21.32		33	67
P3Bkg3b	IV	-5.4	-3.2	-230	-19.24		48	52
P4Bkgb	III	-8.8	-3.7	-230	-22.61		24	76
TT2Bk1	IIc	-2.9	-3.7	-36	-16.76		66	34
TT2Bk2	IIc	-2.7	-3.8	-77	-16.56		67	33
TT2Bk3	IIc	-6.1	-4.6	-148	-19.93		43	57
TT2Bk1b	IIc	-6.0	-3.8	-262	-19.83		44	56
TT2Bk2b	IIc	-5.5	-3.8	-295	-19.34		48	52
TT5Bssk	Ic	-3.7	-3.8	-120	-17.55		60	40
TT5Bk	Ic	-5.2	-3.8	-178	-19.04		50	50
TT6Bk1	IIc	-0.7	-4.1	-43	-14.58		82	18
TT6Bk2	IIc	-2.2	-4.0	-82	-16.07		71	29
Average:		-4.5	-3.8					

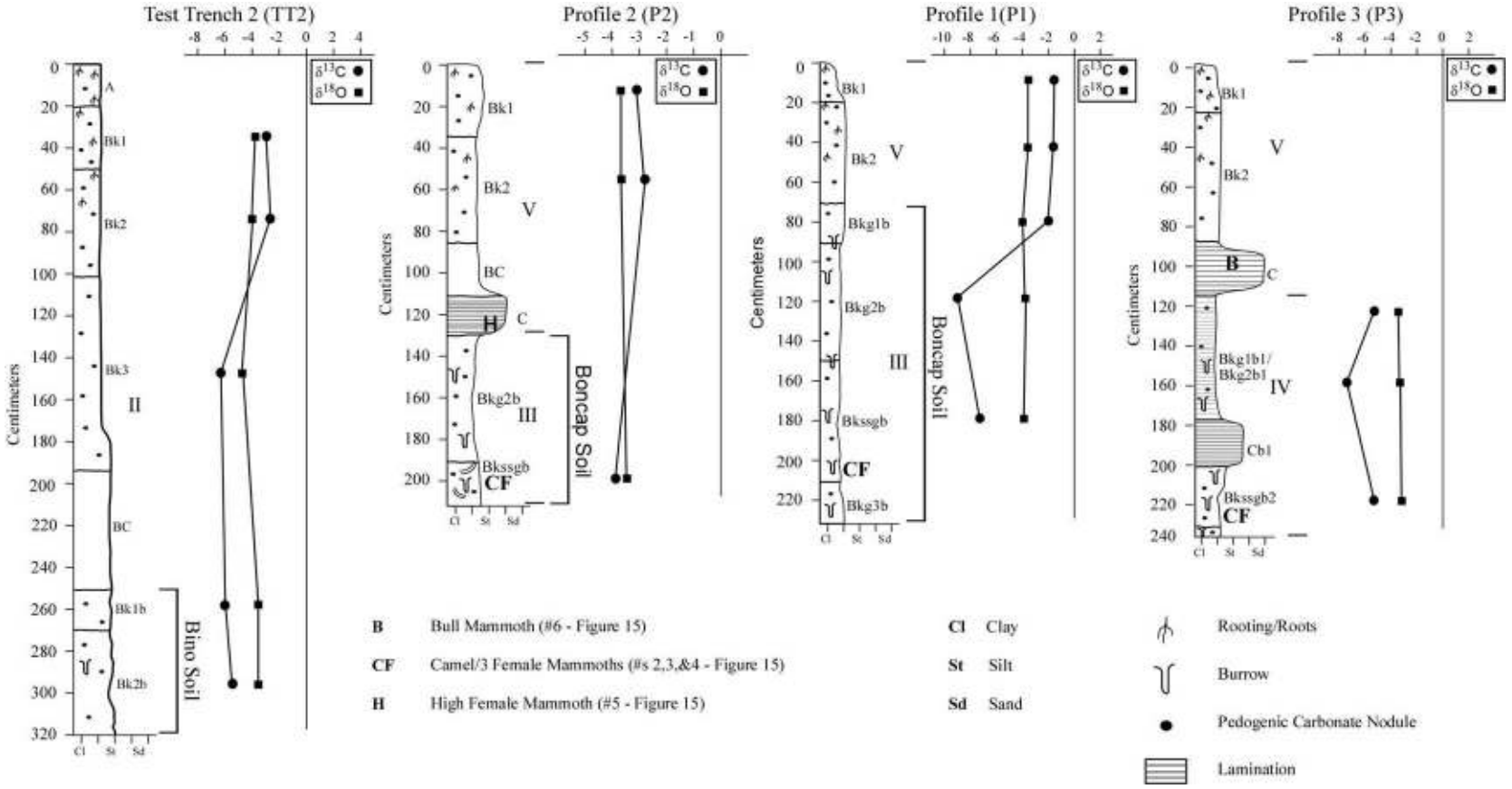

Figure 22. $\delta^{13}C$ and $\delta^{18}O$ values of pedogenic carbonate nodules from soil profiles selected for paleoenvironmental analysis.

et al., 2002), SOM concentrations were used to calculate the relative contributions to C_4 (warm season grasses) and C_3 (cool season grasses) biomass from each carbon isotope sample (Table 2). The upper two horizons of Unit V and first horizon of the Boncap soil in Unit III of Profile 1 contain SOM that is predominantly from C_4 vegetation, whereas the lower two horizons of the Boncap soil contain SOM dominated by C_3 vegetation (Figure 22; Table 2). Profile 2 (P2),Test Trench 2 (TT2; Unit IIc), Test Trench 5 (TT5; Unit Ic), and Test Trench 6 (TT6; Unit IIc) all appear to have SOM that was derived from an ecosystem dominated by C_4 vegetation. Profile 3 (P3; Unit IV) contains SOM that is predominantly C_3-contributed (Table 2).

The $\delta^{13}C$ value from the upper buried horizon (Bkg1b) of the Boncap soil of Profile 1 (P1; Unit III) was used to calculate a temperature estimate during soil formation. The Bkg1b horizon of the Boncap soil was used due to its spatial relationship to the mammoth strata and its speculated stratigraphic position to the original surface of Unit III (before truncation). Using the Nordt et al. (2007) linear equation, a mean monthly July temperature estimate of 26.7 °C was calculated (Table 2). $\delta^{18}O$ values estimated from pedogenic carbonate averaged 3.8‰, which is similar to the $\delta^{18}O$ average of modern meteoric waters for Central Texas and therefore, the estimated $\delta^{18}O$ values from pedogenic carbonate were assumed to have reached equilibrium with the modern waters. Due to the $\delta^{18}O$ values having been "reset" to modern meteoric waters, a temperature estimate (Dworkin et al., 2005) was not calculated.

CHAPTER FIVE

Discussion

Stratigraphic Interpretation

Subsurface exposures associated with the Waco Mammoth Site represent multiple facies contained within four allostratigraphic units (Figure 14). These allostratigraphic units record the geologic history of the Waco Mammoth Site, spanning a large portion of the Late Quaternary. The elevation of T3, in relation to the T2 and T1 terraces and modern floodplain, demonstrates that it is the oldest terrace within the existing terrace hierarchy, and according to OSL ages was formed sometime prior to 60.0 ± 5.0 ka B.P. (Figures 6, 7, 12, and 19). Initially, a paired alluvial terrace (T3) was formed, constructed from siliceous gravels (Ia) overlain by fine-grained overbank deposits (Ib) to the north and fine-grained, carbonate-rich overbank deposits (Ic) to the south. The siliceous deposits to the north are consistent with the characteristics of the Brazos River (Flawn and Burkett,1965; Hilliard, 1997). The carbonate-rich sediments of the southern portion of T3 terrace suggest they were sourced from the carbonate-alluvium-rich Bosque River (Flawn and Burket, 1965; Hilliard, 1997).

Sometime after the formation of T3, a period of channel widening and incision took place (IIa) downcutting through the T3 terrace valley surface. The channel continued to downcut into the underlying Cretaceous bedrock, before migrating northward across the bedrock surface where it formed a narrow, deeply entrenched channel (Figure 14). Simultaneously, a second, smaller (likely a low-order tributary of the larger incised channel) channel was formed, downcutting into the Cretaceous bedrock

bench north of the Unit IIa channel (Figure 14). Infilling of the main channel (IIa) and floodplain deposition (IIc) by the trunk stream and low order tributary (IIb) through time, completely filled the entrenched valley and constructed the T2 terrace surface. The main channel was completely infilled by sand and gravel (IIa), followed by the partial infilling of the low order tributary (IIb). The low-order tributary remained active, continuing to deposit fine-grained, overbank sediments of Unit III. Some time after Unit III was deposited the low order tributary became a location of slackwater deposition (Unit IV). The clay-rich slackwater sediments and very fine-grained, laminated sands of Unit IV were deposited within the channel and adjacent floodplain, mixing with the sediments derived periodically from erosion of Unit III (Figures 14 and 15). Preceding and during the initial deposition of slackwater deposits, the tributary was inhabited by a variety of fauna, including Columbian mammoths (*Mammuthus columbi*), North American Camels (*Camelops hesternus*), and large-tooth felines.

The bones of 18 semi- to fully articulated Columbian mammoths and a camel are/were situated on of erosional surface of Unit III, having been buried by the sediments of Unit IV (Figures 14 and 15). As the animals died and/or following their deaths, another period of slackwater deposition (IV) occurred, burying them. These slackwater deposits consist of silty clay sediments interbedded with thin (avg. 10-20 cm thick) finely laminated beds of coarse silt to fine sand (Figure 15). These finely laminated beds appear to be slackwater deposits from high-energy flood events from the trunk stream of the ancestral Bosque River to the south. The presence of remains from an unidentified large-tooth feline in the silty clay sediments of Unit IV (Figure 15) suggests that the surfaces of Unit IV were intermittingly exposed, allowing occupation by fauna. However, the feline

tooth does not appear to be spatially or temporally associated with any other fauna within the excavation area (Figure 15). The remains of a bull mammoth (6), small juvenile (7) within Unit IV, and upper female (5) on Unit III surface and buried by Unit IV, which is traceable southward into the south wall (Test Trench 3) of the excavation area (Figures 14 and 15). These remains appear to represent the last mammoth habitation at the Waco Mammoth Site (Figure 15). These three mammoths (Figure 15; 5, 6, and 7) appear to have been buried by silty clay sediments (V) that over time completely filled the tributary valley. Unit V was pedogenically altered, forming a surface soil and the modern geomorphic surface of the T2 valley, before being partially unearthed during the initial excavation phases (Figure 14).

The depositional history of the sediments associated with the Waco mammoths uncovered during Phase II and III excavations is documented by a series of slackwater depositional events captured in Units IV and V (Figures 14 and 15). These deposits over time formed a well-stratified column of sediments, separating a number of the mammoths and other fauna (i.e. camel, large-tooth feline) (Figure 15). There is no sedimentological or stratigraphic evidence for an episodic event associated with the deaths of the Waco mammoths, rather, the sediments are stratified in a number of unconformable (Unit III/Unit IV) and conformable layers (Unit IV/Unit V) (Figures 14 and 15). For example, the sediments exhibit characteristics of a slackwater environment based on the presence of a succession of very fine-grained (i.e. clay and silt), carbonate-rich sediments deposited horizontally across the tributary channel. Sedimentological and stratigraphic evidence suggests several low-energy depositional events that buried the mammoths over time, not from a single episodic event. Furthermore, given that Unit IV consists of a

series of conformable beds with no evidence of surface stability and soil formation, it is therefore speculated that the three events happened within a relatively brief time frame.

Micromorphologic Interpretation

Thin-section samples were taken from the majority of soil test trenches and vertical profiles within the excavation area. Micromorphological analysis of the Waco Mammoth Site was used to identify pedogenic features present throughout each soil profile and to determine weathering factors associated with soil development. In addition to micromorphological interpretation and correlation of soils and paleosols, visible sedimentary structures were identified, when present, and used to correlate sedimentary beds and units within the alluvium of T3 and T2 terraces.

The presence of abundant translocated clay (i.e., grain and root pore argillans) and common Fe and Fe/Mn oxide coatings throughout the Test Trench 1 (TT1) Alfisol (Ib), suggests moderately to well-drained conditions (Figure 18A and 18B). The Fe and Fe/Mn oxide concentrations throughout the soil profile suggest periods of soil saturation, likely due to periodic saturation of the soil column from high amounts of precipitation or rising of the water table. However, the abundance of illuviated clays coating grains and infilling biopores suggest predominantly freely drained soil conditions. The Btss horizon at the base of the TT1 soil profile contains a variety of vertic (Vertisol-like) features including a well defined sepic-plasmic fabric and abundant and thick illuviated clays (Figure 18B).

The Test Trench 5 (TT5) Mollisol (Ic) contains a thick organic-rich surface horizon with abundant rooting. Underlying the surface horizon is a succession of subsurface (B) horizons that show an increase in pedogenic alteration with depth.

Abundant Fe/Mn redoximorphic features throughout the subsurface horizons suggest that the Mollisol is subjected to intermittent periods of soil saturation. The Bss, Bssk and Bk horizons all contain fine-grain matrices with sepic-plasmic fabrics. The distinct orientation of clays within the matrices, suggest prominent wet/dry or shrink/swell conditions during soil development. Illuviated clays are present in the form of grain argillans, thick pore linings and infillings (Figure 18C). Abundant pedogenic carbonate nodules with septarian shrinkage cracks and secondary sparry calcite development in the lowermost Bk horizon (Figure 18D) point to seasonal (wet/dry) moisture conditions during the formation of the horizon.

The Test Trench 2 (TT2) soil (IIc) consists of an organic-rich surface horizon underlain by a series of Bk (calcic) horizons grading down to a coarser grain BC horizon. Abundant calcium carbonate nodules with prominent septarian shrinkage cracks are present with secondary sparry calcite growth (Figure 18E). The abundance of calcium carbonate nodules with septarian cracks and Fe/Mn redoximorphic features suggest seasonal moisture conditions controlled primarily by fluctuations in water table levels.

The Bk1b and Bk2b horizons of the buried Bino soil (IIc), exposed below the TT2 surface soil, contain abundant calcium carbonate (crystalic fabric) disseminated throughout the soil matrix (Figure 18G). The presence of biopores (Figure 18H) and sparse pedogenically altered carbonate indicate that the Bino soil may have been buried quickly, thus retarding further pedogenic alteration of the carbonate.

The Boncap paleosol (III) exposed in Profile 1 and Profile 2 contains micromorphologic features also implying formation under seasonal moisture conditions (Figures 18A, 18B, 18C, and 18D). An abundance of pedogenic carbonate nodules and

filaments (Figure 18D), and the common presence of redoximorphic features (Figure 18C) imply a seasonally controlled water table resulting in alternating wet/dry conditions. The stratigraphic location of the Boncap soil in relation to the ancient tributary channel (IIb) and the abundance of redoximorphic features, further suggests that the paleosol was heavily influenced by the fluctuating position of the water table before burial. Abundant evidence of rooting (root rhizoliths and rhizocretions) indicates that the paleosol formed under a long-term stable surface. The upper surface horizon of the Boncap paleosol does appear to have been erosionally truncated during the deposition of Unit V.

Micromorphologic evidence from Test Trench 3 (TT3) excavated into Unit IV, suggests frequent deposition of thinly stacked soils. The thin soil horizons appear to be weakly developed, with minimal soil ped development and sparse pedogenic features (i.e., fine rooting and Fe staining). The lack of pedogenic alteration and thin horizon development suggests that the TT3 profile (IIc) represents several periods of brief surface stability and intermittent deposition. Micromorphologically, the Cb2/Cb3 horizons contain sedimentary structures (i.e. Fe-stained laminations) and grain size (Figure 19I) similar to that of structures and grain size of the upper laminated sand bed (Figures 14 and 15) of surface or upper sand bed of Unit IV within the excavation area (Figure 19H).

Micromorphological features in Unit I (Alfisols of Ib and Mollisols of Ic) soils suggest fairly well drained soil conditions, with periodic saturation. The close proximity of these two soils suggests formation under similar climate conditions. Conversly, micromorphologic features of these two soils indicate that they have experienced different forms and degrees of pedogenic alteration.

Abundant pedogenic carbonate nodules (with abundant septarian cracks) and Fe/Mn redoximorphic features suggest that the Unit IIc soils formed under seasonal wet/dry conditions. The Bino soil (TT2) in Unit IIc contains few Fe/Mn redoximorphic features and abundant disseminated carbonate that is much less pedogenically altered than the overlying surface soil, indicates a relatively brief period of surface stability and soil formation before burial. The Boncap soil of Unit III contains abundant pedogenic features pointing to seasonally dominated (wet/dry) conditions during soil formation. The Boncap soil appears to have been subjected to additional pedogenic alteration (i.e. rhizolith and rhizocretion development) after burial, following features that formed during pedogenesis. The last surface soil of Unit V contains well-developed calcic horizons with abundant pedogenic nodules throughout, suggesting wet/dry conditions during soil formation. Overall, the buried soils associated with the Waco mammoth events all contain evidence of moderately to well-drained soil conditions and possibly formed under a seasonal (wet/dry) climate.

Environmental Reconstruction

Climate/Ecosystem Reconstruction

$\delta^{13}C$ values of the soils and buried soils of the Waco Mammoth Site suggest multiple shifts from C_3-dominated to C_4-dominated plant ecosystems. Carbon isotopic ratios from subsurface horizons of the Unit Ic Mollisol (TT5) to the south of the Waco Mammoth Site (Table 2) suggest the presence of a mixed C_3/C_4 plant component. Plant ecosystems estimated from isotopic ratios from Unit I (Unit Ib to the north and Unit Ic to the south) are consistent with the presence of Alfisols and Mollisols, respectively mapped

(USDA, 2001) on both sides of the T3 terrace (Figure 8). Commonly associated with tropical to subtropical climates, C_4 vegetation in the North American Great Plains includes warm-season grasses and some dicot and woody species (Paruelo and Lauenroth, 1996; Ehleringer et al., 1997). The $\delta^{13}C$ values from the Unit Ic Mollisol indicate an ~50/50 C_4/C_3 landscape that does not change significantly with depth. This mixed ecosystem signal implies a grassland-dominated ecosystem throughout much of the Bosque (south side) T3 surface history, with C_3 contributions resulting from a historic encroachment of mesquite and other C_3-photosynthetic vegetation.

$\delta^{13}C$ values from the TT2 soil and the buried Bino soil of Unit IIc show that during periods of landscape stability and pedogenesis, approximately 43 to 67% of the soil organic matter (SOM) was contributed by C_4 vegetation (Table 2). The Bino soil horizons and the lowermost Bk horizon of the TT2 Mollisol (IIc) show a slightly more C_3 plant assemblage during soil formation (Table 2). The C_3 vegetation potentially consisted of cool-season grasses, trees or shrubs (Paruelo and Lauenroth, 1996; Ehleringer et al., 1997). The presence of a mixed C_3/C_4 component suggests more temperate climate conditions (Nordt et al., 1994) during early deposition of the Unit IIc. A shift to a more C_4-dominated plant association is apparent in the two upper Bk horizons of the TT2 Mollisol (IIc), which indicates a move towards higher temperature conditions. Another possibility is that the $\delta^{13}C$ values of the TT2 Mollisol and Bino paleosol represent an early (during soil formation of Bino Soil and lower Bk of TT2 Mollisol) C_3 riparian component with the broader landscape being dominantly C_4 grasslands with a historic encroachment by mesquite. Furthermore, the upper Bk horizons of the surface soil (IIc) of Test Trench 6 (Figures 12 and 14) show $\delta^{13}C$ values

suggesting a predominantly C_4 grass ecosystem, which correlates isotopically with the upper Bk horizons of the TT2 Mollisol (IIc) to the north. The presence of a more dominate C_4 component in the TT2 and TT6 Mollisol than the TT5 Mollisol is likely due to the lower density of mesquite (C3 plants) when compared to the TT5 Mollisol (Table 2).

Isotopic evidence from the buried Boncap soil of Unit III points to an overall mixed C_3/C_4 assemblage. $\delta^{13}C$ values from the lowermost horizons of the Boncap soil (III) from Profile 1 (Figure 22, P1) suggest higher C_3 contributions, showing a range of 66 to 79% of the biomass being contributed by C_4 plants (Table 2). A shift (~8‰) from a C_3-dominated to C_4-dominated component occurs between the Bkg2b and Bkg1b horizons of the Boncap paleosol (Figure 22). A much more subtle shift from C_3-dominated to C_4-dominated plant communities occurs in the upper portion of Unit IIc (TT2 soil) and appears to be similar to that of the shift present between Unit III to Unit V, but occurred sometime before the deposition of Unit III. A Mixed C_3/C_4 plant signal is shown throughout the deposition of Unit IV, which is potentially a result of the mixing of detrital SOM prior to and during burial (Table 2; Figure 22).

The presence of a mixed C_3/C_4 plant ecosystem within the fluvial landscape during the mammoth habitation indicates the presence of a C_3 riparian component (channel landscape) within the broader floodplain and terrace landscape that consisted primarily of C_4 grasses. As the riparian zone decreased (due to channel infilling) through time, C_4 grasses (evident in Unit IIb and Unit V) continued to encroach and dominate the landscape. The C_4-dominated modern landscape that blankets the majority of the Waco Mammoth Site supports interpretation of a shift from a mixed grasses and shrubs/trees

ecosystem to a grass-dominated assemblage, with a historic encroachment of non-native C_3 shrub and grass component.

According to Hoppe (2004), $\delta^{13}C$ values obtained from molars representing several mammoths at the Waco site suggest that all the mammoths sampled ate similar diets consisting of 70-80% C_4 grasses. This is consistent with the $\delta^{13}C$ values from the broader floodplain/terrace landscape surrounding the Waco Mammoth Site. For example carbon isotopic ratios from the surface Mollisols north and south of the site indicate a steady C_4-dominated ecosystem with only 20-30% of the mammoths' diets coming from C_3 vegetation.

Paleohydrology

Stratigraphic evidence of the ancient Bosque River (from coring, augering, and electrical resistivity in Figures 14 and 16), as well as the modern location of Bosque River incised into Cretaceous bedrock suggest that the Bosque River has been primarily a bedrock channel. Bedrock channels are relatively stable and highly resistant to erosion or incision from flooding (Wohl, 1999). Incision rates for various bedrock channels have been estimated as ranging from 0.5 to 1000 cm kyr^{-1} (kyr^{-1} = per thousand years) (Wohl, 1999) in relation to a variety of bedrock materials. Two limestone bedrock channels were presented by Wohl (1999), showing average incision rates of 5.7 cm kyr^{-1} (Quaternary channel in limestone in New Guinea after Chappell, 1974) and 2.7 cm kyr^{-1} (Quaternary channel in carbonate in Virginia, USA after Granger et al., 1997), respectively. Several studies have been performed, that record instances, in which bedrock erosion has exceeded the average range of 0.5 to 1000 cm kyr^{-1} (Scott and Gravlee, 1968; Baker, 1978; Shroba et al., 1979; Vuichard and Zimmermann, 1987). A

study by Brackenridge (1984) on the alluvial stratigraphy of Duck River, Tennessee presented the hydrologic history of the bedrock channel on the time scale of 10^2 to 10^4 years. Duck River is a meandering stream that has incised into limestone, with some reaches confined by steep bedrock valley slopes (Brackenridge, 1984). Brackenridge (1984) used stratigraphic and topographic evidence to estimate the minimum average rate of lateral bedrock erosion over the last 30,000 years. Using 10 kyr^{-1}, 20 kyr^{-1}, and 30 kyr^{-1} time spans, Brackenridge (1984) concluded that the Duck River has eroded laterally into bedrock over time at average rates of no less than 0.25 to 0.75 m 100 yr^{-1}, with a slightly broader range of 1.25 to 2.0 m 100 yr^{-1}. These averages are dependent on locality; hence some areas experienced much more lateral erosion than others. Based on stratigraphic evidence and similarity of bedrock (to the Duck River Limestone), the two deeply incised channels underlying the T2 terrace (Unit IIa and IIb) at the Waco Mammoth Site stratigraphically predate the mammoth habitation (Figure 14). Using the published limestone bedrock erosion rates (i.e. 5.7 cm kyr^{-1}) presented by Wohl (1999), the incision of the limestone floor from the base of Unit Ic to the base of Unit IIa occurred over a period of 10^4 years.

Situated within a low-order tributary (Unit IIb)near (closer than its distance from the modern Bosque River) its confluence with the ancestral Bosque River, the Waco Mammoth Site would have been susceptible to elevated slackwater levels backing into the low-order triburtary from periodic flooding of the Bosque trunk stream. Stratigraphic evidence of periodic slackwater deposition (Unit IV sediments) during Columbian mammoth occupation, coupled with the relationship between the present topographic association of the Bosque trunk stream (Figure 23), indicate that sediment was derived

from the Bosque River during flood episodes. Paleoflood analyses have been performed using slackwater deposits (Kochel and Baker, 1988; Kochel, 1988) as a means of estimating flood potential and frequency. Paleoflood modeling can be an effective method in the estimation and determination of paleoflood discharge amounts (O'Connor and Webb, 1988).

A one-dimensional steady-flow model was constructed using a measured reach of the modern Bosque River associated with the confluence of the distal end of the tributary containing the Waco Mammoth Site (Figure 23), in order to examine the backwater flood potential into the low-order tributary. The steady-flow model was computed using the Hydrologic Engineering Centers River Analysis System (HEC-RAS) 4.0 Beta modeling program (USACE, 2006). For this study, eight cross-section locations were randomly chosen from the USGS Waco West 7.5" quadrangle (USGS, 1979), which represented a stretch of the Bosque River starting upstream of the study area and extending downstream to the confluence of the modern Bosque and Brazos Rivers (Figure 23). Because discharge of the Bosque River near the confluence with the Waco Mammoth Site tributary is controlled by the Waco Lake Dam, discharge was calculated using peak streamflow discharge data from the North Bosque gauge site at Valley Mills, Texas (USGS 0809500) (USGS, 2007) (Appendix F). The North Bosque basin drains approximately 2968 km^2 (USGS, 2007). Discharge data from the North Bosque at Valley Mills, Texas gauge station was determined to be significantly less dam-controlled than the Bosque River below Waco Lake Dam, therefore, simulating more realistic discharge amounts for the ancestral Bosque River. Discharge was computed for two, five, 25, 50, 100, and 200-year storms (Table 3), using the Stormwater Management and Design Aid

(SMADA 6) (Appendix G) Distribution Analysis (Distrib 2.13) extention (CEE UCF, updated 1997) (Appendix G). The HEC-RAS steady flow analysis was run using each calculated discharge. A model of the selected reach was constructed for each storm discharge to determine the spatial extent of flood waters produced by each storm discharge. For this study two models (a 25-year and a 50-year storm discharge model) were observed in detail and are presented in Figure 24 (Appendix H). For the application of this model it was assumed that the ancestral Bosque River had already moved southward from its previous location represented by the deeply incised channel filled with the gravel and sands of Unit IIa and was perhaps nearer its present location. Although the ancestral Bosque River basin would not have been dam-controlled and potentially drained a larger area than the modern Bosque basin, conservative discharge estimates were calculated using only the North Bosque discharge information (Appendix F). Furthermore, the backwater potential of the Bosque River from flooding of the Brazos River was not calculated, which would have likely influenced a higher frequency of flooding in the mammoth tributary.

The steady-flow analysis of the selected reach of the Bosque River using a 50-year flood discharge of approximately 4000 m^3/s would cause backwater into the full extent of the Waco Mammoth Site tributary from the trunk stream, significantly inundating the site (Figure 24). The analysis suggests that a flash flood in the ancient Bosque River with a discharge equal to or greater than 4046 m^3/s would have forced water into the steep-sloped tributary associated with mammoths. A significant rise in water level in the low-order tributary could easily have trapped the Columbian

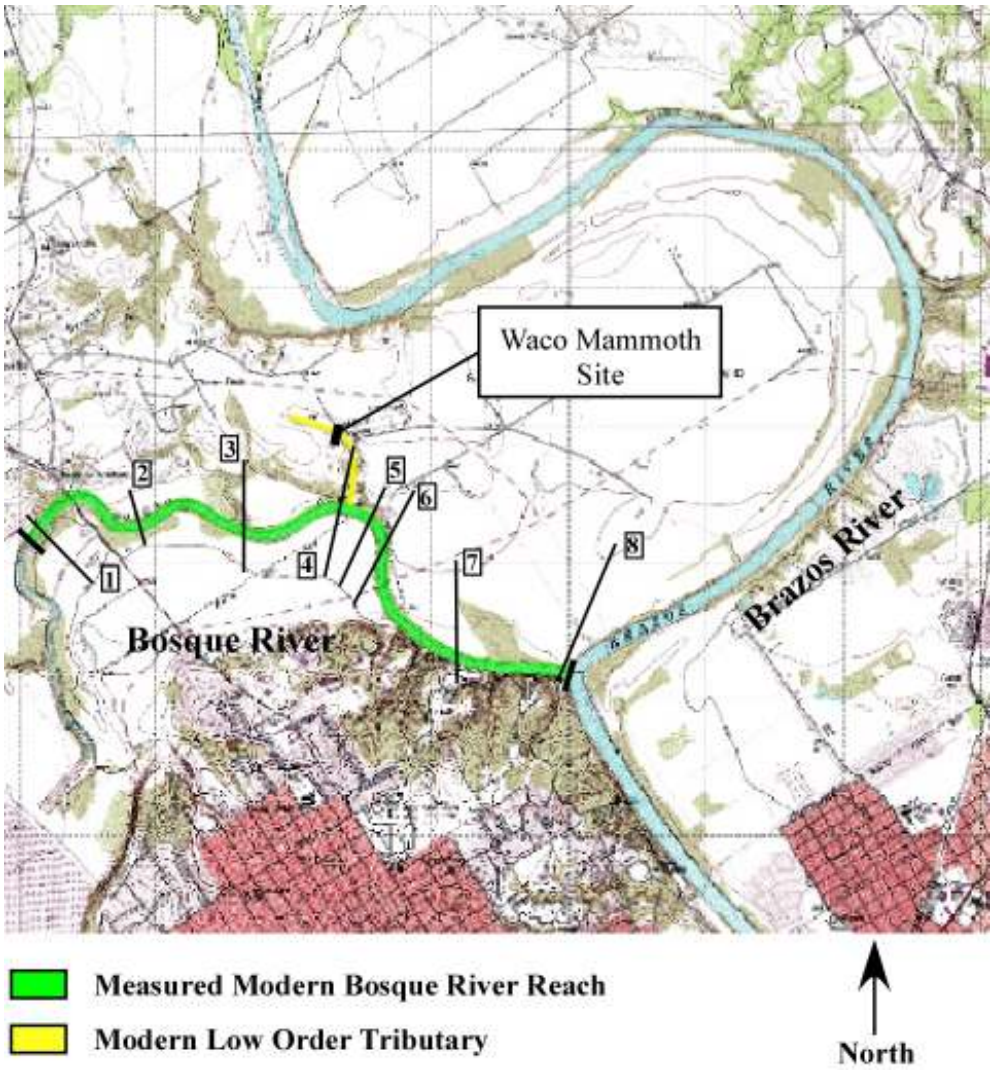

Figure 23. Map of study area, showing measured reach of the modern Bosque River and associated low order tributary containing the Waco Mammoth Site. Measured cross-sections are labeled 1-8.

Table 3. Peak streamflow discharge for the modern North Bosque River at Valley Mills, Texas. Predicted peak streamflow discharge (Prediction) for selected year probability (R Period) flood events calculated from DISTRIB 2.13 (CEE UCF, updated 1997).

Probability	R Period years	Prediction m^3/sec	Std. Dev. m^3/sec
0.995	200	6244.6	2763.6
0.99	100	5066.1	1881.3
0.98	50	4000.7	1224.4
0.96	25	3048.1	759.2
0.9	10	1960.9	381.1
0.8	5	1267.4	222.5
0.667	3	827.1	144.3
0.5	2	516.8	92.6

mammoths (and other fauna) within the tributary channel. Unable to escape the steep slopes of the tributary, trapped fauna could have perished as a result of drowning.

Age of the Mammoths

OSL ages from the Waco Mammoth Site (60 ± 2.5 ka unweighted mean average at 1-sigma) places the mammoth habitation during Marine Oxygen Isotope Stage 4 (OIS 4; Figure 25). This stage begins with the start of the Wisconsinan glaciation and was a time when temperatures would have been nearly as cold as they were during the last glacial maximum 21,000 yr B.P. of OIS 2 (Ruddiman, 2001). The sediments associated with the mammoths (Units III and IV) would have been deposited during the later part of OIS 4. It is speculated from stratigraphic evidence that channel incision (Units IIa and IIb) was initiated during the shift from OIS 5 to OIS 4. This shift in stages correlates with the termination of the Sangamon interglacial (OIS 5) and the subsequent start of the Wisconsinan glaciation (OIS 4) (Figure 25). The transition from interglacial to glacial periods would have resulted in a significant shift in climate (i.e. increase in rainfall), and potentially might have changed fluvial stability and ultimately increased discharge and

incision. Speculating that incision (IIa, IIb) and the deposition of T2 (Units IIc, III, IV, and V) occurred during OIS 4, it is therefore further speculated that T3 (Unit I) deposition occurred during OIS 5 (Figure 25).

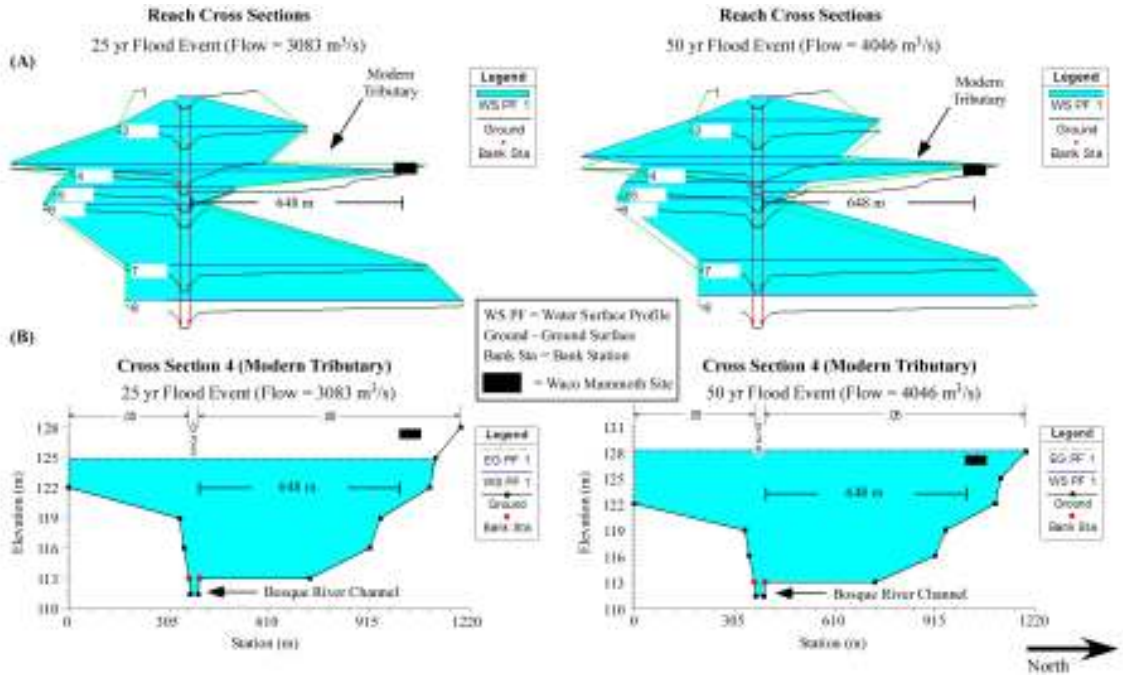

Figure 24. HEC RAS 4.0 Beta steady-flow model of Bosque River channel cross-sections, showing water surface levels using (A) 25-yr flood discharge estimate of 3083 m^3/s and (B) 50-yr flood discharge estimate of 4046 m^3/s calculated from DISTRIB 2.13 (CEE UCF, updated 1997). Waco Mammoth Site is located 648 m north of Bosque River Channel.

Death Events

Stratigraphic, micromorphologic, and isotopic evidence from the Waco Mammoth Site, all suggest that the Columbian mammoths, camel, large-tooth cat, and other potential fauna were inhabiting a slackwater tributary associated with the ancient Bosque River during the time of their death (Figure 26). The deposits of each stratigraphic bed associated with the various fauna uncovered at the site appear to be conformable (Unit

IV; Figures 14, 15, and 19) and were deposited over a relatively short period of time, separated by brief periods of nondeposition or diastems.

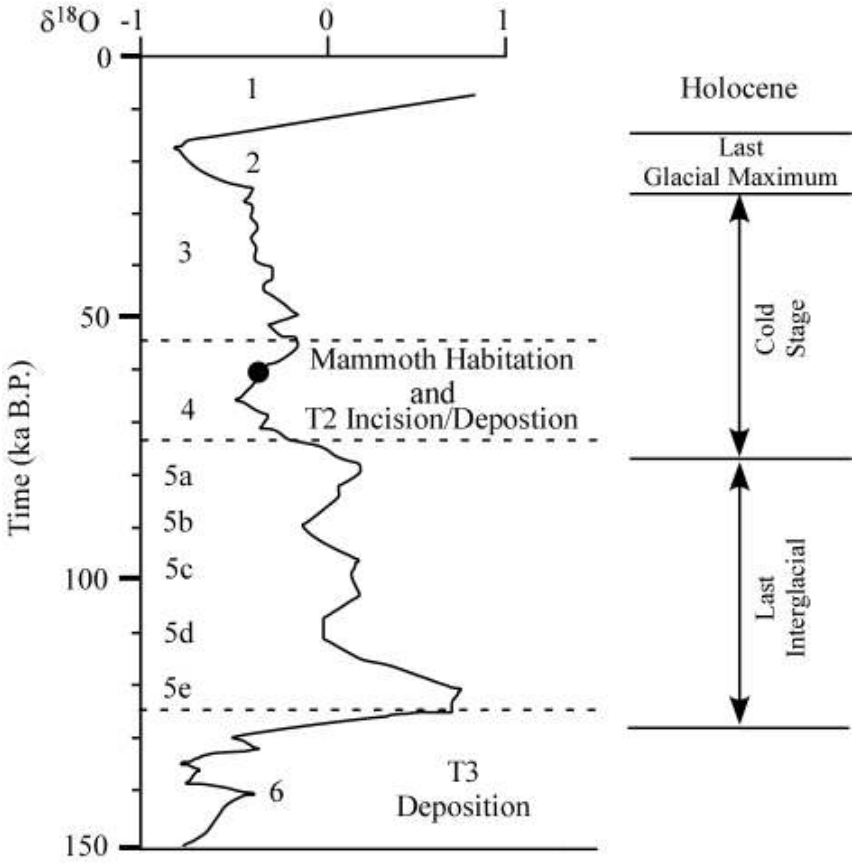

Figure 25. Stacked Marine Oxygen Isotope stages (Martinson et al., 1987), showing associated mammoth habitation and terrace depositional events. Adapted From Lowe and Walker (1997).

Stratigraphically, three separate death events occurred throughout the slackwater deposition within the low-order tributary (Figure 26). Some time after the erosion of Unit III and before the deposition of Unit IV, at least 19 Columbian mammoths (original 16 from Phase I excavation and 3 from Phase II and III excavations) and a camel (Phase III excavation) were apparently trapped by Bosque River-derived flood waters that backed up into the low-order tributary (Figure 26). These animals may have been

confined by the steep-walled tributary channel and ultimately drowned *in situ*, coming to rest on the clay-rich and sand layers (Unit IV slackwater sediments) overlying the ancient tributary gravels and sands (Figure 27). Above the lower sand bed (2nd layer from bottom to top) of Unit IV (overlying the bone bed of the 19 mammoths and camel) lies the tooth of an unidentified large-tooth feline (Figures 15 and 27). Due to the lack of taphonomic data, the cause of death of the large-tooth cat is uncertain. It is speculated however, that the cat was walking on the clayey sediments between the two sand beds (IV) in search of water and food resources and potentially died from drowning within the low order-tributary (Figure 27).

The last death event recorded at the Waco Mammoth Site consists of the adult bull male mammoth and adjacent juvenile, and an adult female mammoth located slightly higher topographically, just north of the bull and juvenile (Figures 15 and 27). These mammoths appear to have been walking on the upper laminated sand bed of Unit IV before their deaths (Figure 27). The location of the mammoth remains in the Shelby tube core by Hilliard (1997) located in the sediments of Unit IIc north of the excavation site, suggests that it was occupied much earlier than the other 22 mammoths unearthed within the excavation site (Figure 15, Units III and IV). As was the case for the initial death event, these mammoths appear to have been within the confines of the low-order tributary as flood waters from the ancestral Bosque River encroached up on them. The mammoths associated with the initial death event (16 from Phase I and 3 from Phase II/III) appear to have been confined within the channel of the ancient tributary (IIb), with three of the mammoths trailing northward (on Unit III surface) away from the channel possibly attempting to escape rising floodwaters (Figure 27). Like these mammoths, the

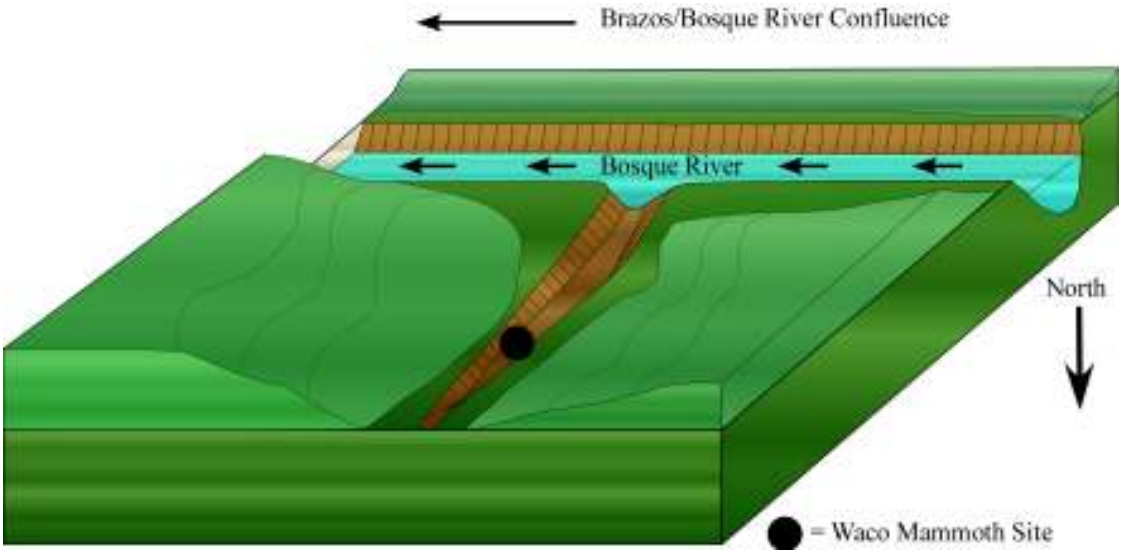

Figure 26. Conceptual geographic map, showing the location of the Waco Mammoth Site within the low-order tributary associated with the ancient Bosque River.

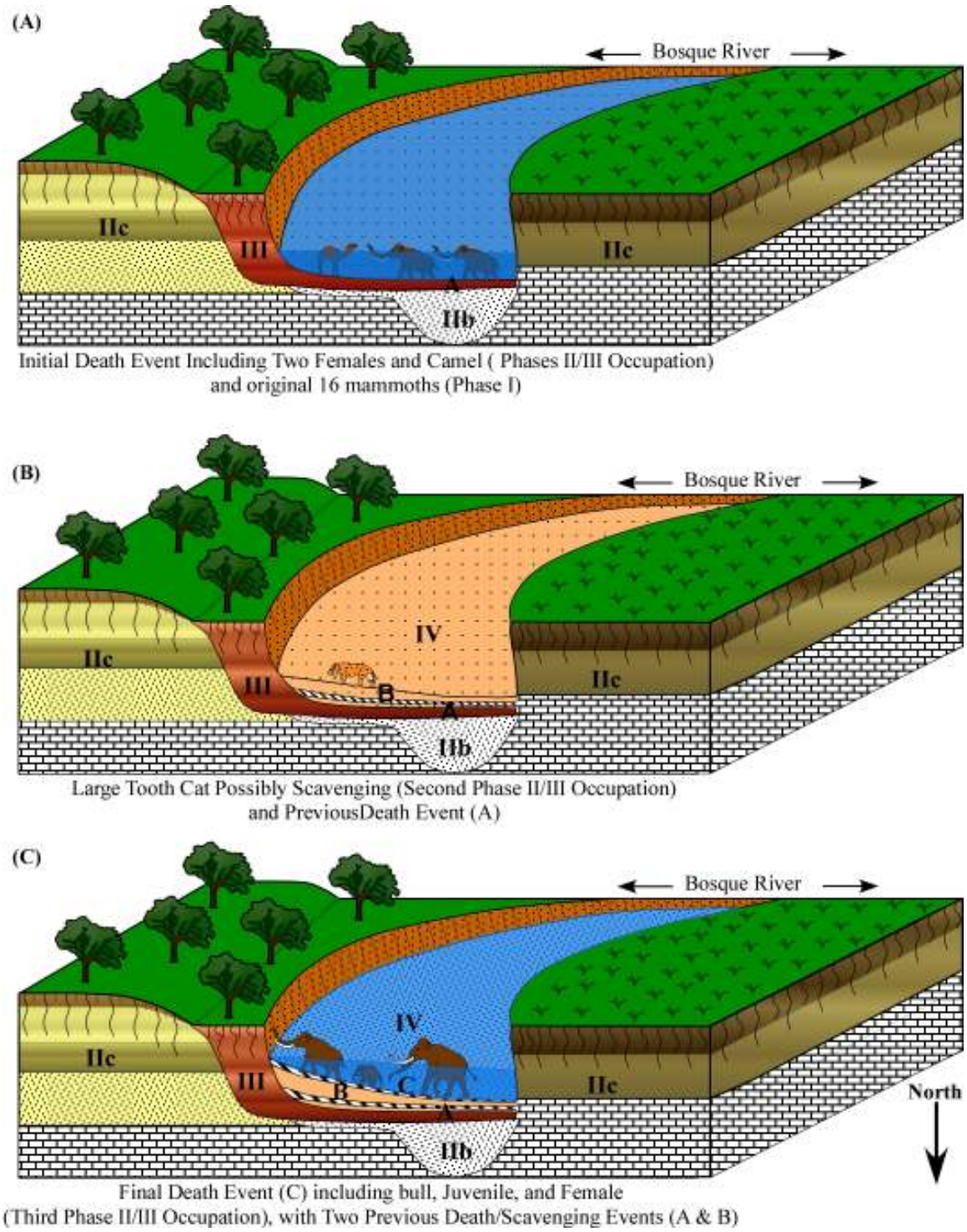

Figure 27. Environmental reconstruction of the three recorded death events at the Waco Mammoth Site, occurring between 53 to 73 ka B.P.

mammoths (Phase II and III) in the final death event appear to have been trailing away from the tributary channel on the Unit IV surface (upper sand bed), possibly attempting to escape the flood waters (Figure 27).

CHAPTER SIX

Conclusion

The Waco Mammoth Site contains the semi- to fully articulated remains of 22 Columbian mammoths (*Mammuthus columbi*), a North American camel (*Camelops hesternus*), and an unidentified large-tooth feline. The stratigraphic, chronological, micromorphological, geochemical, and paleohydrological relationships present at the Waco Mammoth Site are summarized as follow:

1. Four unconformably bound allostratigraphic units were identified in the succession of the Waco Mammoth Site that represent multiple channel, floodplain and slackwater depositional events.
2. Within the four allostratigraphic units, two buried soils (paleosols) were identified. The Boncap paleosol in Unit III formed in the floodplain deposits of the ancient low-order tributary during a period of surface stability. The Boncap paleosol appears to have supported the steep bank wall of the ancient tributary during the mammoth occurrences.
3. A series of optically stimulated luminescence (OSL) ages estimated from sandy fluvial sediments within the Phase III excavation area indicate that the mammoths inhabited the Waco site between 53,000 to 73,000 yr B.P. The unweighted mean average of all ages put the mammoth events around 60.0 ± 2.5 ka B.P. During this time the mammoths perished within the confines of a low-order tributary of the ancient Bosque River. This period places site habitation into the Marine Oxygen Isotope Stage 4 (OIS 4) of the Wisconsinan glaciation, a time when

temperatures were as low as during the last glacial maximum 21,000 yr B.P. (Ruddiman, 2001). The OSL age sharply contrasts the initial standard radiocarbon age of approximately 29,000 yr B.P., which places the mammoth habitation during OIS 3 with slightly warmer temperatures relative to OIS 4. Furthermore, Uranium/Thorium ages (Mckinney, 1990) from two mammoth molars fit within the range of the OSL ages.

4. Isotopic data obtained on pedogenic carbonate nodules from several sediment and soil profiles spatially associated with the Waco Mammoths, suggest that during the mammoth habitation the local environment was covered by a mixed C_3/C_4 (warm season grasses/trees and shrubs) plant ecosystems. Columbian mammoths, as open steppe grazers, would have been attracted to grasslands. The presence of a mixed C_3/C_4 plant ecosystem within the fluvial landscape during the mammoth habitation indicates the presence of a C_3 riparian component (channel landscape) within the broader floodplain and terrace landscape that consisted of primarily C_4 grasses. The likely presence of warm season grasslands bordering the low-order tributary is consistent with Hoppe (2004) conclusion that isotopically, the Waco mammoths age a similar diet of 70-80% C_4 plants. Sometime after the mammoths' deaths, a shift from mixed C_3/C_4 to C_4-dominated vegetation occurred. A mean July temperature estimate of 26°C was calculated using the $\delta^{13}C$ value and a modern analog transfer function from the upper B horizon of the Boncap paleosol of Unit III (associated with mammoth habitation). This temperature estimate suggests that the mean July temperature at the Waco Mammoth Site between 53,000 to 73,000 yr B.P. was approximately four degrees

cooler than the present mean July temperature (~30°C) for Waco, Texas.

5. Micromorphological evidence of the soils and paleosols from the Waco Mammoth Site suggest strong seasonality in climate. Abundant calcium carbonate and Fe/Mn redoximorphic features throughout the Boncap soil (III) and Unit IV sediments associated with the mammoths, indicate seasonal wetting and drying of the soil caused by annual water-table. Surface soils associated with the Waco Mammoth Site include loamy acidic Alfisols (hardwood savannah) to the north and loamy, organic-rich Mollisols (grassland) to the south. The Bino soil consists of two Bk horizons in Unit IIc that appear to have been buried, after a brief period of surface stability, by the surface Mollisol exposed in Test Trench 2.
6. Stratigraphic and paleoclimate history of the site indicates that the Waco mammoths died in an ancient low-order fluvial environment. Sediment and soil conditions during the mammoth habitation are consistent with periodic episodes of slackwater deposition from flooding of the ancestral Bosque River. The spatial distribution of mammoths within the strata suggest that the mammoths died from drowning caused by a rapidly rising backwater derived from the ancestral Bosque River, which trapped the mammoths within the steep-sided tributary channel. As the waters receded from the tributary, the mammoths likely came to rest on the slackwater deposits and then were buried by later depositional events. The bull, juvenile and subadult female appear to have been trailing away from the tributary channel before succumbing to the lack of footing on the slippery silty clay slopes of the channel wall and flood waters.
7. Stratigraphic evidence of the spatial distribution of mammoths at the Waco

Mammoth Site points to at least two mammoth death events and one possible large-tooth feline death. The mammoth found during subsurface coring (Hilliard, 1997) is associated with the sediments of Unit IIc and is significantly older than the other 22 mammoths associated with the sediments of Units III and IV. At least 19 mammoths perished on the same geomorphic surface before being buried by the slackwater deposits of Unit IV. Because situated within the upper sand bed of Unit IV and time-equivalent surface of Unit III, the Bull, juvenile, and adult female mammoths died sometime after the deposition of Unit IV. Because Unit IV consists of a succession of conformable beds and the OSL ages all overlap (within a 2-sigma error), the amount of time between death events cannot be precisely determined. Given that Unit IV consists of a series of conformable beds with no evidence of surface stability and soil formation, it is therefore speculated that the three events happened within a relatively brief time frame.

APPENDICES

APPENDIX A

Test Trench Field Descriptions

Table A.1. Test Trench 1 Alfisol (Unit Ib) field description sheet, showing morphologic characteristics (Soil Survey Staff, 1993) observed in the field.

Depth (cm)	Horizon	Color M/D	Structure	$CaCO_3$ size, type	Consistence M/D	HCl	Texture	Boundary	Comments
0-6	A	10YR 3/4& 5YR 4/6 10YR 5/3& 40% of 5YR5/6	Mod, med Sbk	N/A	V. friable	N/A	SL 15% clay	Abrupt, smooth	
Depth (cm)	Horizon	Color M/D	Structure	$CaCO_3$ size, type	Consistence M/D	HCl	Texture	Boundary	Comments
6-27	Bt1	5YR 4/6	Mod, cs Abk	N/A	V. hard	N/A	SCL 23% clay	Gradual, smooth	2d 5YR 4/3 clay skins
Depth (cm)	Horizon	Color M/D	Structure	$CaCO_3$ size, type	Consistence M/D	HCl	Texture	Boundary	Comments
27-62	Bt2	5YR 4/3 5YR 5/6		N/A	V. hard	N/A	CL 33% clay	Gradual, smooth	>1% Quartz Pebbles (1cm dia); Cd Clay Films 5YR 4/3; f1d FeMn coats
Depth (cm)	Horizon	Color M/D	Structure	$CaCO_3$ size, type	Consistence M/D	HCl	Texture	Boundary	Comments
62-118	Btg	2.5YR 4/6 Ped Interior 10YR 5/4 Ped Exterior		N/A	V. hard	N/A	C	Gradual, smooth	Cd clay films 7.5YR 4/3; f1d FeMn concentrations (2-4mm dia)
Depth (cm)	Horizon	Color M/D	Structure	$CaCO_3$ size, type	Consistence M/D	HCl	Texture	Boundary	Comments
118-156	Btss	7.5YR 6/6 Clay Films 5YR 4/3&4/4		N/A	V. hard	N/A	C	Abrupt, smooth	Cd slicks >20° & grooved
Depth (cm)	Horizon	Color M/D	Structure	$CaCO_3$ size, type	Consistence M/D	HCl	Texture	Boundary	Comments
156-191	Ck	N/A	N/A	N/A	N/A	str	N/A	N/A	Matrix supported poorly sorted Med. Grained (2mm to 3cm dia) subrounded

Additonal Comments
>1% silicious pebbles >1cm dia throughout
Roots throughout, but concentrated in first 3 horizons

Mod = moderate; med = medium; cs = coarse; Abk = angular blocky; Sbk = subangular blocky; HCl = reaction to hydrochloric acid; str = strong; SL = Sandy Loam; SCL = Sandy Clay Loam; CL = Clay Loam; C = Clay; f1d = few fine distinct; 2d = moderate distinct; V. hard = very hard; V. friable = very friable; M/D = moist/dry

Table A.2. Test Trench 5 Mollisol (Unit Ic) Field description sheet, showing morphologic characteristics (Soil Survey Staff, 1993) observed in the field.

Depth (cm)	Horizon	Color M/D	Structure	CaCO3 size, type	Consistence M/D	HCl	Texture	Boundary	Comments
0-17	Ap	10YR 3/1	Mod, cs Abk	N/A	V. hard	N/A	CL	Gradual, smooth	
Depth (cm)	Horizon	Color M/D	Structure	CaCO3 size, type	Consistence M/D	HCl	Texture	Boundary	Comments
17-54	Bw	10YR 5/3 20% of 3/1 mixed	W, cs Abk	N/A	V. hard	str	SiCL	Gradual, smooth	1% FeMn coats (2-4mm dia.)
Depth (cm)	Horizon	Color M/D	Structure	CaCO3 size, type	Consistence M/D	HCl	Texture	Boundary	Comments
54-84	Bss	10YR 5/2 3-5% of 10YR 4/2	Mod, med Abk	1% nod White Hard 2-4mm dia.	V. hard	str	SiCL	Clear, smooth	Clear fine slicks
Depth (cm)	Horizon	Color M/D	Structure	CaCO3 size, type	Consistence M/D	HCl	Texture	Boundary	Comments
84-155	Bssk	10YR 4/2 2% 10YR 5/3 pockets	Mod, cs Abk	5-8% nod White Hard 3-8mm dia.	V. hard	vstr	CL	Clear, smooth	Clear distinct slicks 20-40° dip Same FeMn same as above
Depth (cm)	Horizon	Color M/D	Structure	CaCO3 size, type	Consistence M/D	HCl	Texture	Boundary	Comments
155-200	Bk	7.5YR 5/4 - 4/6	Weak, cs Abk	3-5% nod White Hard 0.5-1cm dia.	V. hard	vstr	SiCL	N/A	1% biocast 10YR 3/2 (2-3mm dia.)

Mod = moderate; W = weak; med = medium; cs = coarse; Abk = angular blocky; nod = nodule;
V. hard = very hard; vstr = very strong; str = strong; CL = Clay Loam; SiCL = Silty Clay Loam; M/D = moist/dry

Table A.3. Test Trench 2 Surface soil and Bino Soil (Unit IIc) Field description sheet, showing morphologic characteristics (Soil Survey Staff, 1993) observed in the field.

Depth (cm)	Horizon	Color M/D	Structure	CaCO3 size, type	Consistence M/D	HCl	Texture	Boundary	Comments
0-21	A	7.5YR 4/3	Mod, med Abk	2% nodules 3-8mm dia white/hrd	V. hard	vstr	CL	Clear, smooth	
Depth (cm)	Horizon	Color M/D	Structure	CaCO3 size, type	Consistence M/D	HCl	Texture	Boundary	Comments
21-52	Bk1	7.5YR 4/3	Mod, med Abk	5-7% nodules .5-1.5cm dia white/hrd	V. hard	vstr	CL	Clear, smooth	
Depth (cm)	Horizon	Color M/D	Structure	CaCO3 size, type	Consistence M/D	HCl	Texture	Boundary	Comments
52-102	Bk2	7.5YR 5/6	Mod, med-cs Abk	15% nodules .5-1.5cm dia white/hrd	V. hard	vstr	CL 38% clay	Gradual, smooth	Cd coats 7.5YR 3/2, 10cm thick at base of this horizon; majority of CaCO3 in middle of horizon
Depth (cm)	Horizon	Color M/D	Structure	CaCO3 size, type	Consistence M/D	HCl	Texture	Boundary	Comments
102-194	Bk3	10YR 5/4 & 10YR 6/4	W, cs Pr	3% nodules .5-1.5cm dia white/hrd	V. hard	vstr	CL 35% clay	Distinct, smooth	5% biocasts (3-6mm dia), 7.5YR 4/4
Depth (cm)	Horizon	Color M/D	Structure	CaCO3 size, type	Consistence M/D	HCl	Texture	Boundary	Comments
194-254	BC	10YR 6/4	M	N/A	V. hard	vstr	SiCL-CL 30% clay	Abrupt, smooth	5% biocasts 3-6mm dia, 7.5YR 4/6 &10YR 5/6 Rysoliths (2mm-5cm dia), extend 20cm through horizon Termite traces
Depth (cm)	Horizon	Color M/D	Structure	CaCO3 size, type	Consistence M/D	HCl	Texture	Boundary	Comments
254-270	Bk1b	10YR 6/8 & 10YR 7/4 mixed	M	1% nodules .5-1.5cm dia white/hrd 5% 2-4cm	Hard	vstr	SiCL-CL 33% clay	Clear, Smooth	
Depth (cm)	Horizon	Color M/D	Structure	CaCO3 size, type	Consistence M/D	HCl	Texture	Boundary	Comments
270-320	Bk2b	7.5YR 5/6 & 5% of 7.5YR 6/6	M	5% nodules .5-1cm dia	Hard	vstr	SiCL-CL 35% clay	N/A	2% biocasts (2-4cm dia), 7.5YR 4/6

Additional Comments
Most roots are in 1st 3 horizons

Mod = moderate; med = medium; Abk = angular blocky; Pr = prismatic; M = massive; W = weak; hrd = hard; V. hard = very hard; vstr = very strong; CL = Clay Loam; SiCL = Silty Clay Loam; M/D = moist/dry

Table A.4. Test Trench 3 Surface soil (Unit IIc) and Unit IIb field description sheet of upper portion of TT3 showing morphologic characteristics (Soil Survey Staff, 1993) of fill to C2b3 horizons observed in the field.

Depth (cm)	Horizon	Color M/D	Structure	CaCO3 size, type	Consistence M/D	HCl	Texture	Boundary	Comments
0-20	Fill	N/A	N/A	N/A	N/A	vstr	N/A	Clear, smooth	
Depth (cm)	Horizon	Color M/D	Structure	CaCO3 size, type	Consistence M/D	HCl	Texture	Boundary	Comments
20-71	Bwb1	10YR 6/6 10YR 7/3 10YR 6/4	W	Filaments	Hard	vstr		Gradual, smooth	
Depth (cm)	Horizon	Color M/D	Structure	CaCO3 size, type	Consistence M/D	HCl	Texture	Boundary	Comments
71-103	Cb1	10YR 6/6 10YR 6/4 10YR 6/4 10YR 6/6	N/A	N/A	N/A	vstr	N/A	Gradual, smooth	Weak horizontal Lamination
Depth (cm)	Horizon	Color M/D	Structure	CaCO3 size, type	Consistence M/D	HCl	Texture	Boundary	Comments
103-144	Bwb2	10YR 6/4 10YR 6/3 10YR 6/4	W	Filaments	Hard	vstr		Gradual, smooth	Black Mn coats 10YR 2/1 (1%) 2cm thick bed 10YR 4/3
Depth (cm)	Horizon	Color M/D	Structure	CaCO3 size, type	Consistence M/D	HCl	Texture	Boundary	Comments
144-165	Cb2	2.5Y 6/4 2.5Y 7/4	N/A	N/A	N/A	vstr	N/A	Gradual, smooth	Upper part - Cross-lamination and grades downward to horizontal Lamination
Depth (cm)	Horizon	Color M/D	Structure	CaCO3 size, type	Consistence M/D	HCl	Texture	Boundary	Comments
165-196	Bgb3	10YR 7/4 10YR 6/4 2.5Y 7/4 2.5Y 7/2	W	N/A	Hard	vstr		Gradual, smooth	
Depth (cm)	Horizon	Color M/D	Structure	CaCO3 size, type	Consistence M/D	HCl	Texture	Boundary	Comments
196-222	C1b3	2.5Y 7/4 2.5Y 7/6 2.5Y 7/3 2.5Y 6/4	N/A	N/A	N/A	vstr	N/A	Gradual, smooth	Faint to v.faint horz lamination 1% Mn coats 2.5Y 2/1 sandy cross Lamination

Table A.4. Continued

Depth (cm)	Horizon	Color M/D	Structure	CaCO3 size, type	Consistence M/D	HCl	Texture	Boundary	Comments
222-239	C2b3 upper lower upper lower	 2.5Y6/4 2.5Y7/3 2.5Y 7/2 2.5Y 7/4 2.5Y 7/3 2.5Y 7/3	N/A	N/A	N/A	 vstr	N/A	Gradual, smooth	up: clay loam 30% clay few clay lamin-ation (red-brown) lo: horz lam. grading down to cross-lam
Depth (cm)	Horizon	Color M/D	Structure	CaCO3 size, type	Consistence M/D	HCl	Texture	Boundary	Comments
239-260	Bgb4	2.5Y 6/1 2.5Y 5/6 5Y 6/2 5% of 2.5Y 6/6	W	N/A	Hard	vstr		Gradual, smooth	>1% 2.5Y 2/1 Mn coats
Depth (cm)	Horizon	Color M/D	Structure	CaCO3 size, type	Consistence M/D	HCl	Texture	Boundary	Comments
260-281	Cgb4	2.5Y 7/2 5Y 7/2	N/A	N/A	N/A	vstr	N/A	Gradual, smooth	V. faint horz Lamination
Depth (cm)	Horizon	Color M/D	Structure	CaCO3 size, type	Consistence M/D	HCl	Texture	Boundary	Comments
281-289	2C1		N/A	N/A	N/A	N/A	N/A	Gradual, smooth	Gravel: Avg- 1cm wide Clast supported; poorly sorted
Depth (cm)	Horizon	Color M/D	Structure	CaCO3 size, type	Consistence M/D	HCl	Texture	Boundary	Comments
289-356	2C1		N/A	N/A	N/A	N/A	N/A	Gradual, smooth	Avg- 5cm wide weakly embricated to the north; discotle and prolate Clast supported; v. poorly sorted
Depth (cm)	Horizon	Color M/D	Structure	CaCO3 size, type	Consistence M/D	HCl	Texture	Boundary	Comments
356-406	3C1		N/A	N/A	N/A	N/A	N/A	Abrupt	Crude horz lamination Predomenantly CaCO3 Avg- 2-3cm pebbles

Table A.4. Continued

Depth (cm)	Horizon	Color M/D	Structure	CaCO3 size, type	Consistence M/D	HCl	Texture	Boundary	Comments
406-416	Red Clay		N/A	N/A	N/A	N/A	N/A	Abrupt	Sand matrix red & brown; redox boundary from upper to lower gravel
Depth (cm)	Horizon	Color M/D	Structure	CaCO3 size, type	Consistence M/D	HCl	Texture	Boundary	Comments
416-429	Flaggy		N/A	N/A	N/A	N/A	N/A	Abrupt	Similar to upper gravel graphia-rich
Depth (cm)	Horizon	Color M/D	Structure	CaCO3 size, type	Consistence M/D	HCl	Texture	Boundary	Comments
429-439	Red Clay		N/A	N/A	N/A	N/A	N/A	N/A	

W = weak; vstr = very strong; v poorly = very poorly; M/D = moist/dry

Table A.5. Test Trench 4 Surface soil (Unit IIc) Field description sheet, showing taxonomic characteristics (Soil Survey Staff, 1993) observed in the field.

Depth (cm)	Horizon	Color M/D	Structure	CaCO3 size, type	Consistence M/D	HCl	Texture	Boundary	Comments
0-21	Ap	7.5YR 4/6 7.5YR 5/4	Mod, med Abk	2% nodules White Hard 3-5mm dia.	V. hard	vstr	C 35% clay	Abrupt, smooth	
Depth (cm)	Horizon	Color M/D	Structure	CaCO3 size, type	Consistence M/D	HCl	Texture	Boundary	Comments
21-96	Bk1	7.5YR 5/4	Str, med Abk	5-10% nod White Hard 5mm - 0.5cm	V. hard	vstr	CL 30% clay	Gradual, smooth	>1% black Mn coats
Depth (cm)	Horizon	Color M/D	Structure	CaCO3 size, type	Consistence M/D	HCl	Texture	Boundary	Comments
96-132	Bk2	7.5YR 6/6	W, med-cs Sbk	1% nod 5-7mm dia.	V. hard	vstr	CL 30% clay	Clear, smooth	Root traces infilled w/ CaCO3 (2%) Modern snell shells
Depth (cm)	Horizon	Color M/D	Structure	CaCO3 size, type	Consistence M/D	HCl	Texture	Boundary	Comments
132-165	Bw	10YR 6/4	W, cs Sbk		V. hard	vstr	SiCL 25% clay	Gradual, smooth	Rabdotus ?
Depth (cm)	Horizon	Color M/D	Structure	CaCO3 size, type	Consistence M/D	HCl	Texture	Boundary	Comments
165-181	BC1	10YR 6/4	N/A	Root traces infilled 2%	Hard	vstr	N/A	Gradual, smooth	Siliceous pebbles termites 1% black Mn coats
Depth (cm)	Horizon	Color M/D	Structure	CaCO3 size, type	Consistence M/D	HCl	Texture	Boundary	Comments
181-232	BC2	10YR 6/4 w/ 10YR 5/4 &10YR 7/4	N/A		N/A	vstr	N/A	Gradual, smooth	
Depth (cm)	Horizon	Color M/D	Structure	CaCO3 size, type	Consistence M/D	HCl	Texture	Boundary	Comments
232-410 (+132)	C	10YR 6/6			N/A	vstr	N/A		Massive weakly horz lamination in lower 30cm

Mod = moderate; Str = strong; med = medium; Abk = angular blocky; Sbk = subangular blocky; nod = nodule
V. Hard = very hard; vstr = very strong; M/D = moist/dry

Table A.6. Test Trench 6 Surface soil (Unit IIc) Field description sheet, showing taxonomic characteristics (Soil Survey Staff, 1993) observed in the field.

Depth (cm)	Horizon	Color M/D	Structure	CaCO3 size, type	Consistence M/D	HCl	Texture	Boundary	Comments
0-16	Ap	7.5YR 4/3	Mod, med Abk	1%, 2-5 mm White hard	V. hard	N/A	N/A	Gradual, smooth	
Depth (cm)	Horizon	Color M/D	Structure	CaCO3 size, type	Consistence M/D	HCl	Texture	Boundary	Comments
16-69	Bk1	7.5YR 5/4 2% 7.5YR-4/3	Mod, med Abk	7-8%, 3-8 mm White hard	V. hard	vstr	N/A	Gradual, smooth	
Depth (cm)	Horizon	Color M/D	Structure	CaCO3 size, type	Consistence M/D	HCl	Texture	Boundary	Comments
69-95	Bk2	7.5YR 5/4, 7.5YR 6/6	Mod, cs Abk	3-5% 3-8 mm White hard	V. hard	vstr	N/A	Gradual, smooth	1% biocasts- 7.5YR 4/3
Depth (cm)	Horizon	Color M/D	Structure	CaCO3 size, type	Consistence M/D	HCl	Texture	Boundary	Comments
95-185	Bw	10YR 6/4	W	>1%, Same as above	Hard	str	N/A	Abrupt, smooth	5% biocasts- 7.5YR 4/3; Snail shell fragments
Depth (cm)	Horizon	Color M/D	Structure	CaCO3 size, type	Consistence M/D	HCl	Texture	Boundary	Comments
185-205	BC1	10YR 7/4	N/A	N/A	N/A	N/A	N/A	Abrupt, smooth	10% biocasts- 10YR 5/4

Mod = moderate; W = weak; med = medium; cs = coarse; Abk = angular blocky; V. Hard = very hard; vstr = very stong; str = strong; M/D = moist/dry

Table A.7. Test Trench 7 Surface soil (Unit Ib) Field description sheet, showing taxonomic characteristics (Soil Survey Staff, 1993) observed in the field.

Depth (cm)	Horizon	Color M/D	Structure	CaCO3 size, type	Consistence M/D	HCl	Texture	Boundary	Comments
0-15	Ap	7.5YR 4/4	Mod, med Abk	1%, 1-3 mm White hard	Hard	str	SiCL	Abrupt, smooth	
Depth (cm)	Horizon	Color M/D	Structure	CaCO3 size, type	Consistence M/D	HCl	Texture	Boundary	Comments
15-70	Bk1	5YR 4/4, 7.5YR 4/6	Mod, med Abk	2-3% 5 mm-0.5 cm White hard	Hard	str	SiCL	Abrupt, smooth	
Depth (cm)	Horizon	Color M/D	Structure	CaCO3 size, type	Consistence M/D	HCl	Texture	Boundary	Comments
70-150	Bk2	7.5YR 4/4 7.5YR 5/6	Mod, cs Abk	10-15%, nodules and rysoliths, 0.5-1.5 cm White hard	Hard	vstr	SiCL	Abrupt, smooth	>1% Mn coats- Black
Depth (cm)	Horizon	Color M/D	Structure	CaCO3 size, type	Consistence M/D	HCl	Texture	Boundary	Comments
150-189	Bk3	7.5YR 4/6	Str, med Abk	5-10%, 1-2 cm White hard	Hard	vstr	SiCL	Abrupt, smooth	>1% Mn coats- Black f1d; 1%, 1-5 mm in length Root traces infilled w/ carbonate (white)
Depth (cm)	Horizon	Color M/D	Structure	CaCO3 size, type	Consistence M/D	HCl	Texture	Boundary	Comments
189-218	BCk	7.5YR 5/6 7.5YR 5/8	Mod, med Abk	2-5%, 1-2.5 cm White hard	Hard	str	SiCL	Abrupt, smooth	Mn coats and root traces, Same as above

Mod = moderate; Str = strong; med = medium; cs = coarse; Abk = angular blocky; vstr = very strong; str = strong; SiCL = Silty Clay Loam; M/D = moist/dry

Table A.8. Test Trench 8 Surface soil (Unit Ib) Field description sheet, showing taxonomic characteristics (Soil Survey Staff, 1993) observed in the field.

Depth (cm)	Horizon	Color M/D	Structure	CaCO3 size, type	Consistence M/D	HCl	Texture	Boundary	Comments
0-12	A	5YR 4/4	W, cs Sbk	N/A	V. hard	N/A	SiCL	Gradual, smooth	
Depth (cm)	Horizon	Color M/D	Structure	CaCO3 size, type	Consistence M/D	HCl	Texture	Boundary	Comments
12-38	Bt	7.5YR 4/3	Mod, cs Abk	N/A	Hard	N/A	SiCL	Abrupt, smooth	1% Mn coats-Black
Depth (cm)	Horizon	Color M/D	Structure	CaCO3 size, type	Consistence M/D	HCl	Texture	Boundary	Comments
38-75	Bk1	7.5YR 4/3, 7.5YR 4/4	Mod, med Abk	3%, 3-8 mm White hard nod	Hard	str	SiCL	Abrupt, smooth	
Depth (cm)	Horizon	Color M/D	Structure	CaCO3 size, type	Consistence M/D	HCl	Texture	Boundary	Comments
75-123	Bk2	Same as above	Mod, med Abk	10%, 5 mm-1 cm White hard nod	Hard	str	SiCL	Gradual, smooth	
Depth (cm)	Horizon	Color M/D	Structure	CaCO3 size, type	Consistence M/D	HCl	Texture	Boundary	Comments
123-179	BC	10YR 7/4, 5YR 4/4, 5YR5/6	W, cs Abk	3%, 1-2 cm White hard nod	Hard	str	L	Abrupt, smooth	
Depth (cm)	Horizon	Color M/D	Structure	CaCO3 size, type	Consistence M/D	HCl	Texture	Boundary	Comments
179-193	C2	7.5YR 8/3, 7.5YR 6/6	N/A	1%, 2-3 cm White hard nod	N/A	str	N/A	N/A	

Mod = moderate; W = weak; med = medium; cs = coarse; Abk = angular blocky; nod = nodule; str = strong; SiCL = Silty Clay Loam; L = Loam; M/D = moist/dry

APPENDIX B

Test Trench and Vertical Profiles

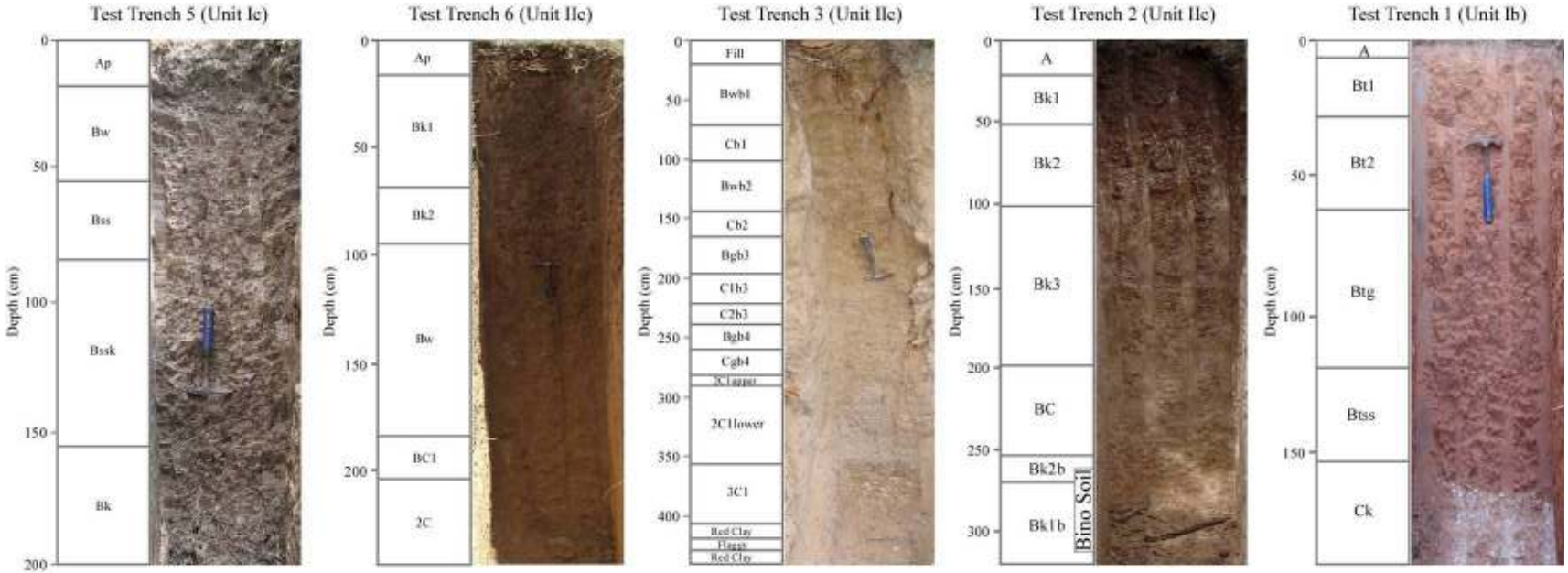

Figure B.1. Field photos of Test Trenches 5, 6, 3, 2, and 1 showing taxonomic soil horizons and depth of horizons. Photo plate is oriented top-down from north to south.

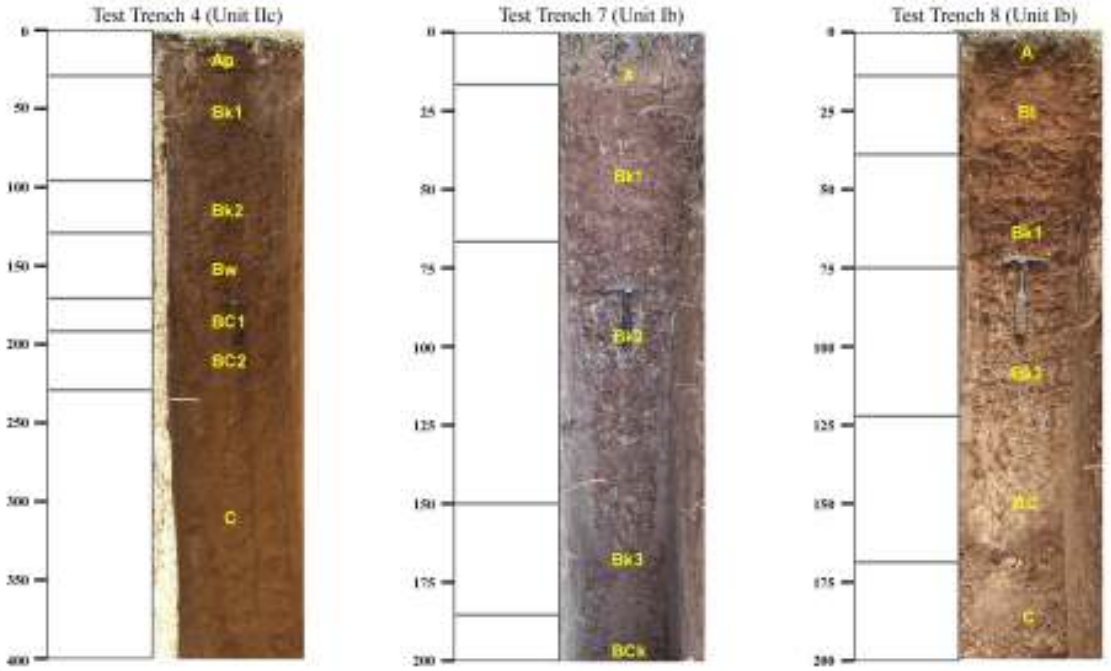

Figure B.2. Field photos of Test Trenches 4, 7, and 8, showing taxonomic soil horizons and depth of horizons. Photo plate is oriented right to left from north to south.

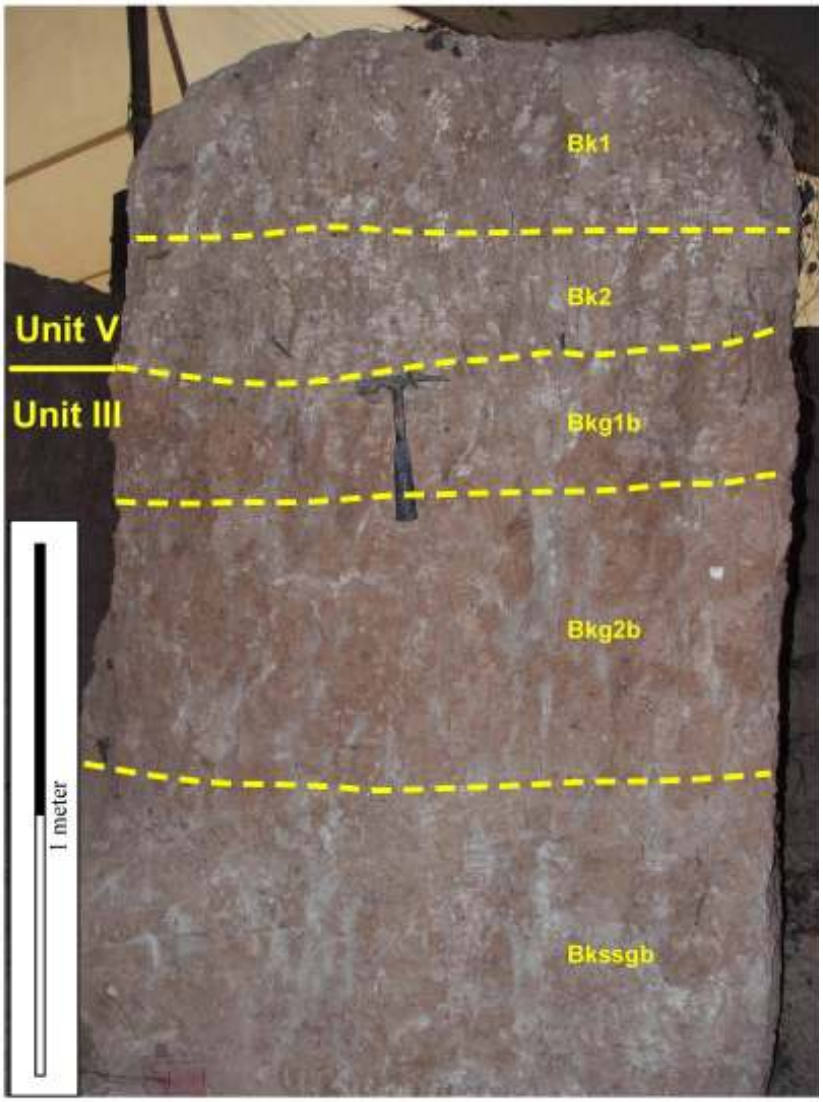

Figure B.3. Photo of Profile 1 (Unit III), showing taxonomic soil horizons and horizon boundaries.

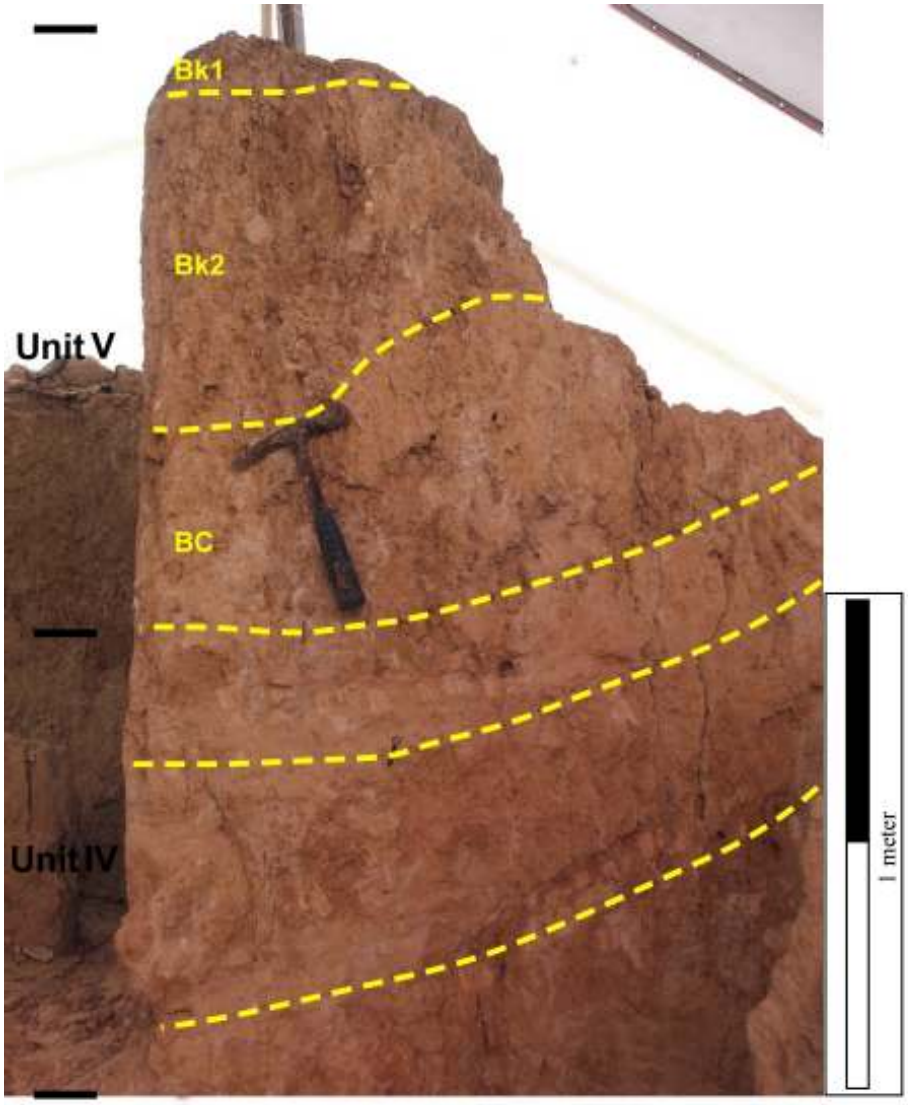

Figure B.4. Photo of Profile 2 (Unit IV), showing morphological soil horizons and horizon boundaries. Unit IV shown with pedogenic properties inherited from erosion and redeposition of the Boncap paleosol.

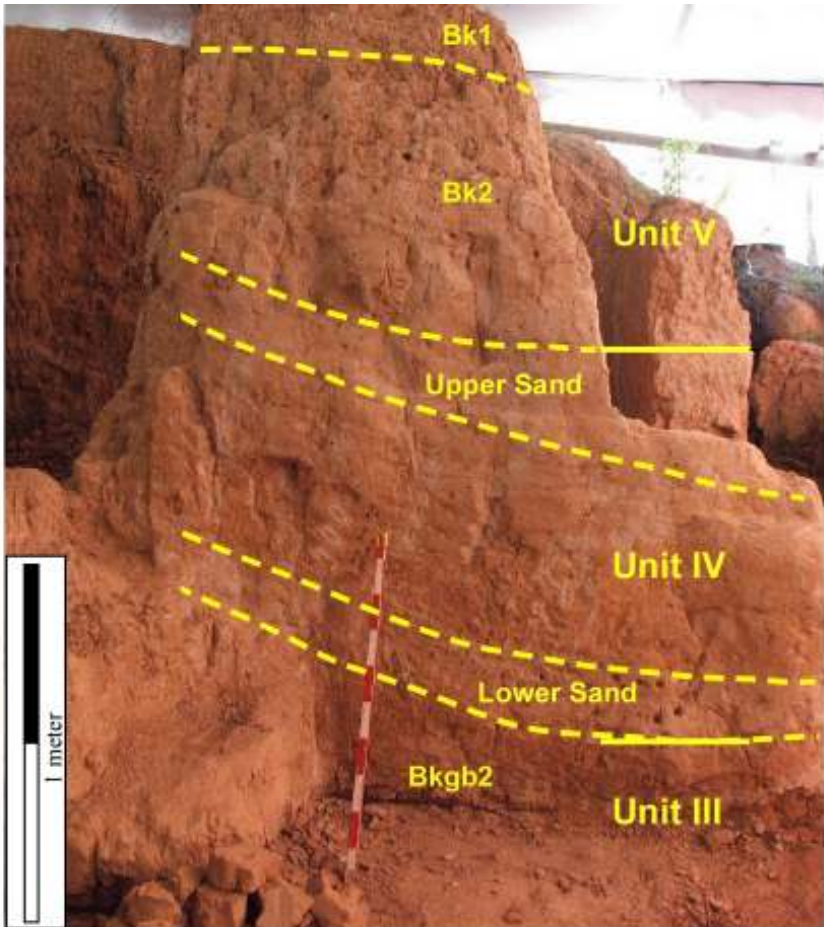

Figure B.5. Photo of Profile 2 (Units III, IV, and V), showing morphological soil horizons, horizon boundaries, and stratigraphic contacts.

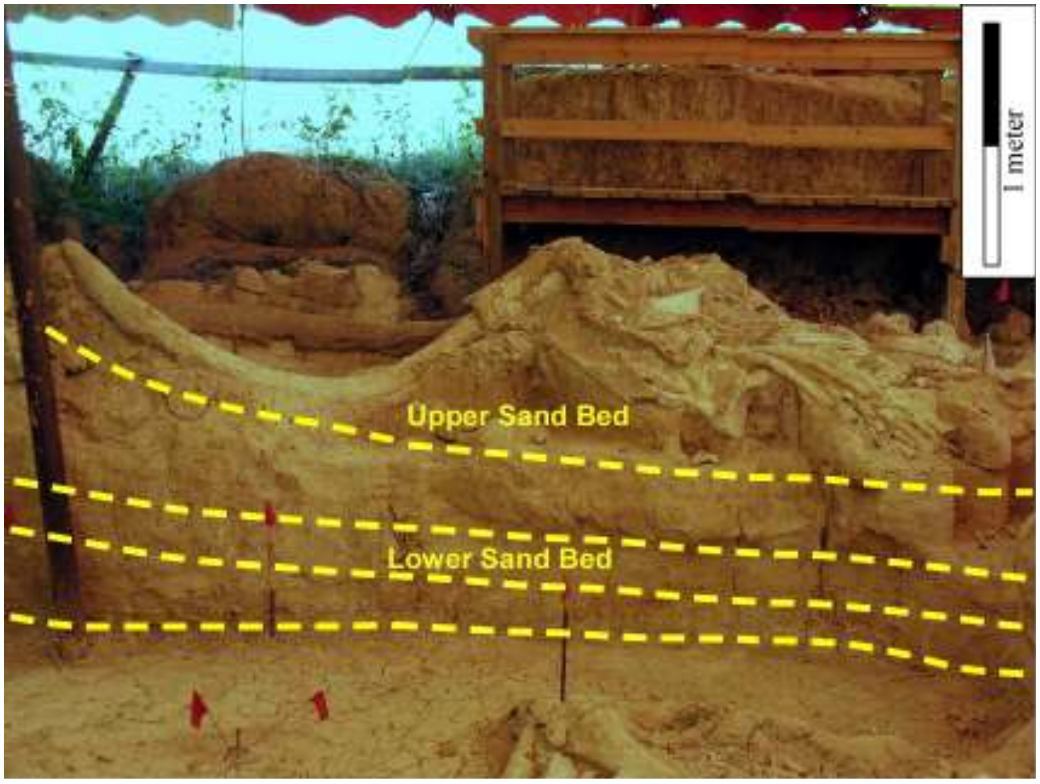

Figure B.6. Photo of the Bull Profile (Unit IV), showing two finely laminated sand beds and interbedded silty clay sediments.

APPENDIX C

Wall Profiles

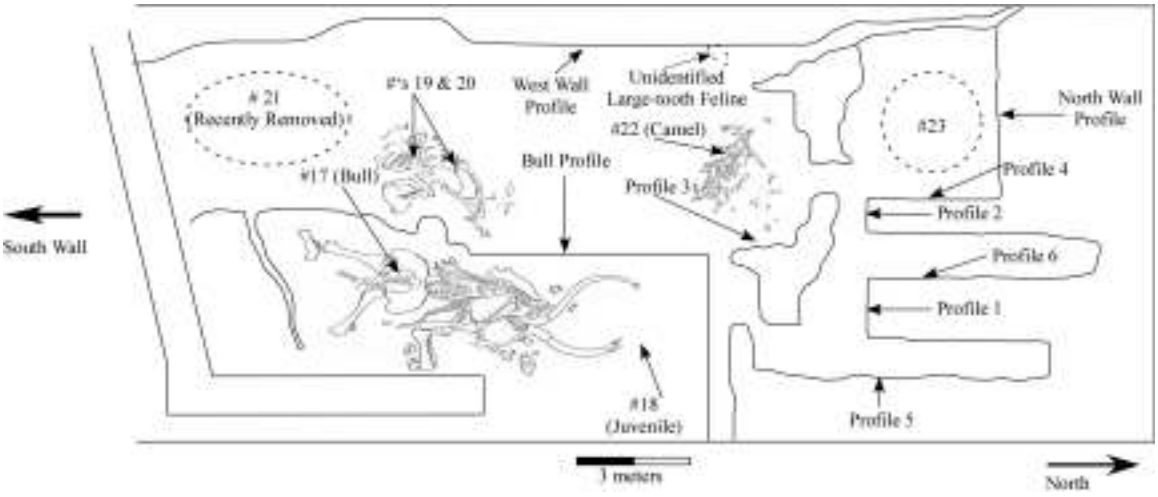

Figure C.1. Plan map of Phase II and III excavation area, showing associated animals, vertical profiles, and wall profiles.

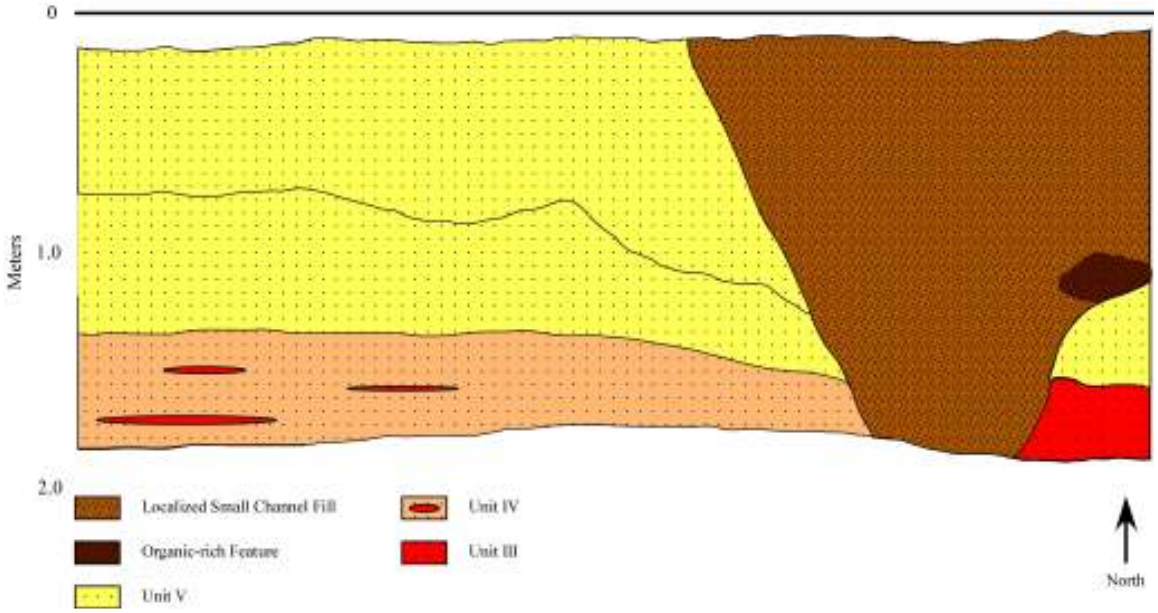

Figure C.2. North wall profile in Phase II and III excavation area, showing associated facies and allostratigraphic units.

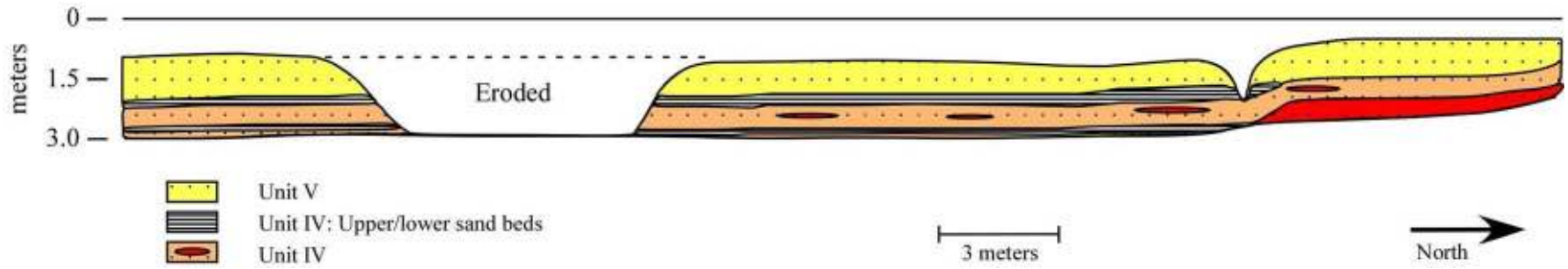

Figure C.3. West wall profile in Phase II and III excavation area, showing associated facies and allostratigraphic units.

APPENDIX D

Particle Size Distribution Analysis

Table D.1. Particle size analysis (Gee and Bauder, 1986) of bulk sediment samples obtained from test trenches and vertical profiles, showing Hydrometer temperature readings, corrected reading, and percent clay, silt, and sand for each sample.

Sample	Bulk Sample Dry Wt. (g)	Hydrometer Reading	Hydrometer Temp.	Corrected Reading	Sample Wt. After Drying	% Clay	% Silt	% Sand
TT1A	50.0	9.0	24	10.4	26.3	20.9	52.6	26.6
TT1Bt1	50.0	9.5	24	10.9	28.6	21.9	57.2	20.9
TT1Bt2	50.0	12.0	24	13.4	25.1	26.9	50.1	23.0
TT1Btss	50.0	20.0	24	21.4	18.1	42.9	36.1	21.0
TT1Btg	50.0	18.5	24	20.0	19.5	39.9	39.0	21.1
TT2A	50.0	15.0	23	16.1	15.2	32.1	37.4	30.4
TT2Bk1	50.0	18.0	23	19.1	11.0	38.2	39.9	22.0
TT2Bk2	50.0	19.0	23	20.1	6.8	40.2	46.2	13.6
TT2Bk3	50.0	18.0	23	19.1	5.8	38.2	50.3	11.5
TT2Bk1b	50.1	13.0	23	14.1	11.6	28.1	48.7	23.2
TT2Bk2b	50.0	15.0	23	16.1	7.1	32.2	53.7	14.2
TT2BC	50.0	13.0	23	14.1	11.1	28.2	49.7	22.1
TT3Bwb1	50.0	9.0	23	10.1	22.3	20.2	35.3	44.5
TT3Cb1	50.0	6.5	23	7.6	31.1	15.2	22.7	62.1
TT3Bwb2	50.0	11.0	23	12.1	16.7	24.2	42.4	33.5
TT3Cb2	50.0	3.0	23	4.1	40.3	8.2	11.3	80.5
TT3Bgb3	50.0	10.0	23	11.1	17.9	22.2	42.0	35.8
TT3C1b3	50.0	10.0	23	11.1	21.7	22.2	34.5	43.3
TT3C2b3	50.0	6.0	23	7.1	34.9	14.2	16.1	69.7
TT3Bgb4	50.0	16.5	23	17.6	10.4	35.2	44.0	20.8
TT3Cgb4	50.0	8.5	23	9.6	27.7	19.2	25.5	55.3
TT5Ap	50.0	13.0	23	14.1	12.5	28.2	46.9	24.9
TT5Bw	50.0	17.0	23	18.1	9.9	36.2	44.1	19.7
TT5Bss	50.0	18.5	23	19.6	9.1	39.2	42.6	18.3
TT5Bssk	50.0	20.0	23	21.1	9.2	42.2	39.4	18.4
TT5Bk	50.0	16.0	23	17.1	7.4	34.2	51.1	14.8
P1Bk1	50.0	16.0	23	17.1	8.4	34.2	49.0	16.9
P1Bk2	50.0	13.5	23	14.6	10.7	29.2	49.4	21.4
P1Bkg1b	50.0	12.0	23	13.1	20.4	26.2	33.0	40.8
P1Bkg2b	50.0	13.0	23	14.1	17.1	28.2	37.7	34.2
P1Bkssg	50.0	15.0	23	16.1	11.6	32.2	44.6	23.2
P2Bk1	50.0	17.0	23	18.1	8.5	36.2	46.9	16.9
P2Bk2	50.0	13.0	23	14.1	11.6	28.2	48.6	23.2
P2BC	50.0	13.0	23	14.1	14.0	28.2	43.9	27.9
P2C	50.0	9.0	23	10.1	22.4	20.2	35.0	44.8
P2Bkg2b	50.0	13.0	23	14.1	12.6	28.2	46.7	25.1
P2Bkssgb	50.0	15.0	23	16.1	11.0	32.2	45.9	22.0
P3Cb1	50.0	9.0	23	10.1	18.9	20.2	42.0	37.9
P3Bkg2b	50.0	13.0	23	14.1	12.9	28.2	46.0	25.8
P3Cb2	50.0	14.0	23	15.1	8.8	30.2	52.2	17.6
P3Bkssgb	50.0	16.0	23	17.1	9.7	34.2	46.4	19.4
P3Marsh	50.0	15.5	23	16.6	12.9	33.2	41.0	25.8

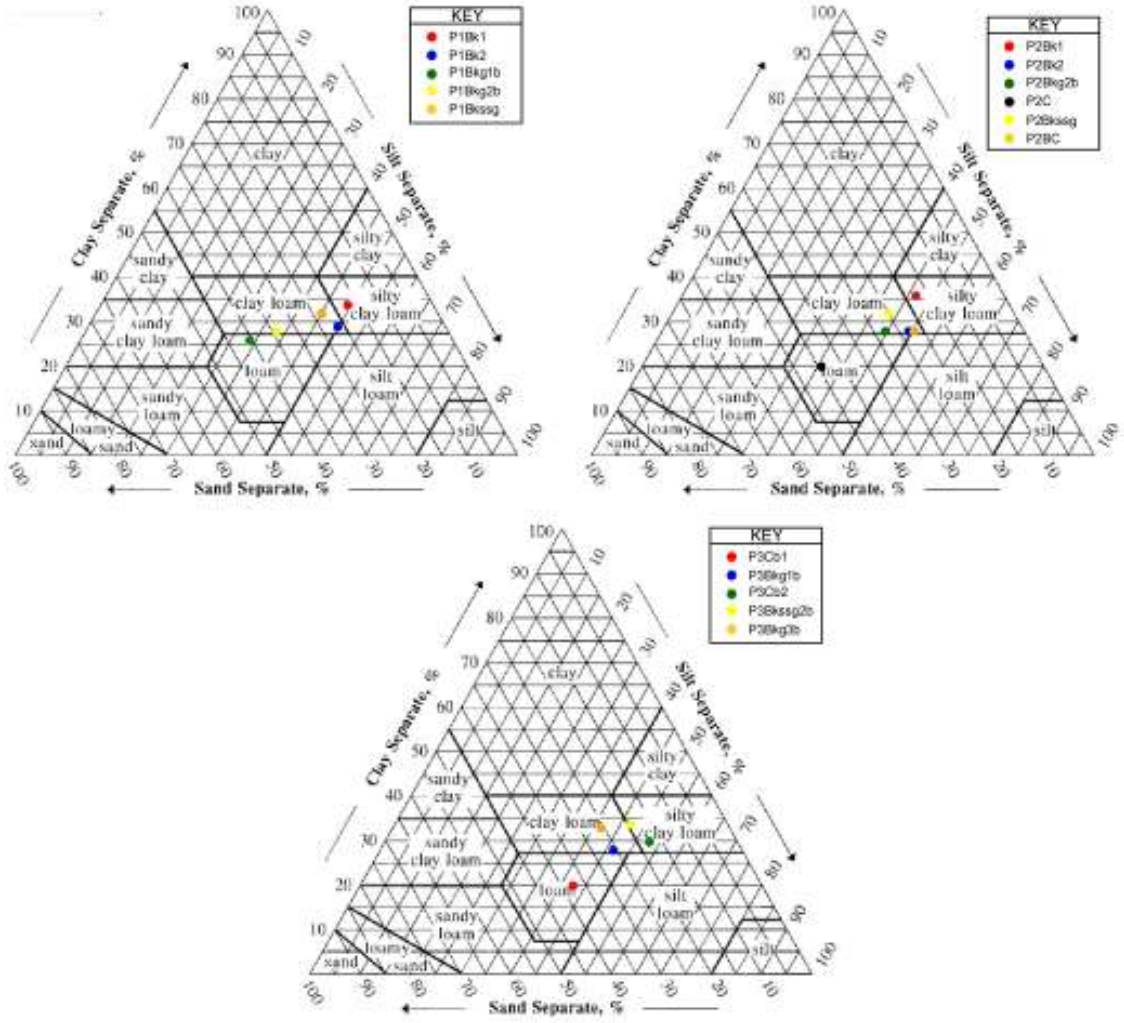

Figure D.1. Textural classes determined from particle size analysis for each profile sampled.

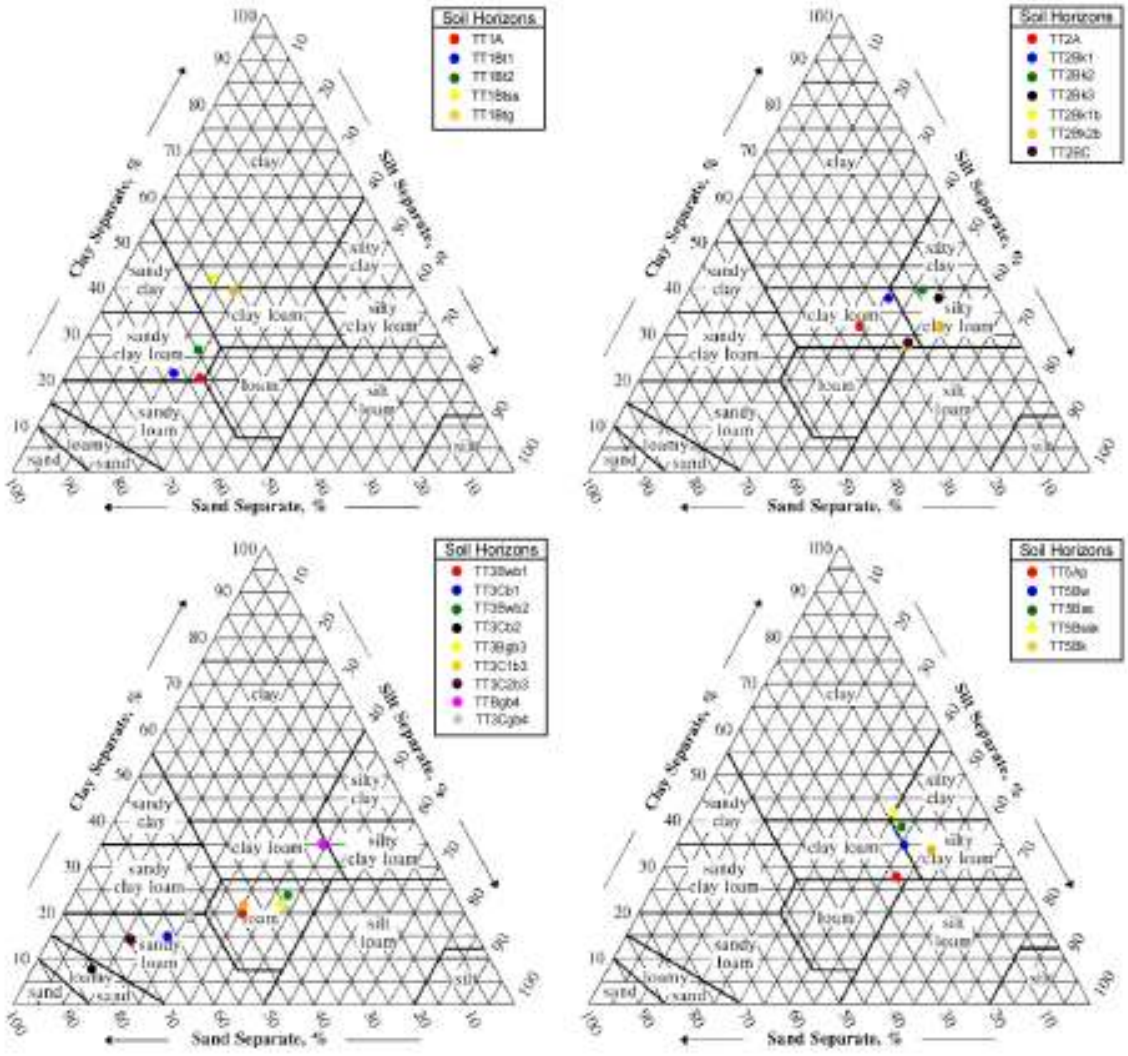

Figure D.2. Textural classes determined from particle size analysis for each test trench sampled.

APPENDIX E

Micromorphologic Descriptions

Table E.1. Detailed micromorphologic summary of all thin section samples.

Profile/ Horizon	Speciman Designation	% Composition Estimate		Distinguishing Properties/Features
Profile 1/ Bk1	P1-01	Skeletal grains%	55	Fine grain, carbonate-rich matrix with common silt-size quartz grains
		Pedogenic features%	20	Common carbonate nodules and soft masses Illuviated clay accumulation along biopores and grains
		Soil matrix%	25	Common Fe/Mn concentrations with embedded silt
Profile 1/ Bk2/Bkg Contact	P1-02	Skeletal grains%	65	Fine grain carbonate-rich matrix (similar to above) Few illuviated clay features (i.e. pore linings)
		Pedogenic features%	15	Abundant calcium carbonate nodules and soft masses Abundant organic material (i.e. roots, root nodes)
		Soil matrix%	20	Common Fe/Mn concretions with difuse boundaries, engulfing surrounding matrix materia Abundant biopores and soil pores
Profile 1/ Bkg2b	P1-03	Skeletal grains%	25	Slightly coarser grain, reduced matrix with a slight bimasepic plasmic fabric
		Pedogenic features%	10	Abundant calcium carbonate nodules and soft masses Common septarian shrinkage cracking within
		Soil matrix%	65	carbonate nodules, showing sparry calcite development Sparse Fe staining throughout thin section Common biopores throughout thin section
Profile 1/ Bkssgb3	P1-04	Skeletal grains%	35	Fine grain matrix showing mosepic plasmic fabric Abundant carbonate nodules, showing
		Pedogenic features%	25	septarian shrinkage cracks and formation of microspar Abundant root pores, some infilled with
		Soil matrix%	40	detrital silt and matrix material Few Fe/FeMn masses and concentrations Very few K-feldspar grains, showing little weathering Possible gastropod fragment
Profile 2/ BC	P2-01a	Skeletal grains%	55	Well rounded, well sorted fine silt Finely laminated
		Pedogenic features%	10	Fe staining and CaCO3 accumulation along laminations
		Soil matrix%	35	

Profile 2/ C	P2-01b	Skeletal grains%	70	Well rounded, well sorted fine silt Finely laminated
		Pedogenic features%	10	Fe staining and CaCO3 accumulation along laminations
		Soil matrix%	20	
Profile 3/ C	P3-01	Skeletal grains%	55	Fine-grain CaCO3-rich clay matrix engulfing fine silt to silt Abundant Fe/Mn concentrations and staining of matrix
		Pedogenic features%	10	Lg. root pores with common root fragments Few areas of illuviated clay accumulations,
		Soil matrix%	35	primarily along root pores Abundant Fe staining of matrix
Profile 3/ Bkg1b/2b	P3-02	Skeletal grains%	35	Fine-grain CaCO3-rich clay matrix w/ embedded sand-size grainsfine silt to silt-size quartz grains
		Pedogenic features%	20	and few larger fine sand-size grains Sparse Fe accumulations
		Soil matrix%	45	Common biopores and soil cracks Some CaCO3 accumulation within the matrix and (microspar) along biopores CaCO3 replaced bone/organic features Few K-feldspar and clinopyroxene grains
Profile 3/ Cb1/Bkg	P3-03	Skeletal grains%	40	Similar matrix as P3-01, w/ slightly finer quartz grain size and abundance
		Pedogenic features%	20	Very few Fe/Mn nodules (~500 μm in dia.) Biopores infilled with fine-grain detrital clay
		Soil matrix%	40	Few biopores with illuviated clay argillans CaCO3 replaced bone/plant material/fragments
Profile 3/ Cb1	P3-04	Skeletal grains%	20	Drab matrix with common silt-size quartz grains Common Fe/Mn and organic features
		Pedogenic features%	20	embedded in biopore infilled matrix Very abundant biopores infilled with
		Soil matrix%	60	fine clay matrix
Profile 3/ Bkgb2	P3-05	Skeletal grains%	20	Carbonate-rich fine-grain matrix with abundant embedded silt-size quartz grains
		Pedogenic features%	25	Abundant CaCO3 soft masses and nodules Common Fe/Mn masses and concentrations
		Soil matrix%	55	Abundant biopores, few infilled with detrital matrix material

Profile 3/ Bkssgb2	P3-06	Skeletal grains%	30	-Similar matrix as P1 Bkssgb -Abundant CaCO3 nodules and soft masses
		Pedogenic features%	25	-Common Fe/Mn concentrations and argillans -Carbonate nodule with megaquartz overgrowth
		Soil matrix%	45	
Profile 4/ Cb1	P4-01	Skeletal grains%	60	-Carbonate-rich Silt to very fine sand matrix -Abundant silt to fine sand-size carbonate features
		Pedogenic features%	10	-Few fairly unweathered K-feldspar grains -Possible fining upward lamina throughout
		Soil matrix%	30	
Profile 4/ Cb2	P4-02	Skeletal grains%	15	Slightly finer matrix than P4-02 with similar carbonate features
		Pedogenic features%	10	Common Fe staining in the form of linear features between lamina
		Soil matrix%	75	few small root pores and root nodes with preserved whewellite
Bull Upper	Bull-upper	Skeletal grains%	10	Abundant carbonate in matrix Fine-grain clay matrix with
		Pedogenic features%	20	weak mosepic plasmic fabric, ingulfing primarily v. fine to fine sand-size quartz grains
		Soil matrix%	70	Very few unweathered K-feldspars Abundant biopores infilled w/ detrital clay and fine silt
Bull Middle	Bull-middle	Skeletal grains%	5	Similar carbonate rich matrix as Bull-upper with no apparent plasmic fabric
		Pedogenic features%	25	Abundant silt to v. fine sand-size quartz grains Abundant biopores (e.g. burrows and root pores)
		Soil matrix%	70	infilled with detrital clay and silt Some root pores with organic fragments remaining
Bull Lower/C	Bull-L/C	Skeletal grains%	10	Same matrix and plasmic fabric as Bull-upper Few unweathered K-feldspar grains and
		Pedogenic features%	20	v. few clinopyroxixe (CPX) grains Carbonate-replaced organic features,
		Soil matrix%	70	showing cellular structure Similar infilled biopores as Bull-upper and Bull-middle Common Fe staining and Fe/Mn accumulation

Bull Marsh	Bull-Marsh	Skeletal grains%	10	Similar matrix, plasmic fabric and quartz grain size and abundance as Bull-upper
		Pedogenic features%	25	Common Fe/Mn concretions and banded nodules
		Soil matrix%	65	Both Fe/Mn concretions and nodules w/ embedded matrix material Abundant carbonate nodules and hard masses Organic (e.g. plant/root) material, some root nodes Common biopores (e.g. root traces and possible burrows) Some Fe staining of matrix and carbonate features Very few small relatively unweathered K-feldspar grains
TT1/ A	TT1-01	Skeletal grains%	25	silty clay matrix with abundant quartz grains and few unweathered K-feldspar grains
		Pedogenic features%	40	Very abundant illuviated clay in the form of grain argillans Common roots, few with preserved whewellite present
		Soil matrix%	35	
TT1/ Bt1	TT1-02	Skeletal grains%	25	Silty clay matrix slightly finer matrix-supported quartz grains
		Pedogenic features%	45	Very abundant illuviated clays in the form of grain argillans and biopore infillings Abundant Fe staining of matrix and overprinting of argillans
		Soil matrix%	30	Few Fe/Mn concretions with both sharp and diffuse boundaries Fewer roots than TT1-01, some with whewellite preserved
TT1/ Bt2	TT1-03	Skeletal grains%	30	Clay matrix with common sand-size embedded quartz grains and few K-feldspar grains
		Pedogenic features%	40	Very abundant illuviated clay features including grain argillans and pore linings
		Soil matrix%	30	Common Fe staining of matrix and concentrations Few subangular chert grains, heavily Fe stained Much fewer roots than TT1-01 and TT1-02
TT1/ Btg	TT1-04	Skeletal grains%	25	Clay matrix showing sepic plasmic fabric and containing abundant coarse silt-size quartz grains
		Pedogenic features%	45	Abundant illuviated clays forming grain argillans
		Soil matrix%	30	Common Fe/Mn nodules and concentrations, nodules with both diffuse and sharp boundaries Much few roots than TT1-01, TT1-02 and TT1-03
TT1/ Btss	TT1-05	Skeletal grains%	25	Clay matrix with sepic plasmic fabric and containing similar quartz grains at TT1-04
		Pedogenic features%	45	Few illuviated clay features
		Soil matrix%	30	Common Fe/Mn concentrations and nodules, nodules with primarily sharp boundaries Preserved organic material Common biopores and soil cracks

TT2/ A	TT2-01	Skeletal grains%	30	Clay matrix with abundant silt to fine sand-size quartz grains
		Pedogenic features%	35	Common pedogenic carbonate nodules with distinct septarian shrinkage cracks
		Soil matrix%	35	Shrinkage cracks show sparry calcite development Few Fe/Mn nodules with sharp boundaries Common roots and root traces
TT2/ Bk1	TT2-02	Skeletal grains%	25	Same matrix as TT2-01
		Pedogenic features%	35	Very Abundant carbonate nodules, with common stress cutans and septarian shrinkage cracks Sparry calcite development within cracks
		Soil matrix%	40	Common (.25-.5 mm dia) Fe/Mn concretions engulfing surrounding matrix material
TT2/ Bk2	TT2-03	Skeletal grains%	15	Fine-grain, carbonate-rich matrix engulfing common silt to fine sand quartz grains
		Pedogenic features%	30	Common carbonate nodules with common shrinkage cracks Common apatite features throughout (possible bone material)
		Soil matrix%	55	Few illuviated clay argillans Large biopore infilled with detrital matrix material
TT2/ Bk3	TT2-04	Skeletal grains%	15	Carbonate-rich, drab-colored engulfing silt-size quartz grains Common Fe/Mn concentrations engulfing surrounding matrix
		Pedogenic features%	35	Common biopores, few with thin clay argillans Common stress/soil cracking
		Soil matrix%	50	
TT2/ BC	TT2-05	Skeletal grains%	10	Similar matrix a TT2-04 with slightly finer embedded quartz grains
		Pedogenic features%	30	Common angular carbonate nodules with common microspar overgrowths
		Soil matrix%	60	Fe argillans on carbonate nodules
TT2/ Bk1b	TT2-06	Skeletal grains%	15	Carbonate-rich fine-grain matrix with concentrations of larger embedded sand-size quartz grains
		Pedogenic features%	30	Common Fe/Mn accumulations throughout engulfing surrounding matrix
		Soil matrix%	55	Possible biopores infilled with detrital matrix and carbonate material

TT2/ Bk2b	TT2-07	Skeletal grains%	15	Very fine-grain, carbonate-rich matrix with fine silt to very fine sand
		Pedogenic features%	35	Common carbonate nodules with common septarian shrinkage cracking
		Soil matrix%	50	Common apatite features (possible bone fragments) Common Microcodium features at bases of root traces Very few illuviated clays
TT3/ Bwb2	TT3-03	Skeletal grains%	10	Fine-grain, carbonate-rich matrix Abundant carbonate nodules and masses
		Pedogenic features%	30	Abundant silt to fine sand-size carbonate grains Common microspar development along
		Soil matrix%	60	soil cracks and biopores Common Fe and Fe/Mn concentrations and staining
TT3/ Cb2	TT3-04	Skeletal grains%	75	Very carbonate-rich matrix (almost cemented appeared) Abundant carbonate masses and grains
		Pedogenic features%	10	Common Microcodium associated with root traces Common apatite features (possible bone fragments)
		Soil matrix%	15	
TT3/ Bgb3	TT3-05	Skeletal grains%	10	Similar, but finer-grained matrix than TT3-03 Same abundance and type of carbonate features as TT3-03,
		Pedogenic features%	30	with few hard masses diffused in matrix Same abundance and type of biopores as TT3-03
		Soil matrix%	60	
TT3/ C1b3	TT3-06	Skeletal grains%	50	Very fine-grain matrix (more fine than TT3-04) Possible fining upward lamina (mm-scale)
		Pedogenic features%	20	Abundant carbonate masses, grains, and concentrations along lamina
		Soil matrix%	30	Common Fe and Fe/Mn concentration in matrix
TT3/ C2b3	TT3-07	Skeletal grains%	35	Same as TT3-06 with more abundant carbonate dispersed throughout thin section
		Pedogenic features%	25	Weak nodules with common cracking Common apatite features
		Soil matrix%	40	Common recrystallized carbonate features

TT3/ Bgb4	TT3-08	Skeletal grains%	15	Fine-grain, carbonate-rich matrix
		Pedogenic features%	25	Very abundant carbonate masses, some with recrystallized (sparry calcite) carbonate
		Soil matrix%	60	Common Fe/Mn accumulations within matrix Few apatite features Abundant biopores, few infilled with detrital quartz silt and matrix material
TT3/ Cgb4	TT3-09	Skeletal grains%	20	Same as TT3-08 with slightly finer matrix and similar features
		Pedogenic features%	15	
		Soil matrix%	65	
TT5/ Ap	TT5-01	Skeletal grains%	10	Fine-grain clay matrix with mosepic plasmic fabric engulfing silt to very fine sand
		Pedogenic features%	30	Common Fe/Mn concretions, most with sharp boundaries Common organic material (i.e. root nodes, plant fragments)
		Soil matrix%	60	
TT5/ Bw	TT5-02	Skeletal grains%	15	Fine-grain matrix,drab in color compared to TT5-02 Common Fe/Mn redoximorphic features
		Pedogenic features%	10	(i.e. concretions and reduced masses) Common biopores (i.e. root nodes, roots, and root pores)
		Soil matrix%	75	
TT5/ Bss	TT5-03	Skeletal grains%	20	Same matrix with slight plasmic fabric Common carbonate nodules (bifurcated) with
		Pedogenic features%	25	shrinkage cracks Common organic features (i.e. roots and root nodes)
		Soil matrix%	55	Few small (.25-.5 mm dia) Fe/Mn concretions with sharp boundaries
TT5/ Bssk	TT5-04	Skeletal grains%	10	Same matrix as TT5-03 Very abundant carbonate nodules with
		Pedogenic features%	45	common septarian shrinkage cracks and stress cutans Microspar development within shrinkage cracks
		Soil matrix%	45	Common Fe/Mn concentrations Few Fe/Mn concretions with sharp boundaries Possible biopores
TT5/ Bk	TT5-05	Skeletal grains%	10	Similar matrix as TT5-04 with more abundant carbonate Few thin clay argillans
		Pedogenic features%	30	Common Fe/Mn masses and concretions
		Soil matrix%	60	

APPENDIX F

USGS Peak Stream Flow Data

Table E.1. Peak stream flow data from North Bosque River at Valley Mills, Texas, gage station # 8095200. Data represents peak stream flow in ft^3/sec recorded from October 4, 1959 to March, 20, 2006. For definitions of abbreviations see USGS-NWIS.

agency_cd 5s	site_no 15s	peak_dt 10d	peak_va 8s	peak_cd 27s	gage_ht 8s
USGS	8095200	10/4/1959	107000	5	40.22
USGS	8095200	1/8/1961	22400	5	30.47
USGS	8095200	10/10/1961	73500	5	38.82
USGS	8095200	10/9/1962	8990	5	20.1
USGS	8095200	9/22/1964	20200	5	29.35
USGS	8095200	5/16/1965	54000	5	38
USGS	8095200	4/25/1966	23400	5	31.91
USGS	8095200	4/11/1967	5380	5	14.61
USGS	8095200	5/11/1968	27800	6	34.45
USGS	8095200	5/7/1969	24800	6	32.84
USGS	8095200	10/30/1969	10300	6	20.6
USGS	8095200	10/27/1970	1860	6	9.59
USGS	8095200	10/20/1971	36700	6	36.67
USGS	8095200	4/24/1973	18600	6	28.54
USGS	8095200	9/17/1974	8220	6	18.15
USGS	8095200	4/8/1975	16100	6	26.69
USGS	8095200	6/25/1976	11900	6	22.49
USGS	8095200	5/1/1977	36800	6	36.88
USGS	8095200	5/3/1978	2000	6	9
USGS	8095200	5/4/1979	31600	6	35.48
USGS	8095200	5/15/1980	2000	6	9.7
USGS	8095200	6/16/1981	47100	6	38.26
USGS	8095200	5/6/1982	11900	6	22.5

USGS	8095200	5/31/1983	1890	6	9.21
USGS	8095200	3/21/1984	5320	6	14.78
USGS	8095200	10/19/1984	5310	6	14.76
USGS	8095200	6/6/1986	19700	6	29.67
USGS	8095200	5/29/1987	16800	6	27.33
USGS	8095200	6/1/1988	24500	6	32.7
USGS	8095200	3/29/1989	31800	6	35.53
USGS	8095200	4/26/1990	56900	6	39.1
USGS	8095200	6/3/1991	5610	6	14.02
USGS	8095200	12/21/1991	220000	6	44.6
USGS	8095200	2/4/1993	9790	6	15.85
USGS	8095200	5/11/1994	36600	6	30.55
USGS	8095200	5/8/1995	42400	6	32.48
USGS	8095200	8/30/1996	24700	6	26.27
USGS	8095200	2/21/1997	46500	6	35.64
USGS	8095200	3/16/1998	92000	6	39.4
USGS	8095200	12/10/1998	3580	6	10.6
USGS	8095200	6/15/2000	21300	6	27.08
USGS	8095200	3/12/2001	17400	6	24.04
USGS	8095200	3/20/2002	15800	6	23.28
USGS	8095200	9/19/2003	8090	6	15.32
USGS	8095200	5/1/2004	42600	6	34.78
USGS	8095200	11/17/2004	36200	6	33.36
USGS	8095200	3/20/2006	5690	6	13.6

APPENDIX G

SMADA DISTRIB 2.13 Output Data

Table E.1. SMADA, DISTRIB 2.13 output data from Log Pearson Type III distribution.

Distribution Analysis: Log Pearson Type III
Summary of Data
First Moment (mean) = 29638.9
Second Moment = 1.329e09
Skew = 3.291e+00

Point Number	Weibull Probability	Actual Value	Predicted Value	Standard Deviation	Point Number	Weibull Probability	Actual Value	Predicted Value	Standard Deviation
1	0.0208	1860	1461.395	661.7704	25	0.5208	21300	19559.66	3489.868
2	0.0417	1890	2211.479	792.233	26	0.5417	22400	20725.05	3683.727
3	0.0625	2000	2872.72	889.6567	27	0.5625	23400	21960.22	3889.129
4	0.0833	2000	3497.127	975.3981	28	0.5833	24500	23273.03	4107.41
5	0.1042	3580	4104.846	1056.871	29	0.6042	24700	24672.59	4340.196
6	0.125	5310	4706.429	1137.581	30	0.625	24800	26169.6	4589.486
7	0.1458	5320	5308.428	1219.468	31	0.6458	27800	27776.72	4857.765
8	0.1667	5380	5915.415	1303.713	32	0.6667	31600	29509.09	5148.155
9	0.1875	5610	6530.884	1391.088	33	0.6875	31800	31384.97	5464.633
10	0.2083	5690	7157.704	1482.126	34	0.7083	36200	33426.68	5812.34
11	0.2292	8090	7798.378	1577.222	35	0.7292	36600	35661.9	6198.027
12	0.25	8220	8455.2	1676.683	36	0.75	36700	38125.39	6630.719
13	0.2708	8990	9130.357	1780.768	37	0.7708	36800	40861.7	7122.736
14	0.2917	9790	9826.006	1889.71	38	0.7917	42400	43929.07	7691.292
15	0.3125	10300	10544.32	2003.737	39	0.8125	42600	47405.52	8361.089
16	0.3333	11900	11287.56	2123.08	40	0.8333	46500	51398.7	9168.745
17	0.3542	11900	12058.09	2247.987	41	0.8542	47100	56062.77	10170.69
18	0.375	15800	12858.41	2378.729	42	0.875	54000	61628.66	11458.16
19	0.3958	16100	13691.24	2515.613	43	0.8958	56900	68463.84	13188.34
20	0.4167	16800	14559.51	2658.987	44	0.9167	73500	77202.6	15656.19
21	0.4375	17400	15466.46	2809.249	45	0.9375	92000	89077.09	19489.25
22	0.4583	18600	16415.64	2966.864	46	0.9583	107000	106981.1	26324.71
23	0.4792	19700	17411	3132.37	47	0.9792	220000	140766.9	42570.47
24	0.5	20200	18457.28	3306.445					

Predictions

Exceedence Probability	Return Period	Calculated Value	Standard Deviation	Deviation
0.995	200	223022.1	98701.43	
0.99	100	180932.9	67189.94	
0.98	50	142882.1	43727.18	
0.96	25	108859.5	27114.71	
0.9	10	70031.77	13609.59	
0.8	5	45265.34	7945.341	
0.667	3	29537.92	5153.001	
0.5	2	18457.28	3306.445	

APPENDIX H

HEC RAS 4.0 Beta Output Data

Table H.1. Detail steady flow analysis summary table computed from HEC RAS 4.0 Beta Flow Analysis for 25 year flood event. For definitions of abbreviations see USGS-NWIS.

Reach	River Sta	Profile	Q Total (cfs)	Min Ch El (ft)	W.S. Elev (ft)	Crit W.S. (ft)	E.G. Elev (ft)	E.G. Slope (ft/ft)	Vel Chnl (ft/s)	Flow Area (sq ft)	Top Width (ft)	Froude # Chl
1	8	PF 1	108859	360	410.45		410.53	0.000062	4.27	63559.06	3700	0.11
1	7	PF 1	108859	361.3	410.25		410.36	0.000077	4.73	56609.11	3300	0.12
1	6	PF 1	108859	363.8	409.48		409.84	0.000204	7.51	32127.9	1800	0.2
1	5	PF 1	108859	364.8	409.33		409.61	0.000172	6.82	35637.26	1996.67	0.18
1	4	PF 1	108859	364.5	409.46		409.49	0.000015	2.04	97068.11	3600	0.05
1	3	PF 1	108859	364.2	409.25		409.45	0.000143	6.25	43137.32	2812.3	0.17
1	2	PF 1	108859	366	408.7	398.14	409	0.000202	7.25	34629.83	2100	0.2
1	1	PF 1	108859	368	390	390	405.75	0.012032	36.24	4179.19	299.97	1.37

Table H.2. Detail steady flow analysis summary table computed from HEC RAS 4.0 Beta Flow Analysis for 50 year flood event. For definitions of abbreviations see USGS-NWIS.

Reach	River Sta	Profile	Q Total (cfs)	Min Ch El (ft)	W.S. Elev (ft)	Crit W.S. (ft)	E.G. Elev (ft)	E.G. Slope (ft/ft)	Vel Chnl (ft/s)	Flow Area (sq ft)	Top Width (ft)	Froude # Chl
1	8	PF 1	142882	360	421.03		421.07	0.000024	3.01	102716.4	3700	0.07
1	7	PF 1	142882	361.3	420.95		421	0.000029	3.34	91929.92	3300	0.08
1	6	PF 1	142882	363.8	420.63		420.8	0.000082	5.51	52186.63	1800	0.13
1	5	PF 1	142882	364.8	420.57		420.71	0.000067	4.95	58114.6	2000	0.12
1	4	PF 1	142882	364.5	420.63		420.65	0.000009	1.8	137265.7	3600	0.04
1	3	PF 1	142882	364.2	420.55		420.64	0.000046	4.1	75352.42	2850	0.1
1	2	PF 1	142882	366	420.36	390	420.49	0.000068	4.94	59109.69	2100	0.12
1	1	PF 1	142882	368	390	390	417.13	0.020718	47.56	4180.37	300.13	1.8

Table H.1. Detailed summary of channel cross section output data computed from HEC RAS 4.0 Beta Flow Analysis for a 25 year flood event. For definitions of abbreviations see HEC RAS 4.0 Beta at U. S. Army Corp of Engineers.

Plan: Plan 01	Bosque	1 RS: 8	Profile: PF 1			
E.G. Elev (ft)		410.53	Element	Left OB	Channel	Right OB
Vel Head (ft)		0.08	Wt. n-Val.	0.05	0.035	0.05
W.S. Elev (ft)		410.45	Reach Len. (ft)	2500	2500	2500
Crit W.S. (ft)			Flow Area (sq ft)	10769.04	4944.84	47845.18
E.G. Slope (ft/ft)		0.000062	Area (sq ft)	10769.04	4944.84	47845.18
Q Total (cfs)		108859	Flow (cfs)	17032.36	21111.04	70715.59
Top Width (ft)		3700	Top Width (ft)	600	100	3000
Vel Total (ft/s)		1.71	Avg. Vel. (ft/s)	1.58	4.27	1.48
Max Chl Dpth (ft)		50.45	Hydr. Depth (ft)	17.95	49.45	15.95
Conv. Total (cfs)		13830100	Conv. (cfs)	2163892	2682073	8984130
Length Wtd. (ft)		2500	Wetted Per. (ft)	612.53	108.28	3012.45
Min Ch El (ft)		360	Shear (lb/sq ft)	0.07	0.18	0.06
Alpha		1.82	Stream Power (lb/ft s)	0.11	0.75	0.09
Frctn Loss (ft)		0.17	Cum Volume (acre-ft)	5200.53	1471.79	8065.82
C & E Loss (ft)		0	Cum SA (acres)	328.28	33.98	467.29

Table H.4. Detailed summary of channel cross section output data computed from HEC RAS 4.0 Beta Flow Analysis for a 50 year flood event. For definitions of abbreviations see HEC RAS 4.0 Beta at U. S. Army Corp of Engineers.

Plan: Plan 01	Bosque	1 RS: 8	Profile: PF 1			
E.G. Elev (ft)		421.07	Element	Left OB	Channel	Right OB
Vel Head (ft)		0.04	Wt. n-Val.	0.05	0.035	0.05
W.S. Elev (ft)		421.03	Reach Len. (ft)	2500	2500	2500
Crit W.S. (ft)			Flow Area (sq ft)	17118.88	6003.15	79594.39
E.G. Slope (ft/ft)		0.000024	Area (sq ft)	17118.88	6003.15	79594.39
Q Total (cfs)		142882	Flow (cfs)	22609.65	18087.1	102185.3
Top Width (ft)		3700	Top Width (ft)	600	100	3000
Vel Total (ft/s)		1.39	Avg. Vel. (ft/s)	1.32	3.01	1.28
Max Chl Dpth (ft)		61.03	Hydr. Depth (ft)	28.53	60.03	26.53
Conv. Total (cfs)		29272310	Conv. (cfs)	4632051	3705513	20934750
Length Wtd. (ft)		2500	Wetted Per. (ft)	623.11	108.28	3023.03
Min Ch El (ft)		360	Shear (lb/sq ft)	0.04	0.08	0.04
Alpha		1.35	Stream Power (lb/ft s)	0.05	0.25	0.05
Frctn Loss (ft)		0.07	Cum Volume (acre-ft)	8831.37	1814.89	13165.57
C & E Loss (ft)		0	Cum SA (acres)	328.28	33.98	468.72

REFERENCES

Aitken, M. J., and Bowman, S. G. E. 1975, Thermoluminescent dating: Assessment of alpha particle contribution: Archaeometry, v. 17, p. 132-138.

Aitken, M.J., 1985, Thermoluminescence Dating: Academic Press, New York, 359 pp.

Aitken, M.J., 1998, An Introduction to Optical Dating: The dating of Quaternary Sediments by the use of Photon-stimulated luminescence: Oxford University Press, New York, 267 pp.

Agenbroad, L.D., 2004, North American Proboscideans: Mammoths: The State of Knowledge, 2003: Quaternary International, p. 126-128 (2005) p. 73-92.

Advanced Geosciences Inc., 2006, Instruction manual for SuperSting R8 automatic earth resistivity and IP system: Austin, Texas.

Baker, V.R., 1978, Large-scale erosional and depositional features of the Channeled Scabland, in Baker, V.R., and Nummedal, D. (Eds.), The Channel Scabland: NASA, Washington, D.C., p. 81-115.

Bishop, A.L., 1977, Flood Potential of the Bosque Basin: Baylor Geological Studies Bull., No. 33, p. 37.

Brakenridge, G.R., 1984, Alluvial stratigraphy and radiocarbon dating along the Duck River, Tennessee: Implications regarding flood-plain origin: Geological Society of America Bulletin, v. 95, p. 9-25.

Brewer, R., 1976, *Fabric and Mineral Analysis of Soils*, 2nd edition: Huntington, New York, Robert E. Krieger Publishing Co., 482 p.

Bullock, P, Fédoroff, N., Jungerius, A., Stoops, G., Tursina, T., and Babel, U., 1985, *Handbook for Soil Thin Section Description*: Wolverhampton, UK, Waine Research Publications, 152 p.

CEE-UCF, 1999, Stormwater Management and Design Aid, Distribution Analysis 2.13: Civil for Environmental Engineering, University of Central Florida, Orlando, Florida, http://cee.ucf.edu/software/.

Cheng, H., Edwards, R.L., Hoff, J., Gallup, C.D., Richards, D.A., Asmerom, Y., 2000, The half-lives of uranium-234 and thorium-230, Chemical Geology, no. 169, p. 17-33.

Claerbout J. F. and Muir, F., 1973, Robust modeling with erratic data: Geophysics, v. 38, p. 826-844.

Darwin R. L., Ferring, R.C., and Ellwood, B.B., 1990, Geoelectric stratigraphy and subsurface evaluation of quaternary stream sediments at the Cooper Basin, NE Texas: Geoarchaeology, v., 5 p. 53-79.

Davis, L.C., Eshelman, R.E., and Prior, J.C., 1972, A Primary Mammoth Site with Associated Fauna in Pottawattamie County, Iowa: Iowa Academy of Science Proceedings, v. 79, n. 2, p. 62-65.

Dahlin, T. and Zhou, B., 2004, A numerical comparison of 2D resistivity imaging with 10 electrode arrays: Geophysical Prospecting, v. 52, p. 379-398.

Dutrow, B.L., 1980, Metric Analysis of a Late Pleistocene Mammoth Assemblage, Hot Springs, South Dakota: unpublished Southern Methodist University Master of Science thesis, p. 165.

Dworkin, S.I., Nordt, L.C ., and Atchley, S.C., 2005, Determining terrestrial paleotemperatures using the oxygen isotopic composition of pedogenic carbonates, Earth and Planetary Science Letters, v. 237 p. 56-68.

Ehleringer, J.R., Cerling, T.E., and Helliker, B.R., 1997, C_4 photosynthesis, atmospheric CO_2, and climate: Oecologia, v. 112, p. 285-299.

Elder, W.R., 1965, Urban Geology of Greater Waco Part II: Soils: Baylor Geological Studies Bull., n.9, 66 p.

Epps, L.W., 1973, A Geologic History of the Brazos River: Baylor Geological Studies Bull., n. 24, p. 45.

Falconer, H., 1863, On the American fossil elephant of the regions bordering the Gulf of Mexico (*E. columbi* Falc.); with general observations on the living and extinct Species: Nat. Hist. Rev., v. 5, n. 3, p. 43-114.

Feathers, J.K., Holliday, V.T., and Meltzer, D.J., 2006, Optically stimulated luminescence dating of Souther High Plains archaeological sites: Journal of Archaeological Sciences, v. 33, p. 1651-1665.

Flawn, P.T., Burket, J.M., 1965, Urban Geology of Greater Waco Part 1: Geology: Baylor Geological Studies Bull., n. 8, p. 45.

Forman, S.L. and Pierson, J., 2002, Late Pleistocene luminescence chronology of loess deposition in the Missouri and Mississippi river valleys, United States: Palaeogeography Palaeoclimatology Palaeoecology, v. 186, n. 1-2, p. 25-46.

Fox, F.W., Smith, C.B., and Lintz, D.O., 1992, Herd Bunching at the Waco Mammoth Site: Preliminary Investigations, 1978-1987. Pp. 51, *in* J.W. Fox, C.B. Smith, and K.T. Wilkins, (Eds.), Proboscidean and Paleoindian Interactions: Baylor University Press, Waco, Texas, 233p.

Furman, A., Ferre, P.S., and Warrick, A.W., 2003, A sensitivity analysis of electrical resistivity tomography array types using analytical element modeling: Vadose Zone Journal, v. 2, p. 416-423.

Gee, G.W., Bauder, J.W., 1986, Particle-Size Analysis, *in* Klute, A., (Ed.), Methods of Soil Analysis, Part 1. Physical and Mineralogical Methods: Agronomy 2nd Edition, Madison, Wisconsin, USA, p. 383-411.

Guthrie, R.D., 2001, Origin and causes of the mammoth steppe: a story of cloud Cover, woolly mammal tooth pits, buckles, and inside-out Beringia: Quaternary Science Reviews v.20, p. 549-574.

Graham, R., 1986, Taxonomy of North American mammoths, *in* Frison, G., Todd, R., eds., The Colby mammoth site: University of New Mexico Press, Albuquerque, New Mexico, p. 165-169.

Greiner, J.J., 1978, Erosion and Sedimentation by Water in Texas: Texas Department of Water Resources, USCS, Report 268.

Grun, R., Abeyratne, M., Head, J., Tuniz, C., and Hedges, R.E.M., 1997, AMS ^{14}C analysis of teeth from archaeological sites showing anomalous ESR dating results: Quaternary Science Reviews, v. 16, n. 3, p. 437-444.

Haury, E.W., 1953, Artifacts with mammoths remains, Naco, Arizona, I: discovery of The Naco mammoth and the associated projectile points: American Antiquity, v. 19, p. 1-14.

Hay, O., 1924, The Pleistocene of the middle region of North America and its vertebrated Animals: Carnegie Institute, Washington Publication. v, 322, p. 1-385.

Haynes, G., 1985, On Watering Holes, Mineral Licks, Death, and Predation, *in* J. Mead and D. Meltzer (Eds.), Environment and Extinctions: Man in Late Glacial North America: Center for the Study of Early Man, Orona, Maine, p. 53-71.

Haynes, G., 1988, Mass Deaths and Serial Predation: Comparative Taphonomic Studies of Modern Large Mammal Death Sites, Journal of Archaeological Science, no. 15, p. 219-235.

Haynes, G., 1991, Mammoths, mastodonts, and elephants: biology, behavior, and the Fossil record: Cambridge University Press, Cambridge, England, 413 p.

Haynes, G., 1992, The Waco Mammoths: Possible Clues to Herd Size, Demography, and Reproductive Health. Pp. 111, *in* J.W. Fox, C.B. Smith, and K.T. Wilkins, (Eds.), Proboscidean and Paleoindian Interactions: Baylor University Press, Waco, Texas, 233p.

Heinrich, P.V., 1985, Sedimentology at the Waco Mammoth Site: Manuscript, Strecker Museum, Baylor University, Waco, Texas, 16 p.

Hilliard, L.K., 1997, Late Quaternary Geology of the Waco Mammoth Site, Waco, Texas: unpublished Baylor University Bachelor of Science thesis, Waco, Texas, 61p.

Holen, S.R., 2006, Taphonomy of two last glacial maximum mammoth sites in the Central Great Plains of North America: A preliminary report on La Sena and Lovewell: Quaternary International, v. 142-143, p. 30-43.

Holliday, V.T., Haynes, V.C., Hofman, J.L., and Meltzer, D.J., 1994, Geoarchaeology and Geochronology of the Maimi (Clovis) Site, Southern High Plains of Texas: Quaternary Research, v. 41, p. 234-244.

Hoppe, K.A., 2004, Late Pleistocene mammoth herd structure, migration patterns, and Clovis hunting strategies inferred from isotopic analysis of multiple death assemblages: Paleobiology, v.30, n.1, p. 129-145.

Jain, M., Murray, A.S., Bøtter-Jensen, L., 2003, Characterization of blue-light stimulated luminescence components in different quartz samples: implications for dose measurements: Radiation Measurements, v. 37, p. 411–449.

Koch, P.L., K.A. Hoppe, and S.D. Webb, 1998, The isotopic ecology of late Pleistocene mammals in North America Part 1. Florida: Chemical Geology, v. 152, p. 119-138.

Koch, P.L., N.S. Diffenbaugh, K.A. Hoppe, 2004, The effects of late Quaternary Climate and pCO_2 change on C_4 plant abundance in the south-central United States: Paleogeography, Paleoclimatology, Paleoecology, v. 207, p. 331-357.

Kochel, R.C., and Baker, V.R., 1988, Paleoflood analysis using slackwater deposits, *in* Baker, V.R., Kochel, R.C., and Patton, P.C. (Eds.), Flood Geomorphology: John Wiley & Sons, Inc., New York, p. 357-376.

Kochel, R.C., 1988, Extending stream records with slackwater paleoflood hydrology: Examples from West Texas, *in* Baker, V.R., Kochel, R.C., and Patton, P.C. (Eds.), Flood Geomorphology: John Wiley & Sons, Inc., New York., p. 377-391.

Kurten, B., Anderson, E., 1980, Pleistocene mammals of North America: Columbia University Press, New York, 442 p.

Loke, M.H., and Barker, R.D., 1996, Rapid least-square inversion of apparent resistivity pseudosections by quasi-Newton method: Geophysical Prospecting, v. 44, p. 131-152.

Loke, M.H, 2000, Electrical imaging surveys for environmental and engineering studies: available at: http://www.georentals.co.uk/Lokenote.pdf (accessed January 20, 2007, verified February 5, 2007).

Loke M. H., Acworth, I., and Dahlin, T., 2003, A comparison of smooth and blocky inversion methods in 2D electrical imaging surveys: Exploration Geophysics, v. 34, p. 182-187.

Lowe J.J., and Walker M.J.C., 1997, Reconstructing Quaternary Environments, 2nd Edition: Longman, London. 446 pp.

Lundelius, E.L., 1972, Fossil vertebrates from the Late Pleistocene Ingleside fauna, San Patricio County, Texas: University of Texas Bureau of Economic Geology, Rept. Inv. 77, p. 1-74.

Lundelius, E.L., 1992, Quaternary Paleofaunas of the Southwest. Pp. 35, *in* J.W. Fox, C.B. Smith, and K.T. Wilkins, (Eds.), Proboscidean and Paleoindian Interactions: Baylor University Press, Waco, Texas, 233p.

Maglio, V.J., 1973, Origin and evolution of the Elephantidae: Transactions of the American Philosophical Society, Philadelphia, Pennsylvania, New series, v. 63, n. 3, p. 1-149.

Marean, C.W., and Ehrhardt, C., 1995, Paleoanthropological and paleoecological implications of the taphonomy of a sabertooth's den: Journal of Human Evolution, v. 29, p. 515-547.

Martinson, D.G., Pisias, N.G., Hays, J.D., Imbrie, J., Moore, T.C., and Shackleton, N.J., 1987, Age dating and the orbital theory of the ice ages: Development of a high-resolution 0 to 300 000-year chronostratigraphy: Quaternary Research, v. 27, p. 1–29.

McDonald, Gregory, 2005, Personal Communication, National Park Service, Fort Collins, Colorado.

McGrew, P.O., 1961, The Rawlins mammoth: Wyoming Geological Association Annual Field Conference Guidebook, v. 16, p. 315-317.

McKinney, C.R., 1991, The Determination of the Reliability of Uranium Series Dating Of Enamel, Dentine, and Bone: Unpublished Southern Methodist University Doctor of Philosophy Dissertation, Dallas, Texas, 186 p.

Murry, A.S., Olley, J.M., 2002, Precision and Accuracy in the Optically Stimulated Luminescence Dating of Sedimentary Quartz: A Status Review, Geochronometria, v. 21, p. 1-16.

Naryshkin, G.F., 1981, The Significance of the Waco Mammoth Site To Central Texas Pleistocene History: unpublished Baylor University Bachelor of Science thesis, Waco, Texas, 59 p.

Nelson, D.W., Sommers, L.E., 1982, Total Carbon, Organic Carbon, and Organic Matter, *in* Page, A.L., Miller, R.H., Keenley, D.R., (Eds.), Methods of Soil Analysis, Part 2. Chemical and Microbiological Properties: Agronomy, 2nd Edition, n. 9, p. 539-577.

Nordt, L.C., Boutton, T.W., Hallmark, C.T., and Waters, M.R., 1994, Late Quaternary vegetation and climate changes in Central Texas based on the isotopic composition of organic carbon: Quaternary Research, v. 41, p. 109-120.

Nordt, L.C., Hallmark, C.T., Wilding, L.P., and Boutton, T.W., 1998, Quantifying pedogenic carbonate accumulations using stable carbon isotopes: Geoderma v. 82, p. 115-136.

Nordt, L.C., 2001, Stable Carbon and Oxygen Isotopes in Soils, *in* Goldberg, P., Holliday, V.T., Ferring, R.C., (Eds.), Earth Sciences and Archaeology: Kluwer Academic/Plenum Publishers, New York, 514 p.

Nordt, L.C., Boutton, T.W., Mandel, R., and Jacob, J.S. 2002, C4 Plant Productivity and Climate-CO_2 Variations in the Southern Great Plains During the Late Quaternary: Quaternary Research*, v.* 58, p. 182-188.

Nordt, L., von Fischer, J., and Tieszen, L. 2007, Late Quaternary temperature record from buried soils of the North American Great Plains: Geology, v. 35, p. 159-162.

O'Connor, J.E., and Webb, R.H., 1988, Hydraulic modeling for paleoflood analysis, *in* Baker, V.R., Kochel, R.C., and Patton, P.C. (Eds.), Flood Geomorphology: John Wiley & Sons, Inc., New York., p. 403-418..

Olayinka, A.I. and Yaramanci, U., 2000, Use of block inversion in the 2-D interpretation of apparent resistivity data and its comparison with smooth inversion: Journal of Applied Geophysics, v. 45, p. 63-81.

Olley, J.M., Caitcheon, G.G., and Roberts, R.G., 1999, The origin of dose distributions in fluvial sediments, and the prospect of dating single grains from fluvial deposits using optically stimulated luminescence: Radiation Measurements, v. 30, p. 207-217.

Osborn, H.F., 1922, Species of American Pleistocene Mammoths, Elephas jeffersonii, New Species: American Museum of Natural History, Novitates, New York, n. 41, p. 1-16.

Osborn, H.F., 1942, Proboscidea: A Monograph of the Diversity, Evolution, Migration, and Extinction of the Mastodons and Elephants of the World: Volume II. Stegodontoidea and Elephantoidea: The American Museum of Natural History, New York.

Osella A., de la Vega, M., and Lascano, E., 2005, 3D electrical imaging of an archaeological site using electrical and electromagnetic method: Geophysics, v. 4, p. 101-107.

Papadopoulos N. G., Tsourlos, P., Tsokas, G.N., and Sarris, A., 2006, Two-dimensional and three-dimensional resistivity imaging in archaeological site investigation: Archaeological Prospection, v. 13, p. 163–181.

Paruleo, J.M., and Lauenroth, W.K., 1996, Relative abundance of plant functional types in grasslands and shrublands of North America: Ecological Applications, v. 6, p. 1212-1224.

Prescott, J.R. and Hutton, J.T., 1994, Cosmic ray contributions to dose rates for luminescence and ESR dating: large depths and long-term time variations: Radiation Measurements, v. 23, p. 497-500.

Proctor, Jr., C.V., McGowen, J.H., Haenggi, W.T., and Barnes, V.E., 1970, Geologic Atlas of Texas, Waco Sheet (reprented 1998): Bureau of Economic Geology, The University of Texas, Austin, Texas.

Ruddiman, W.F., 2001, Earth's Climate Past and Future: W.H. Freeman and Company, New York, New York, p. 465.

Saunders, J., 1990, Immanence, configuration, and the discovery of America's past, *in* Agenbroad, L.D., Mead, J. I., Nelson, L., (Eds.), Megafauna And Man: The Mammoth site of Hot Springs, South Dakota, Inc., Hot Springs, p. 136-143.

Scollar, I., Tabbagh, A., Hesse, A., Herzog, I., Arvidson, R. E., and Rycroft, M.J., 1990, Archaeological Prospecting and Remote Sensing: Cambridge University Press, Cambridge, England, 692 p.

Scott, K.M., and Gravlee, Jr., G.C., 1968, Flood surge on the Rubicon River, California-Hydrology, hydraulics, and boulder transport: U.S. Geological Survey Professional Paper 422-M, Reston, Virginia, M1-M38.

Sellards, E.H., 1952, Early man in America: a study in prehistory: The University of Texas Press, Austin, Texas, 211 p.

Sellards, E.H., Adkins, W.S., Plummer, F.B., 1981, The Geology of Texas: Bureau of Economic Geology, The University of Texas, p. 1007.

Shroba, R.R., Schmidt, P.W., Crosby, E.J., Hensen, W.R., and Soule, J.M., 1979, Geologic and geomorphic effects in the Big Thompson Canyon area, Larimer County, Colorado: U.S. Geological Survey Professional Paper, v. 1115B, p. 87-152.

Singhvi, A.K., Sharma, Y.P. and Agrawal, D.P., 1982, Thermoluminescence dating of dune sands in Rajasthan, India: Nature, v. 295, p. 313-315.

Soil Survey Division Staff, 1993, Soil Survey Manual, U.S. Department of Agriculture Handbook No. 18: Washington D.C., U.S. Government Printing Press.

Spencer, J.M., 1966, Urban Geology of Greater Waco Part III: Water: Baylor Geological Studies Bull., n. 10, p. 49.

Strickland, S.S., 1988, Site Formation Processes at the Waco Mammoth Site: a thanatocose and its implications: Manuscript, Division of Anthropology, Baylor University, Waco, Texas, 14 p.

Suhm, R., 1978, Preliminary investigation of the La Paloma mammoth site (Late Pleistocene), Kenedy County, Texas: TAIUS, Texas A&M University, College Station, Texas, v. 11, n. 1, p. 13-36.

Tharp, T.L., 1988, Aspects of Leon River Drainage History with Implications to Other Central Texas Streams: unpublished Baylor University Bachelor of Science thesis, Waco, Texas, 260 p.

USACE, 2006, HEC RAS 4.0 Beta Flow Analysis: U.S. Army Corps of Engineers, http://www.hec.usace.army.mil/.

USDA-NRCS, 2001, Soil Survey of McLennan County, Texas, U.S. Department of Agriculture, Natural Resources Conservation Service, in cooperation with Texas Agriculture Experimental Station.

USDA-NRCS, 2007, NCSS Web Soil Survey, http://websoilsurvey.nrcs.usda.gov/app/.

USGS-NWIS, 2007, Peak stream flow data from North Bosque River at Valley Mills, Texas: site number USGS 8095200: National Water Information System, U.S. Geological Survey, accessed 2007, http://waterdata.usgs.gov/nwis/sw.

Vuichard, D., and Zimmerman, M., 1986, The Langmoche flash flood, Khumb Himal, Nepal: Mountain Research and Development, v. 6, n. 1, p. 90-93.

Wallinga, J., Murray, A.S., Duller, G.A.T., and Tōrnqvist, T.E., 2001, Testing optically stimulated luminescence dating of sand-size quartz and feldspar from fluvial deposits: Earth and Planetary Science Letters, v. 193, p. 617-630.

Wallinga, J., 2002, Optically stimulated luminescence dating of fluvial deposits: a review: Boreas, v. 31, n. 4, p. 303-322.

Waters, R.M., L.C. Nordt, 1995, Late Quaternary Floodplain History of the Brazos River in East-Central Texas: Quaternary Research, v. 43, p. 311-319.

Weir, G.H., 1978, Preliminary investigation of the La Paloma mammoth site (Late Pleistocene), Kenedy County, Texas: TAIUS, Texas A&M University, College Station, Texas, v. 11, n. 1, p. 15-36.

Wintle, A.G., and Murray, A.S., 2006, A review of quartz optically stimulated luminescence characteristics and their relevance in single-aliquot regeneration dating protocols: Radiation Measurements, v. 41, p. 369-391.

Wohl, E.E., 1999, Incised Bedrock Channels *in* Darby, S.E., and Simon, A., (Eds.), Incised River Channels: Processes, Forms, Engineering and Management: Wiley & Sons Ltd., West Sussex, England, 452 p.

Wyckoff, D.G., Carter, B.J., Flynn, P., Martin, L.D., Branson, B.A., and Theler, J.L., 1992, Interdisciplinary Studies of the Hajny Mammoth Site, Dewey County, Oklahoma: Studies of Oklahoma's Past, Oklahoma Archeological Survey, The University of Oklahoma, Norman, Oklahoma, n. 17, 134 p.

Yelderman, J.C., and Cervenka, R.E., 1992, Environmental atlas of McLennan County: Baylor Geological Studies Bull, Dept. of Geology, Baylor University, Waco, Texas, . n. 13/14, 19 p.

Zhang, J.F., Zhou, L.P., and Yue, S.Y., 2003, Dating fluvial sediments by optically stimulated luminescence: selection of equivalent doses for age calculation: Quaternary Science Reviews, v. 22, p. 1123-1129.